

Department of Precision and Microsystems Engineering

**Planar Ferrofluid Bearings
Modelling and Design Principles**

S.G.E. Lampaert

Report no : MSD 2015.039
Coach : ir. J.W. Spronck
Professor : Prof. dr. ir. J.L. Herder
Specialisation : Mechatronic System Design
Type of report : Master Thesis
Date : 16 December 2015

Planar Ferrofluid Bearings

Modelling and Design Principles

By

Stefan G.E. Lampaert

in partial fulfilment of the requirements for the degree of

Master of Science
in Mechanical engineering

at the Delft University of Technology,
to be defended publicly on Wednesday December 16, 2015 at 9:30 AM.

Supervisor:	ir. Jo W. Spronck	TU Delft
Thesis committee:	Prof. dr. ir. Just L. Herder	TU Delft
	dr. ir. Ron A.J. van Ostayen	TU Delft
	dr. ir. Dick H. Plettenburg	TU Delft

This thesis is confidential and cannot be made public until December 16, 2020.

An electronic version of this thesis is available at <http://repository.tudelft.nl/>.

“Let us endeavour so to live that when we come to die
even the undertaker will be sorry.”

Mark Twain

List of symbols

Parameter	Definition	Unit	Parameter	Definition	Unit
α	Langevin parameter	–	k_{ff}	Stiffness ferrofluid	N / m
A	Surface area	m^2	k_{setup}	Stiffness of setup	N / m
A_p	Surface area pocket	m^2	k_{mes}	Measured stiffness	N / m
β	Angle between magnetic field and vorticity	rad	k_{top}	Stiffness top	N / m
γ	Ratio of the specific heats	–	$L(\alpha)$	Langevin function	–
d_g	Distance between magnet faces	m	λ	Dipolar diffraction parameter	–
d	Diameter	m	m	Dipolar moment	Am^2
\underline{f}	Body force	N / m^3	M	Magnetization	A / m
$f_{fit,x}$	Fit constant x-direction	–	M_s	Saturation magnetization	A / m
$f_{fit,y}$	Fit constant y-direction	–	M_d	Domain magnetization	A / m
f_{vol}	Volume fraction	–	μ_0	Magnetic permeability	N / A^2
f_0	Larmor frequency	Hz	μ_r	Relative permeability	–
g	Gravitational acceleration	m / s^2	p_i	Pressure inside the pocket	Pa
ϕ	Volume fraction	–	p_0	Pressure outside the pocket	Pa
$\tilde{\phi}$	Volume concentration including surfactant	–	p	Pressure	Pa
F_B	Force bottom	N	p_{seal}	Pressure seal	Pa
F_T	Force top	N	ρ	Density	kg / m^3
F_L	Load capacity	N	R	Radius	m
h	Flight height	m	R^*	Mean radius of ring	m
\bar{h}	Order of magnitude flight height.	m	r	Radius	m
H_i	Magnetic field inner fluid interface	A / m	\bar{r}	Order of magnitude displacement	m
H_0	Magnetic field outer interface	A / m	σ	Surface tension	N / m
$H_{i,B}$	Inner fluid interface bottom	A / m	t	Time	s
$H_{o,B}$	Outer fluid interface bottom	A / m	τ	Time constant	s
$H_{i,T}$	Inner fluid interface top	A / m	T	Temperature	K
$H_{o,T}$	Outer fluid interface top	A / m	\underline{u}	Fluid velocity	m / s
H_{max}	Magnetic field at saddle point	A / m	V_p	Volume of nonmagnetic fluid pocket	m^3
H	Magnetic field strength	A / m	V_i	Initial volume	m^3
\bar{H}	Order of magnitude magnetic field intensity.	A / m	\tilde{V}	Volume of ferrofluid particle including surfactant layer	m^3
I	Area moment of inertia	m^4	\underline{r}	Distance vector	m
J	Polar area moment of inertia	m^4	r_0	Initial pocket radius	m
η	Viscosity	kg / ms	r_{in}	Increase in pocket radius	m
k_B	Boltzman constant	J / k	w_m	Width magnet	m
K_a	Anisotropy constant	J / m^3	x	Displacement	m
k	Stiffness	N / m	\bar{x}	Order of magnitude displacement	m
k_{air}	Stiffness air	N / m	z	Coordinate out-of-plane direction.	m

List of definitions

Term	Definition
Aggregation	Formation of clusters of particles.
Bearing capacity	The maximum force that the bearing can withstand without having a permanent change in flight height.
Bearing configuration	See section 1.3 and Fig. 1-2
Bearing length	The length of the bearing in the direction of the flow.
Bearing performance	See section 1.3 and Fig. 1-2
Bearing surfaces	The surface area of the bearing that carries the load.
Colloidal stability	A suspension that does not show any sedimentation or aggregation.
Damping	The out-of-plane reaction force due to an out-of-plane velocity.
Ferrofluid	A colloidal suspension of magnetic particles
Ferrofluid pocket bearing	A bearing that uses an encapsulated pocket of air to carry a load
Ferrofluid pressure	Both ferrofluid pressure bearings and ferrofluid pocket bearings
Ferrofluid pressure bearing	A bearing that uses solely the magnetic pressure to carry load
Flight height	The distance between the bearing surfaces
Flow field	The velocity profile of the fluid over space
Fluid reservoir	The extra fluid added to a ferrofluid pocket bearing that does not contribute significantly to the load, but reduces the effect of trail formation
Friction	The in-plane force in reaction to an in-plane velocity.
Fully saturated magnetic fluid	Situation at which the magnetization of the fluid cannot increase more with an increase in external magnetic field intensity.
Inherent stability	Stability without the additional need of a controller.
In-plane	The plane tangent to the bearing surfaces
Load capacity	The counteracting force that can be delivered at a certain configuration.
Magnetic body force	The pressure induced in a ferrofluid due to an external magnetic field
Magnetic fluid	A fluid that is attracted to a magnet
Magnetorheological fluid	A magnetic fluid without a colloidal stability; viscosity react aggressively on the presence of a magnetic field
Maximum load capacity	See bearing capacity
Out-of-plane	The line perpendicular to the bearing surfaces
Particle chain formation	The formation of chains of magnetic particles in the fluid
Rotational viscosity	The viscosity due to in increased resistance to rotation of the magnetic particles
Seal capacity	The maximum pressure before air pops through the seal.
Shear thinning effect	The decreasing viscosity with increasing shear rate.
Single domain particles	Particles at which the magnetization does not vary over the volume. These are in general small particles ($< 50nm$).
Stick-slip	The effect of a reduced friction when translating the bearing
Stiffness	The out-of-plane stiffness of the bearing
Trail formation	Fluid that sticks behind during translation

Glossary of abbreviations

Abbreviation	Definition
DOF	Degree of freedom
PID	Proportional-Integral-Derivative
PME	Precision and Microsystems Engineering

Preface

My fascination for engineering started with my science project at the secondary school. My friends and I wanted to do something awesome which ended up in building a 7.5 meters tall trebuchet that could throw a bowling ball about 150 meters far away. After this project I was convinced, I wanted to become an engineer! So I went to Delft, the university where the sky is the limit. I joined the Formula Student Team Delft that designs and builds a race car every year to compete in the largest student design competition in the world: "Formula Student". It started as a project for doing besides my studies, but it rapidly changed in doing my studies beside the project. The three years I participated in the project really shaped me as an engineer, but the main thing I learned from it is not related to this. The main thing I learned is that you learn more from losing than from winning. Being punched to the ground is the only thing that really stops you to think about what to improve.

Looking back at my time in Delft I can say that I gathered a tremendous amount of knowledge at this fascinating institute with endless possibilities. Thank you for this opportunity.

Stefan Lampaert
Delft, December 2015

Acknowledgements

The first people I want to thank are my parents and my family. Not only for this thesis, but also for all the support they gave during my studies. You really helped in getting the best out of me. My apologies for being this busy lately, I promise to spend more time with you in the near future. I am looking forward spending the Christmas holidays with you.

I want to thank my fiancé Lisanne Fernhout for supporting me during my studies and my graduation project. I am looking forward to spend the rest of my life with you.

I want to thank the people of the Taylor board, Thomas van der Linde, Anton Driessen, Sarah Aalbers and Rolf Swuste for the wonderful year we had together on the board. We had some tough discussion during the year, but we always ended up in good agreement. I really enjoyed organizing all the event with you guys with as pinnacle the study trip to Japan.

I want to thank all the people of the Formula Student Racing Team Delft. I really enjoyed the years with you guys. Especially the people on the board of the DUT12, I really appreciate the trust you had in me when the times got rough for me.

I want to thank the technical support staff of PME, Rob Luttjeboer, Patrick van Holst and Harry Jansen for helping me out with everything I needed for the experiments. I really appreciate the advice you gave on all the practical things of the experiments. We students might be good in solving equation, but you guys really know how to turn those equations into something physical.

I want to thank the teaching staff of PME for all the things you guys learned me during the courses. The courses are very well given and I learned a lot of it. I especially appreciate your skill to make the student sweat close to the deadline. You guys really know how to take the sleep away from the students.

I want to thank all my fellow students for all the discussions we had on the famous study platform. I learned a lot from the courses, but a think in learned even more from you guys. You guys really made the difference for me.

I want to thank Bart Joziasse, Thomas van der Linde, Felix de Boer, Eline Veenema, Timo Fernhout, Mieneke Fernhout, Lisanne Fernhout, Martijn van Beek, Paul Ouwehand, Joep Nijssen and Emiel van de Ven for proofreading parts of my thesis. I could not have done this without you.

I want to thank the people of the workshop, Gerard van Vliet and Rene van Ommen for helping me out when I wanted things to be produced.

I want to thank the group of Bachelor student I am supervising now, Aaron Alkemade, Chiwai Kan, Mart Beeftink and Wouter de Roos. It is a lot of fun helping you guys with your research. You, probably without knowing, inspire me a lot for my own research. The different discussions we had on the subject led to a lot of new insights for my own work.

I want to thank Just Herder, Jo Spronck, Dick Plettenburg and Ron van Ostayen for making time to be a member of my graduation committee.

I want to thank Ron van Ostayen for the interesting discussion we had and the proofreading you did for this thesis. I am looking forward to working together the coming four years.

The last person I want to thank is my supervisor Jo Spronck. I really enjoined the discussion we had on the project. You really helped me to get the best out of me. I especially appreciate that you are more than only a supervisor. Apart from being interested in the projects of the students, you are also interested in the students themselves. That really means a lot to me. I have much appreciation for the atmosphere you managed to create among the graduate students. You created a really nice environment to graduate in. I could not have wished for a better supervisor than you.

Abstract

A ferrofluid is a type of fluid that due to its magnetic properties is attracted to a magnetic field. These properties are generated by suspending tiny magnetic particles ($\sim 10\text{nm}$) in a fluid forming a suspension with colloidal stability. Subjecting the fluid to a magnetic field develops an internal pressure in the fluid that is capable of carrying a load. This pressure can be used to make a ferrofluid bearing that can be seen as a type of hydrostatic bearing. The bearing distinguishes itself from other bearings by its low price, compactness, inherent stability, low (viscous) friction, absence of pumps and absence of stick-slip. These properties make the bearing interesting to be used for applications that require fast and precise positioning or applications in the absence of gravity.

In this thesis we will be focussing on planar bearings, viz. bearings that allow movement in a plane while carrying a load perpendicular to that plane. Two different types of ferrofluid bearings can be categorized. The first concept is the ferrofluid pressure bearing that uses solely the magnetic pressure developed by an external magnetic field for creating a load carrying capacity. The second concept is the ferrofluid pocket bearing that encapsulates a pocket of air (or any other nonmagnetic fluid) with a ferrofluid seal (Fig. 0-1). The maximum load capacity of this bearing is determined by the maximum pressure across the seal which is typically 0.2bar for commercial ferrofluids. The stiffness of the bearing is determined by the stiffness of the pocket and the seal together.

A problem of these types of bearings is the repeatability in flight height. Moving the bearing in plane leaves behind a trail of ferrofluid that causes less fluid to be available for carrying a load. In the case of a pocket bearing this might cause air to escape from the seal, resulting in a permanent change in flight height. Another problem is that no methods exist on how the characteristics of this bearing are described by the configuration of the bearing.

In this thesis it is discussed how the different parameters like the geometry, shape of the magnetic field and properties of the ferrofluid influence the specifications of a ferrofluid bearing. The different specifications that are covered are the out-of-plane load, stiffness and damping, the rotational stiffness, the friction and the trail formation.

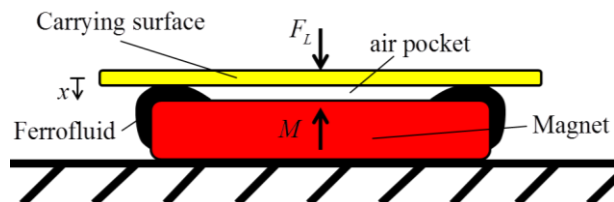


Fig. 0-1. The figure presents a cross section of a disk shaped magnet. The ferrofluid is attracted to the corners of the magnet because the field intensity is highest there. The ferrofluid forms a seal that encapsulates a pocket of air. The air pocket increases the load capacity of the bearing since the pressure is defined by the largest value of magnetic field intensity which is at the corner of the magnet.

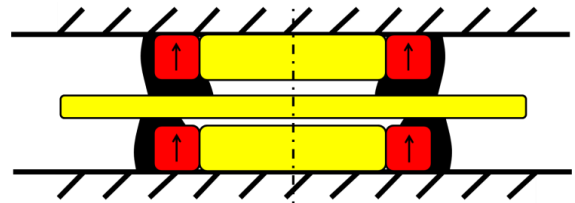


Fig. 0-2. The cross section in the figure presents the fluid interfaces at a deformed configuration. It can be seen that there is a slight movement at the outer interfaces, but this influence is minimal since they are located at a position with low magnetic field gradient. This demonstrates that the load capacity for this concept is predominantly defined by the change of the inner interfaces.

A method is proposed that can be used for deriving a model for predicting the out-of-plane load and stiffness characteristics of a ferrofluid pocket bearing. The method is experimentally validated by comparing the results of a model with the results of experiments (Fig. 0-3). On the basis of new insight developed by this work, a concept is proposed that uses a sandwich-like structure to achieve a higher stiffness and higher repeatability (Fig. 0-2 and Fig. 0-4). The model of this bearing is experimentally validated and it was shown that the performance can be described completely analytically. The proposed method is shown to be correct for describing the load and stiffness characteristic of any shape of a ferrofluid pocket bearing.

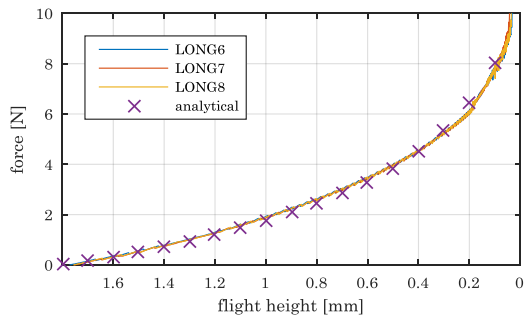


Fig. 0-3. Compressing the bearing will cause air to escape from the seal because the pressure in the pocket of air becomes larger than the pressure that can be counteracted by the seal. The first three datasets in the figure are three different measurements that show that the maximum load curve of the bearing has a high repeatability. The fourth dataset is the result from the theoretical model of this process. The figure shows that the model fits the measurements well.

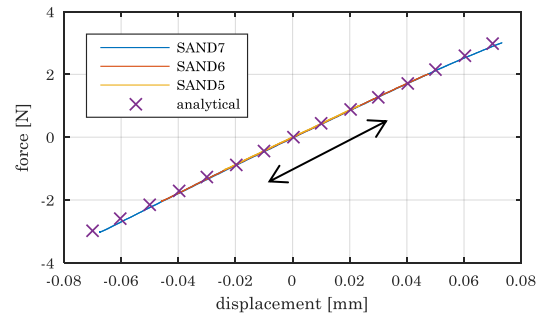


Fig. 0-4. This figure presents the force of the bearing as function of the displacement. Three different measurements are presented from which can be seen that there is no hysteresis and a high repeatability. A model is derived in the thesis that describes this behaviour completely analytical.

Four models are presented that describe the main effects seen in the planar movement of the bearing. The first model discusses the change of viscosity due to the presence of an external magnetic field. This change is caused by two different effects, the rotational viscosity and the particle chain formation. The second and third model describe respectively the translational and rotational friction of a ferrofluid bearing. The fourth model describes the trail formation of the bearing.

It is shown that the influence of the effect of rotational viscosity is limited to an increase of around 10%. The effect of particle chain formation is negligible if all suspended particles have a dipolar interaction parameter smaller than one. The translational friction can be modelled by the summation of a Couette flow and a Poiseuille flow that are such in magnitude that there is no net fluid transport across the length of the bearing. As a result the maximum load capacity of a ferrofluid pocket becomes a function of the bearing velocity since a part of the magnetic force is used for keeping the fluid in place. The derivation of the rotational friction shows that the maximum load capacity of a ferrofluid pocket bearing is not influenced by the rotational velocity of the bearing. The model of the trail formation demonstrates that this is a process depending on the path that the bearing has travelled and time. For precise positioning, the friction force and trail formation force are in the same order of magnitude. This demonstrates that both effects should be taken into consideration when designing a ferrofluid bearing.

This thesis furthermore demonstrates that the ferrofluid pocket bearing is a simple and cheap alternative bearing system for machines now using an air (fluid) bearing or magnetic bearing for achieving absence of coulomb friction and stick-slip.

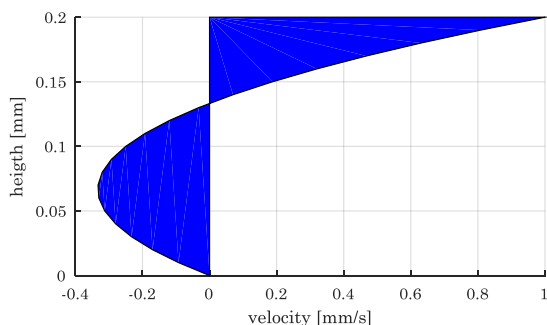


Fig. 0-5. This figure presents the flow field of a ferrofluid bearing during a translational motion. Integrating the blue surface shows a zero net fluid flow that is observed during translation.

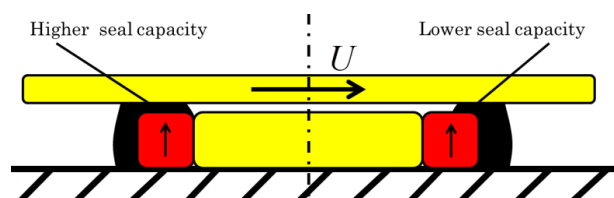


Fig. 0-6. Moving the bearing to the right causes a higher seal capacity at the left and a lower seal capacity at the right. The lowest seal capacity defined the maximum load capacity of the bearing, exceeding this will cause air to escape from the pocket.

Contents

List of symbols	vii
List of definitions	viii
Glossary of abbreviations	ix
Preface	xi
Acknowledgements	xiii
Abstract	xv
Contents	xvii
1 Project introduction	1
1.1 Background.....	1
1.2 Potential of a ferrofluid bearing.....	1
1.3 Problem definition.....	2
1.4 Organization of this thesis	3
2 Introduction to ferrofluids	5
2.1 Brief history.....	5
2.2 Properties of ferrofluids	7
2.3 Ferrohydrodynamics	16
3 Planar ferrofluid bearings in literature.....	19
3.1 Bearing systems found in literature	19
3.2 Conclusion	25
4 Load & Stiffness of a Planar Ferrofluid Pocket Bearing.....	27
4.1 Introduction.....	27
4.2 Method	28
4.3 Ring magnet pocket experiment	30
4.4 Sandwich structure	33
4.5 Conclusion	36
5 Friction Behaviour of a Ferrofluid Bearing.....	39
5.1 Introduction.....	39
5.2 General method.....	39
5.3 Viscosity.....	40
5.4 Translational friction.....	41
5.5 Rotational friction	44
5.6 Trail formation	45
5.7 Conclusion	47
6 Discussion.....	49
6.1 General discussion of results.....	49
6.2 Discussion on bearing configuration for precise positioning.....	52
7 Conclusion and recommendation	55
7.1 General conclusions	55
7.2 Recommendations for future research.....	56

A Useful relations for ferrofluid bearing design 59

B Ferrofluid pressure bearing 61

C Damping 62

D Additional measurements bearings 65

E Change of concentration due to field gradient 68

F Magnetorheological fluids..... 70

G Assumptions 71

H Air pocket stiffness derivation 72

I Specifications magnet 74

J Specifications ferrofluid APG513A from Ferrotec 75

K Zwick..... 76

L Previous projects containing ferrofluids 78

M References..... 79

1 Project introduction

1.1 Background

Where man differs from almost all other creatures on earth is in his unlimited desire of exploring the unknown. We have risked our lives to set sail for new lands and we have been shot to the moon to see what is out there. We all experience this desire of visiting other countries and exploring new cultures. This also feeds our desire of using new technologies like computers and smartphones which pushes this equipment to nowadays high-tech equipment that is fully stuffed with small high-end chips. Besides exploring the world and the space, we are now also exploring the small scale to find these new technologies of tomorrow. Like Richard Feynman told in his famous lecture “Plenty of Room at the Bottom”[1], there is a whole world ready to be explored at the small scale.

One aspect that is important for these developments is precise positioning. The devices we have in our computers and smartphones often have feature sizes in the order of nanometres. This means that the machines that are used in the development, production and inspection of these devices have precision requirements in the same range. One of the big challenges of these systems is the bearing system. A contact based bearing system is in general less interesting due to the drawback of potential stick-slip which leads to a position error by cycling around a set point when used in a control loop [2], [3]. The main alternatives are air (or fluid) bearings and magnetic bearings, though these systems result in general in a complex and therefore expensive system. A cheap alternative for cyclic movements might be flexures, but these can in general have the drawback of having only a small displacement. A ferrofluid bearing might be an interesting alternative [4], [5], although the precise performance of it is up to now only poorly described.

1.2 Potential of a ferrofluid bearing

As men began to explore space, it became relevant to develop efficient techniques to use and store rocket engine propellants in space. In the 1960s, the NASA Research Center developed for this reason a kerosene based magnetic fluid that could be collected at some desired location by the use of a magnetic field [6]. This magnetic fluid consisted of a stable colloidal suspension of tiny magnetic particles ($\sim 10\text{nm}$) giving the fluid paramagnetic properties [7]. This development can be recognized as the first step of all research conducted on these almost magical fluids.

The possibility of having a fluid that is attracted to a magnet has interesting applications in a lot of applications of which one is a bearing system. The ferrofluid bearing distinguishes itself from other bearings by its price, compactness, inherent stability, low (viscous) friction, absence of stick-slip and absence of pumps. These specifications make the bearing especially interesting to be used in applications where fast and precise positioning is important. Applications that can be thought of are (scanning) microscopy and pick and place machines. The bearing has also interesting applications in system placed in space since its performance is not influenced by the absence of gravity and the fluid is near impossible to leak or evaporate.

1.3 Problem definition

All literature found on planar ferrofluid bearings present the performance of a measured system, but fail to link this performance to theoretical models (chapter 3). The only theoretical models that are described, completely neglect the presence of air which makes them inaccurate. This demonstrates that if one is interested in designing a ferrofluid bearing, one has no information at all on how to design the system to meet desired specifications. This leads almost by definition to an unideal configuration of the bearing since it is unknown how the different parameters define the final performance. It is therefore set as a goal of this thesis to develop more knowledge on how a certain configuration leads to the final specifications of the bearing. The following research questions are derived:

- How do the parameters like the geometry, shape of the magnetic field and properties of the ferrofluid influence the following specifications of a ferrofluid bearing (Fig. 1-1 & Fig. 1-2)
 - F_L Load
 - k_{ff} Normal stiffness
 - k_{rot} Rotational stiffness
 - c_{ff} Damping (out-of-plane)
 - F_{fric} Friction (in-plane)
 - F_{trail} Trail formation
- What does this new knowledge mean for the configuration of a ferrofluid bearing for precise positioning.

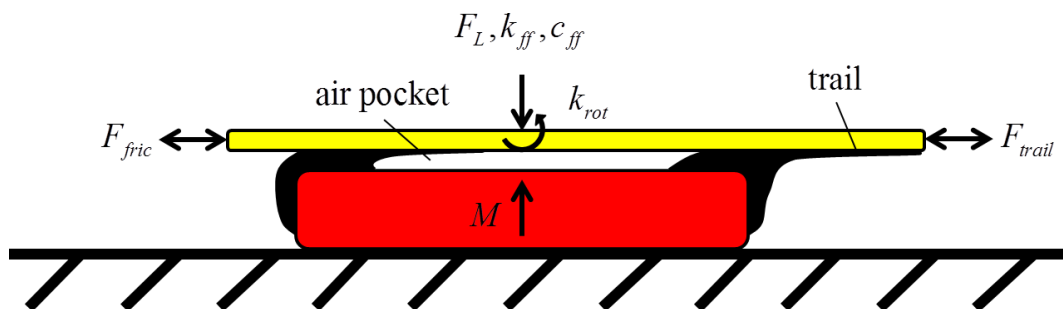


Fig. 1-1. The figure presents an overview of the different parameters of interest in the system. A cross section of a ferrofluid pocket bearing is taken as an example. The magnetic fluid is attracted to the corners of the magnet due to a higher magnetic field intensity there.

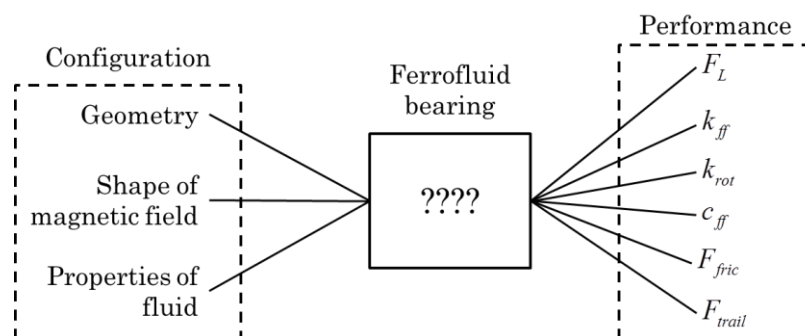


Fig. 1-2. The figure presents a graphical representation of the research objective. The terms at the left are the physical parameters that can be seen as the parameters that determine the performance. The terms at the right are the resulting specifications. This can be seen as the final performance of the bearing. The box in the middle with the question marks presents the ferrofluid bearing of which it is unknown how the configuration leads to the final specifications.

1.4 Organization of this thesis

An overview on how the different chapters interconnect is given in Fig. 1-3. The first three chapters of the thesis can be seen as an introduction since it introduces the reader to the problem, the background and the most important properties of ferrofluids. Chapter 4 and 5 present in paper format the work that is done to answer the research question. Chapter 4 discusses the out-of-plane behaviour like load, normal stiffness and rotational stiffness while chapter 5 discusses the in-plane behaviour like friction and trail formation. These two papers are written such that they should be understandable apart from the rest of the thesis for someone familiar with ferrofluid. Chapter 6 contains a discussion that links together the work of chapter 4 and 5 and some brief things mentioned in the appendices. This is followed by a discussion on what the new knowledge means for the configuration of ferrofluid bearings for precise positioning. The thesis ends at chapter 7 with main conclusions and recommendations for further research.

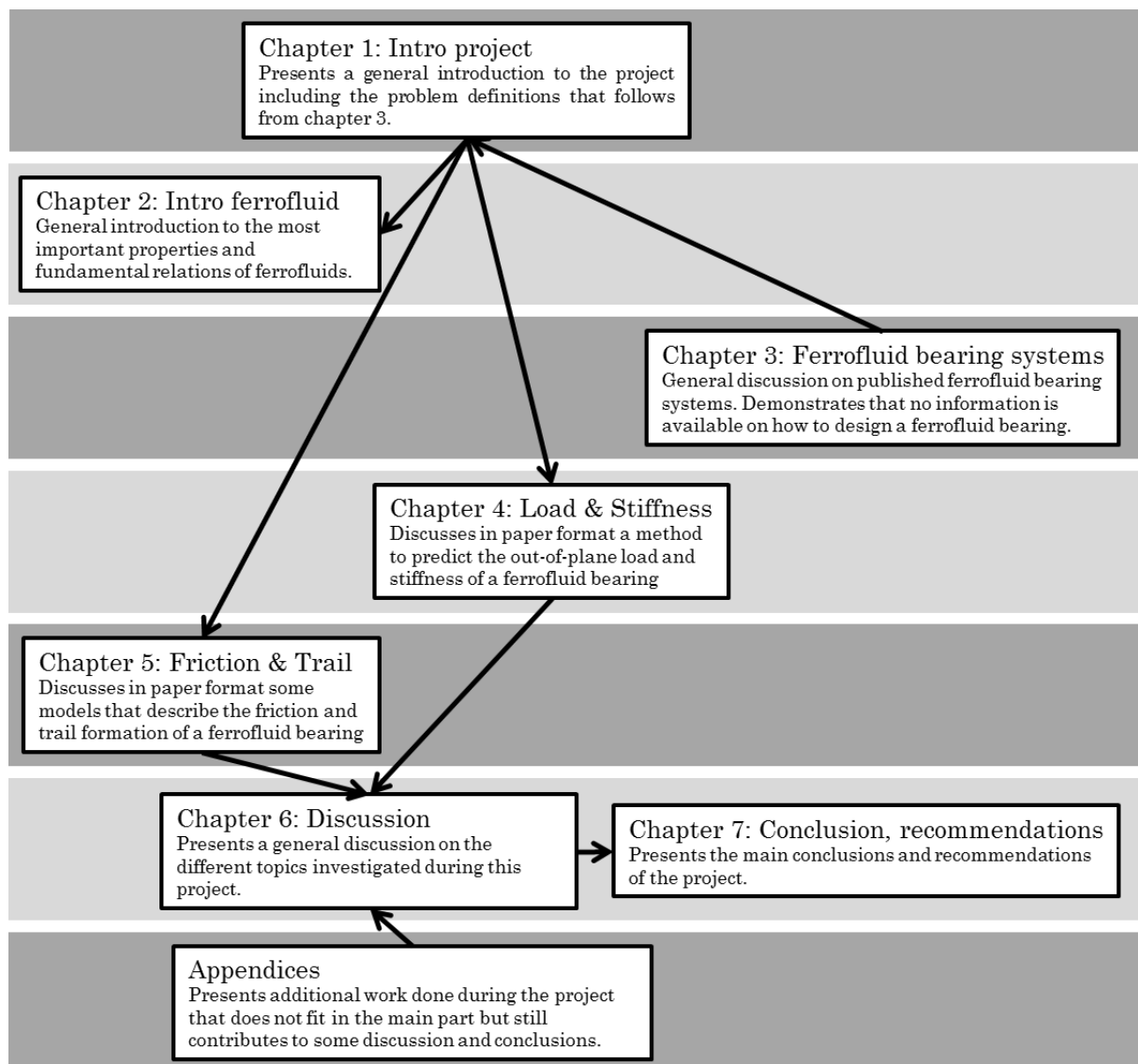


Fig. 1-3. The figure above presents in graphical form the connection between the different chapters of this thesis. The two papers presented in chapter 4 and 5 are written such that someone with experience with ferrofluid can read them apart from the use of the rest of the thesis.

2 Introduction to ferrofluids

This chapter gives an introduction to magnetic fluids and their applications. The main focus is on ferrofluids that is defined as a colloidal suspension of magnetic particles. Magnetorheological fluids are not the scope of this project, see appendix F for more information on subject. The first section gives a brief history of the magnet fluid and it will be explained how the development of the fluid led to the research and applications of today.

2.1 Brief history

A first implementation of magnetic particles suspended in a fluid can be traced back to a patent from 1922 discussing a method for detecting discontinuities on the surface of paramagnetic materials [8]. Discontinuities on the surface will cause a local change in flux density, causing a different rate of sedimentation of magnetic particles (Fig. 2-1). These changes in sedimentation will visualize cracks that would normally not be visible with the ordinary means of that time.

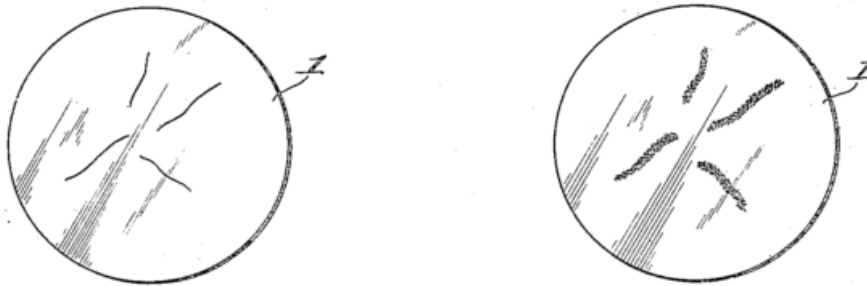


Fig. 2-1. The left picture presents some discontinuities on the surface. The right picture presents sedimentation of particles near the discontinuities of that surface. The sedimentation near those discontinuities increases due to a local increase in flux density. Picture from [8]

Suspending magnetic particles into a fluid causes that fluid to change its rheological properties with the presence of a magnetic field. Jacob Robinow at the U.S. National Bureau of Standards can be credited to be the first to discover this phenomenon in 1948 [9]–[12]. He used the magnetic fluid in a torque and force transmitting device that could be used in for example clutches or brakes (Fig. 2-2). These devices consist of fluid between two independently rotating units. The velocity, force and torque transmitted through these plates can be controlled by changing the rheological properties of the fluid. The invention of Robinow is capable of doing this by using a magnetic fluid and subjecting it to a controllable magnetic field. This concept was able to control from a point of zero slip, up to a point of full force and torque transmission.

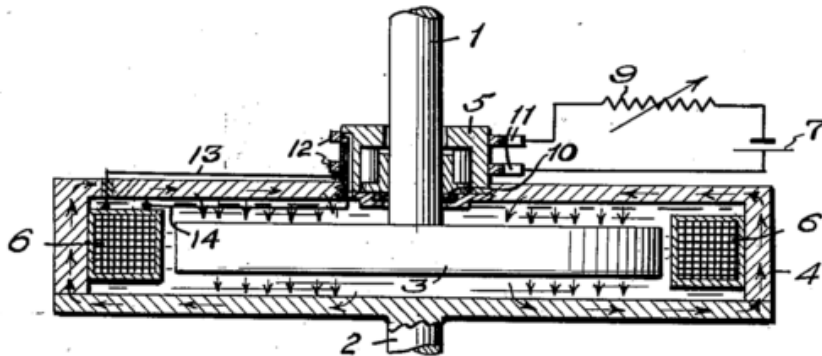


Fig. 2-2. The pictures presents a magnetic fluid clutch from a patent of Rabinow published in 1951 [11]. The two individually rotating discs are indicated with 1 and 2. The arrows in the picture present the flow of the magnetic field. Changing the amplitude of this magnetic field will change the viscosity which will change the torque transmitted between the two discs.

Papell, who was working for NASA, was investigating ways to store rocket engine propellant in space under zero gravity condition. In 1963, he developed a propellant with magnetic properties to achieve an attracting force towards a magnet placed at the inlet of the propulsion system [6], [13]. The propellant was added with a colloidal suspension of magnetic particles to prevent settlement of the particles over time. This was the first time a fluid was developed that had magnetic properties and did not suffer from sedimentation. This colloidal suspension is later referred to as ferrofluid and was further developed in 1965 by Rosensweig et al. with funding of NASA [14]–[16]. Rosensweig showed in 1967 that a magnetic field induces an internal pressure in the fluid that is for example capable of levitating a magnet immersed in ferrofluid [7]. In that same year, Cowley and Rosensweig revealed the cause of the pattern-forming instability of this so called ferrofluid fluid shown in Fig. 2-24 [17]. In 1969 Rosensweig showed that also the rheological properties of a ferrofluid will change with a change of magnetic field [18]. A few months later, the same result was published by McTague by an independent research [19]. These new insights lay the basis for basically all research and development done on ferrofluids from that point on [20].

The first real implementations of ferrofluids are the sealing of a volume [21]–[23]. One application of this sealing is simply the radial sealing of a rotating shaft (Fig. 2-3). This can be achieved by placing a ring magnet around a ferromagnetic shaft and placing ferrofluid between the two surfaces. The ferrofluids wants to stay between the shaft and the magnet, which makes it capable of withstanding a difference in pressure. A bearing could also be made by using the same principle [22]. Assume a ring magnet that is magnetized axially and is placed on top of a surface. Now place ferrofluid on top of the magnet ring and place a nonferrous plate on top of the ferrofluid. The ferrofluid encapsulates the pocket of air because it wants to stay on top of the magnet. The pocket of air is now mainly carrying the force while the ferrofluid makes sure that the air cannot escape.

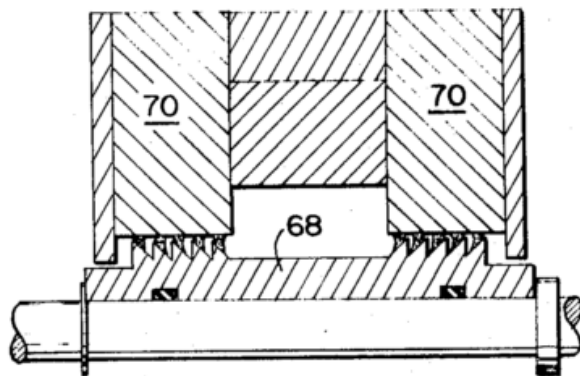


Fig. 2-3. The picture presents a magnetic fluid seal from a patent of Rosensweig published in 1971. The shaft has small triangles to achieve a local increase of the magnetic field in the gab. This is useful to increase the maximum allowable pressure difference across the seal. Multiple of these triangles are used to increase the maximum pressure even more. Figure from [21]

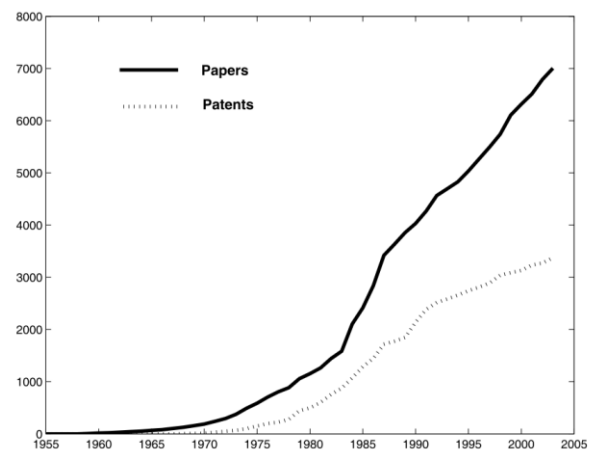


Fig. 2-4. This figure presents the accumulated production of papers and patents on magnetic fluids up 2003. Figure from [24]

These seals and bearings are only two applications of many more to follow. Already about 3500 patents for applications of ferrofluids were granted up to 2003 [24], [25] (Fig. 2-4). Ferrofluids have nowadays found its way into many applications like loudspeakers, ink, power transmissions, stepper motors, lubrication, dampers and sensors. In 1998 it was estimated that the total industrial ferrofluid revenue at that time was about \$150 million [26].

2.2 Properties of ferrofluids

This section introduces the different properties of magnetic fluid. The focus of this research is on ferrofluids and therefore the properties of magnetorheological fluids are not discussed here. The section starts with a general discussion on ferrofluids

2.2.1 Ferrofluids

A ferrofluid can be defined as a fluid that has paramagnetic properties while having a colloidal stability. The magnetic properties are obtained by suspending particles with magnetic properties in a carrier fluid. The colloidal stability is obtained by using small particles that are either coated with long chained organic molecules or stabilized with electric charge [27]. The most commonly used ferrofluids have nearly spherical particles with a size in the order of 10nm and a coating consisting of an organic chain length in the order of 2nm (Fig. 2-5 & Fig. 2-6). The coating has as function to guarantee the colloidal stability against the van der Waals attraction between the particles. This extremely small size of the particles makes them basically single magnetic domain particles. The most often used magnetic material is magnetite (Fe_3O_4), but also cobalt ferrites ($CoFe_2O_4$) are seen a lot [28]. Different carrier fluids can be used like for example water and kerosene.

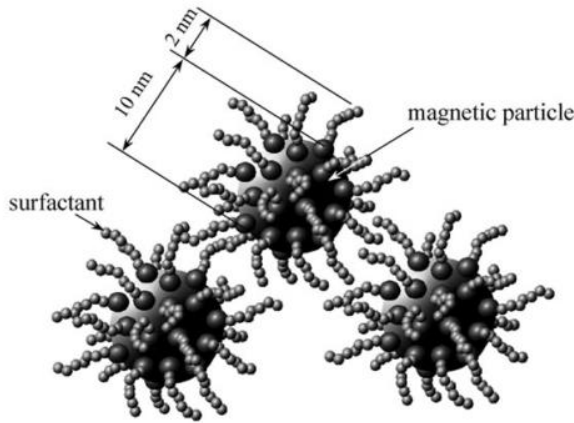


Fig. 2-5: The suspended magnetic particles are coated with a surfactant of long polymer chains to prevent the particles sticking to each other due to van der Waals forces. Figure from [27]

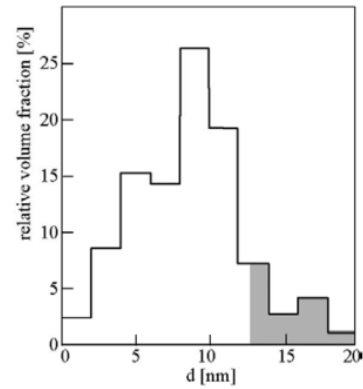


Fig. 2-6: Particle size distribution of the ferrofluid APG513A. The distribution can be seen as typical for a ferrofluid. The white part presents the particles that behave according to the Néelian relaxation and the grey part presents the particles that behave according to the Brownian relaxation. Picture from [27]

Sedimentation and aggregation of the magnetic particles in the fluid does not happen when the thermal energy of the particles (which forces the particles apart) is in the same order of magnitude as the magnetic and gravitational energy of the particles (which try to bring the particles together). The following equations give some typical values of the different energies of interest based on the values given in appendix J.

$$E_{therm} = kT = 1.4 \times 10^{-23} \times 300 = 4.2 \times 10^{-21} J \quad (2.1)$$

$$E_{mag} = \mu_0 M_s H V = 4\pi \times 10^{-7} \times 3.3 \times 10^5 \times 2 \times 10^4 \times \frac{\pi}{6} (10 \times 10^{-9})^3 = 4.3 \times 10^{-21} J \quad (2.2)$$

$$E_{grav} = \Delta\rho g V h = 0.3 \times 10^3 \times 9.81 \times \frac{\pi}{6} (10 \times 10^{-9})^3 \times 1 = 1.5 \times 10^{-21} J \quad (2.3)$$

$$E_{dip} = \frac{\mu_0 M^2 V}{12} = \frac{4\pi \times 10^{-7} \times (3.3 \times 10^5)^2 \frac{\pi}{6} (10 \times 10^{-9})^3}{12} = 6.0 \times 10^{-21} J \quad (2.4)$$

From the results of the calculations above it can be seen that the thermal energy is in the same order of magnitude as the magnetic energy, the gravitational energy and the dipolar interaction energy. This demonstrates that the particles that are suspended in the fluid have a colloidal stability.

2.2.2 Magnetization

The magnetization of the ferrofluid is a function of the external magnetic field applied to it. The orientation of the magnetic particles is random when there is no magnetic field applied to the fluid. This means that in the absence of an external magnetic field, the net magnetization of the ferrofluid equals zero. Applying an external magnetic field to the fluid will give the particles a tendency to align with the field, but this is partly counteracted by thermal agitation. The Langevin function can be used to model this superparamagnetic behaviour between the applied magnetic field and the resulting magnetization of the fluid [14]. The relation between the magnetization of the particle (domain magnetization) and the magnetization of the fluid is given by the following relation.

$$\frac{M}{f_{vol}M_d} = \frac{M}{M_s} = L(\alpha) = \coth \alpha - \frac{1}{\alpha} \tag{2.5}$$

$$\alpha = \frac{\pi}{6} \frac{\mu_0 M_d H d^3}{kT} \tag{2.6}$$

From the shape of the Langevin function presented in Fig. 2-7 it can be seen that the fluid saturates for high values of α , which means in practice that the magnetization of the fluid saturates when a high external magnetic field is applied. The relation also presents that the magnetization of the fluid is linearly related with the particle concentration of the ferrofluid.

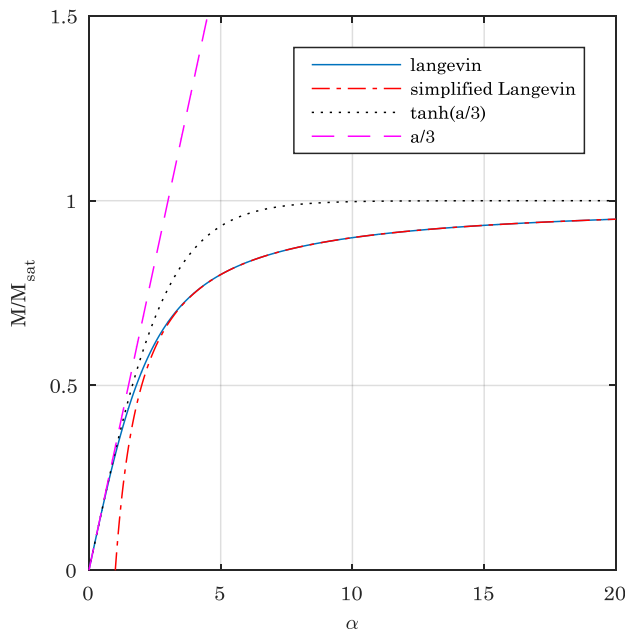


Fig. 2-7. This figure plots the normalized saturation magnetization as function of the Langevin parameter.

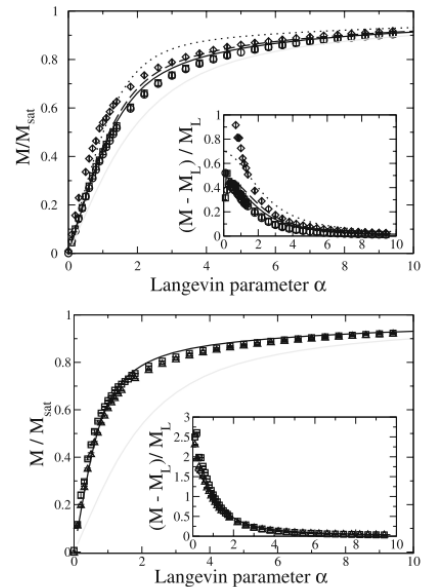


Fig. 2-8. The two figures above present real measurements of the saturation magnetization as function of the Langevin parameter. The data presents a similar shape as presented in Fig. 2-7. Figure taken from [29]

In some situations it might be convenient to use a simplification of the Langevin function. For large magnetic field, (2.5) can be simplified to:

$$M \approx M_s \left(1 - \frac{1}{\alpha}\right) = M_s \left(1 - \frac{6}{\pi} \frac{kT}{\mu_0 M_d H d^3}\right) \quad (2.7)$$

The Langevin function can also be simplified to a tanh function that makes it reasonable for low and high values of α .

$$M \approx M_s \tanh\left(\frac{\alpha}{3}\right) \approx M_s \tanh\left(\frac{\pi}{18} \frac{\mu_0 M_d H d^3}{kT}\right) \quad (2.8)$$

For low values of the Langevin parameter the equation (2.8) can be approximated by the following linear relation:

$$M \approx M_s \frac{\alpha}{3} \approx M_s \frac{\pi}{18} \frac{\mu_0 M_d H d^3}{kT} \quad (2.9)$$

This linear relation can be used to get a relation with the magnetic susceptibility and the relative permeability of the fluid. The flux flowing through the system can be expressed by the following relation.

$$\underline{B} = \mu_0 (\underline{H} + \underline{M}) \quad (2.10)$$

Substituting the linear relation of the magnetization in the relation above gives the relation for the magnetic susceptibility of a ferrofluid.

$$\begin{aligned} \underline{B} &\approx \mu_0 \left(1 + M_s \frac{\pi}{18} \frac{\mu_0 M_d d^3}{kT}\right) \underline{H} \\ &\approx \mu_0 (1 + \chi) \underline{H} \end{aligned} \quad (2.11)$$

$$\underline{M} \approx \chi \underline{H} \quad (2.12)$$

This magnetic susceptibility can be linked to the relative permeability in the following way:

$$\mu_r = 1 + \chi = 1 + M_s \frac{\pi}{18} \frac{\mu_0 M_d d^3}{kT} \quad (2.13)$$

The flux flowing through the system now reduces to:

$$\underline{B} \approx \mu_0 \mu_r \underline{H} \approx \mu \underline{H} \quad (2.14)$$

Some typical parameters of a ferrofluid are calculated based on a typical magnetization curve of a ferrofluid given by Fig. 2-9.

$$\begin{aligned} B_{sat} &= \mu_0 M_{sat} = 4\pi \times 10^{-7} \times 35 \times 10^3 = 44 \text{ mT} \\ \chi &= M_s \frac{\pi}{18} \frac{\mu_0 M_d d^3}{kT} = \frac{\Delta M}{\Delta H} = \frac{1750}{1000} = 1.75 \\ \mu_r &= 1 + \chi = 2.75 \end{aligned} \quad (2.15)$$

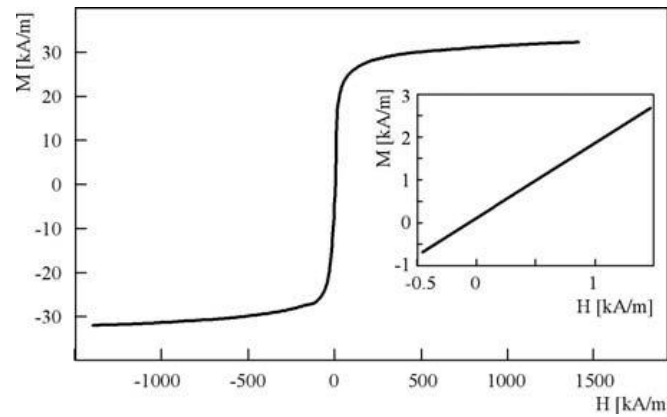


Fig. 2-9. Typical magnetization curve of a ferrofluid. The curve shows that the ferrofluid has a saturation magnetization $M_s \approx 30 \times 10^3 A/m$. The box at the bottom right shows a zoomed in part from which the relative permeability can be calculated to be around $\mu_r \approx 2$. Figure taken from [29]

2.2.3 Ferrofluid viscosity

Applying a magnetic field on a magnetic fluid will cause the rheological properties of the fluid to change. There are two causes for these effects which are rotational viscosity and particle chain formation that is mostly in literature referred to as the magnetoviscous effect [30]. The following section discusses how these two effects are caused and presents how they could be modelled.

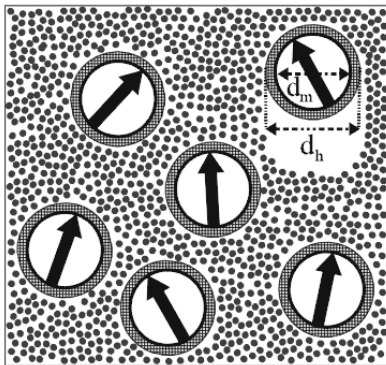


Fig. 2-10. This figure presents some magnetic particles suspended in a liquid of smaller particles. The particles have a net alignment due to an external magnetic field. Figure from [29]

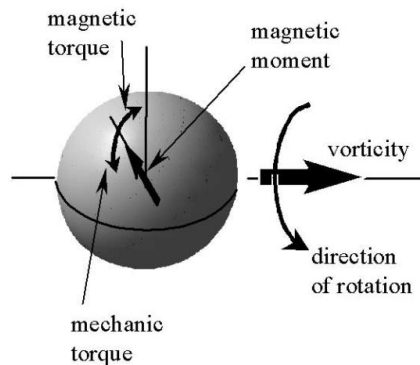


Fig. 2-11. This figure presents a graphical representation of the increase resistance to shear. The alignment of the magnetic moment of the particles with an externally applied field causes a higher shear load due to a vorticity. Figure taken from [30]

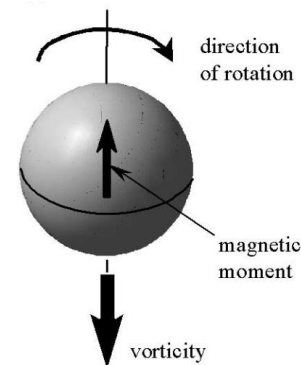


Fig. 2-12. This figure gives a graphical representation on how the particle does not influence the fluid when a vorticity tangent to the magnetic moment is applied. Figure taken from [30]

The rotational viscosity is caused by the interaction of the magnetic alignment torque with the shear related rotational torque. The tendency of the particles to align with the magnetic field increases the viscosity of the fluid. Applying a magnetic field on a ferrofluid introduces an alignment torque on the particles in the direction of the magnetic field that is counteracted by the colliding forces of the molecules in the suspension (Fig. 2-10). Applying a shear force perpendicular to the field develops an additional counteracting torque to that alignment torque, causing a reduced effective alignment torque. Increasing the magnitude of the magnetic field increases the amount of effective alignment torque, which increases the resistance to the shear related torque. This effect can be seen as a change in viscosity in the direction perpendicular to the

direction of the magnetic field (Fig. 2-11 & Fig. 2-12). Assuming that all suspended particles contribute to the change in viscosity, the rotational viscosity can be included by the following relation [31]:

$$\eta = \eta_c \left(1 + \frac{5}{2} \tilde{\phi} + \frac{3}{2} \tilde{\phi} \frac{\alpha - \tanh \alpha}{\alpha + \tanh \alpha} \sin^2 \beta \right) \quad (2.16)$$

The first term of this equation presents the viscosity of the carrier fluid, the second term presents the increase in viscosity due to the suspension of particles and the third term presents the change in viscosity due to the magnetic field. For large values of α this relation has a maximum value of:

$$\eta_{\max} = \eta_c \left(1 + \frac{5}{2} \tilde{\phi} + \frac{3}{2} \tilde{\phi} \right) = \eta_c (1 + 4\tilde{\phi}) \quad (2.17)$$

Datasheets often give the viscosity of the fluid as the viscosity in the absence of the magnetic field:

$$\eta_0 = \eta_c \left(1 + \frac{5}{2} \tilde{\phi} \right) \quad (2.18)$$

In the case of the APG513A, the maximum increase of viscosity can be calculated from [32] by first calculating the viscosity of the carrier liquid and then calculating the maximum viscosity with a magnetic field present. From the result it can be concluded that the increase in viscosity of a typical ferrofluid due to the effect of rotational viscosity is only small.

$$\eta_{\max} = \frac{(1 + 4\tilde{\phi})}{1 + \frac{5}{2}\tilde{\phi}} \eta_0 = \frac{(1 + 4 \times 0.07)}{1 + \frac{5}{2} \times 0.07} 0.15 = 0.16 \text{ kg/m s} \quad (2.19)$$

The alignment of the particles with the magnetic field can happen with two different processes. The first process is the Néel relaxation at which the particle itself is static, but the magnetic moment inside the particle aligns with the magnetic field. This alignment is not instantaneous; the time constant at which it happens can be calculated with the following relation:

$$\tau_N = \tau_0 e^{\frac{K_p V}{kT}} \quad (2.20)$$

The second process is the Brownian relaxation at which the particle aligns with the magnetic field while the magnetic moment inside the particle stays static. Also this alignment is not instantaneous and the time constant at which this occurs can be calculated with the following relation:

$$\tau_B = \frac{3\tilde{V}\eta}{kT} \quad (2.21)$$

The process with the shortest time constant will dominate the alignment with the magnetic field. The Néel relaxation scales exponentially with the particle volume while the Brownian relaxation scales linearly with the particle volume. This means that larger particles will align with the Brownian process and the smaller particles will align with the Néel process as is presented in Fig. 2-13 for the APG513A. This means that only the larger particles should be

considered for the change in viscosity since only the Brownian process can affect the viscosity. This also means that ferrofluids at which the change in viscosity is desired to be negligible, have to use the small particles only. A geometric mean of the two time constants should be considered when the two values are in the same order of magnitude [33]. The particles are called to have a critical diameter in this situation.

$$\tau_{eff} = \frac{\tau_N \tau_B}{\tau_N + \tau_B} \quad (2.22)$$

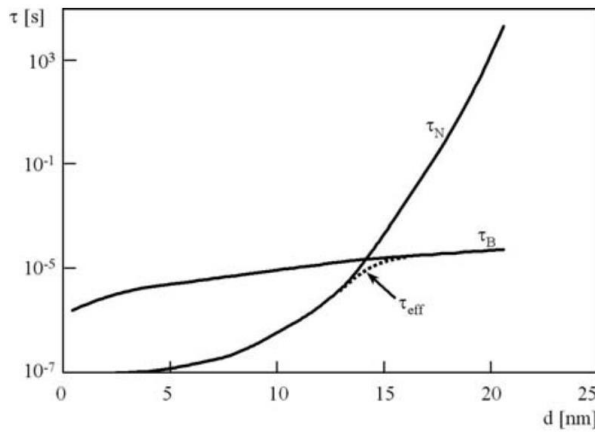


Fig. 2-13. The figure presents the Brownian and Néelian relaxation time as function of the particle diameter. The viscosity of the oil in which the magnetite particles are suspended is $\eta = 0.05 \text{ kg/ms}$. Figure from [29]

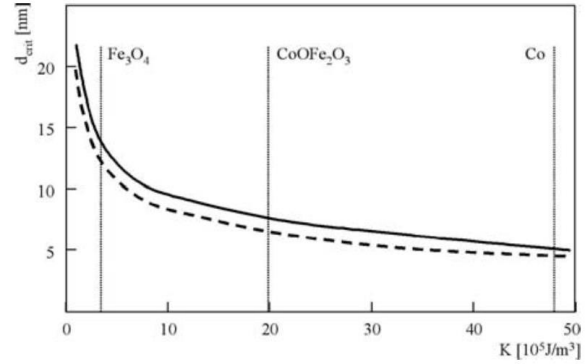


Fig. 2-14. This figure presents the critical diameter for the transition from Néelian to Brownian relaxation as function of the anisotropy constant. The solid line presents a viscosity of $\eta = 0.05 \text{ kg/ms}$ and the dashed line presents a viscosity of $\eta = 0.005 \text{ kg/ms}$. Figure from [29]

The critical diameter of the APG513A can be calculated to be about 13 nm , the data necessary for his calculation can be found in appendix J.

$$\tau_N = 10^{-9} e^{\frac{4.3 \times 10^4 \times \frac{\pi}{6} (13 \times 10^{-9})^3}{1.4 \times 10^{-23} \times 292}} = 1.8 \times 10^{-4} \text{ s} \quad (2.23)$$

$$\tau_B = \frac{3 \times \frac{\pi}{6} (17 \times 10^{-9})^3 \times 0.15}{1.4 \times 10^{-23} \times 292} = 2.8 \times 10^{-4} \text{ s} \quad (2.24)$$

The magnetoviscous effect is caused by chains of particles in the fluid. This effect causes a higher resistance to shear, which results in a higher viscosity. This viscosity increases for larger chain lengths as can be seen from Fig. 2-22. Applying a magnetic field to the fluid will align the chains in the direction of the field. This makes the viscosity perpendicular to the field larger than the viscosity tangent to the field. This also means that the viscosity of the fluid increases by a larger magnetic field strength. Imposing a shear flow on the fluid causes a disassembling force on the chains resulting in a shorter chain length for a larger shear force [34]. A graphical representation of this is given in Fig. 2-19. This shorter length results in a lower viscosity making the ferrofluid have a shear thinning effect. The viscosity of a commercial ferrofluid can increase up to 60 times for low shear values and high field strengths as can be seen from Fig. 2-17 and Fig. 2-18. The increase in viscosity as function of the magnetic field and shear rate for the same fluid is presented in Fig. 2-15, Fig. 2-16 & Fig. 2-17. The change in viscosity $\Delta\eta$ used in these figures is derived by the following relation:

$$\Delta\eta = \frac{\eta_{mes} - \eta_0}{\eta_0} \quad (2.25)$$

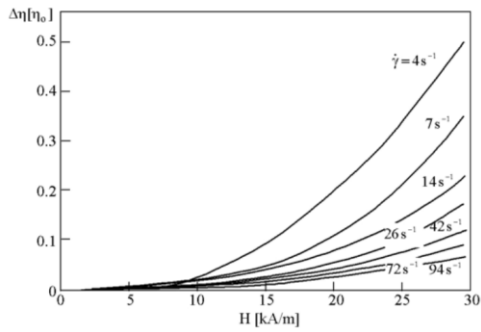


Fig. 2-15. The figure presents the change of viscosity as function of the magnetic field at various high shear rates for the ferrofluid APG513A. It can be observed that the fluid shows a shear thinning effect. Figure from [27]

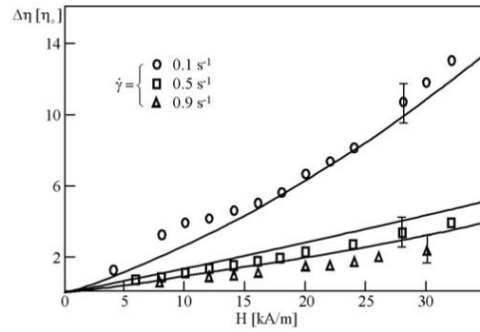


Fig. 2-16. The figure presents the change of viscosity as function of the magnetic field at low various shear rates for the ferrofluid APG513A. It can be observed that there is a shear thinning effect. Figure from [27]

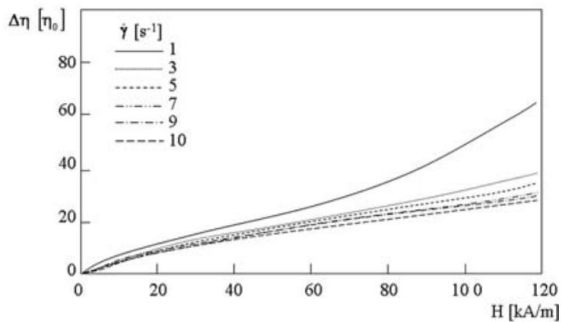


Fig. 2-17. The figure presents the change of viscosity in the function of the magnetic field at various shear rates for the ferrofluid APG513A. It can be observed that there is still an shear thinning effect and an increase in viscosity at high values of the magnetic field. Figure taken from [29]

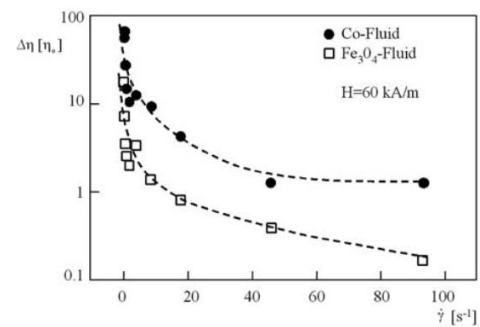


Fig. 2-18 The figure presents the change of viscosity as function of the shear rate for two different types of ferrofluid. The magnetite based ferrofluid is the APG513A. A field strength of $H = 60\text{ kA/m}$ is applied during the measurement. Figure from [29]

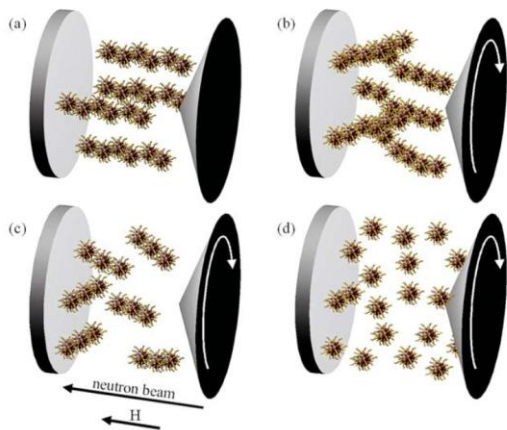


Fig. 2-19. The figure gives a graphical representation of the particle chain formation. Figure a presents the situation at rest at which chains are formed that align with the magnetic field. Figure b presents the rotation of those chains when a vorticity is applied. Figure c presents breakage of those chains due to a too large vorticity. Figure d presents the situation at which the vorticity is that high that no chains exist anymore. Figure from [29]

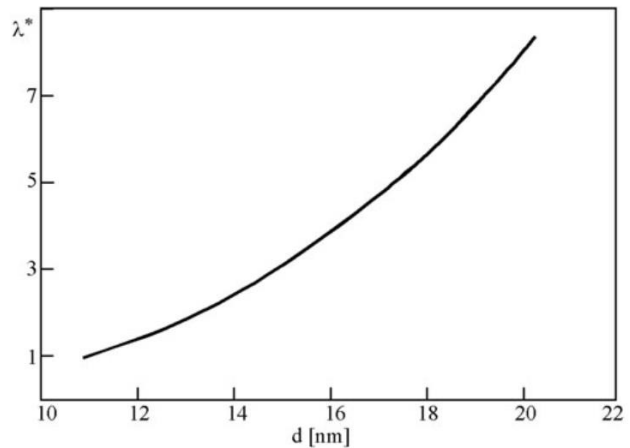


Fig. 2-20. This figure presents the dipolar interaction parameter as a function of the particle diameter. The data presented is of the fluid APG513A. Figure taken from [27]

The particle chain formation is caused by the interacting forces between the magnetic particles that become too large. The dipole-dipole interaction causes the north and south poles of the particles to lock together forming a chain like structure as presented in Fig. 2-19. Chains will form when the interaction between two magnetic particles cannot be counteracted anymore by

the thermal energy of the system. The tendency to create chains is given by the dimensionless dipolar interaction parameter λ [35], values of $\lambda \gg 1$ indicate that chains of particles will be created. Fig. 2-20 presents λ as function of the particle diameter for a typical commercial ferrofluid, it shows that the larger particles in the fluid have a higher tendency to form chains.

$$\begin{aligned} \lambda &= \frac{\mu_0 M_0^2 V}{24 k_B T} = \frac{\mu_0 m^2}{4\pi k_B T d_m^3} \\ &= \frac{4\pi \times 10^{-7} (3.2 \times 10^5)^2 \frac{\pi}{6} (15 \times 10^{-9})^3}{24 \times 1.4 \times 10^{-23} \times 292} = 2.3 \end{aligned} \quad (2.26)$$

The average chain length of in the fluid can generally assumed to be a function of the dipole interaction parameter λ , the volume fraction ϕ , the shear rate $\dot{\gamma}$, the viscosity of the carrier fluid η_0 and the strength of the magnetic field H . Increasing λ , ϕ and H will generally cause the average chain length to increase and increasing $\dot{\gamma}$ and η_0 will generally cause the average chain length to decrease. See [29] for more information about the exact calculation of the chain length. An indication of this length can be generated with the use of formula (2.27) that gives a reasonable description in the absence of a magnetic field and large values of dipolar interaction parameter [29], [36]. Fig. 2-21 presents the chain length as function of λ and ϕ for a typical ferrofluid in this situation.

$$n_{avg} \approx \frac{1}{2} + \sqrt{\frac{1}{4} + \phi Z_2} \quad (2.27)$$

$$Z_2 = \frac{e^{2\lambda}}{3\lambda^3} \quad (2.28)$$

It is showed in [37] that already a large fraction of large particles can be responsible for a large increase in viscosity. The average chain length of the APG513A is given to be about two particles according to [38]. Fig. 2-21 presents the chains length as function of the volume fraction and the dipolar interaction parameter. The figure shows that for small particles almost no chains are formed in the fluid, also not for higher concentrations. Fig. 2-22 shows however that there is still a large increase in viscosity which can only be attributed to chain formation in the fluid. From this it seems reasonable that already a small concentration of large particles in the fluid can have a lot of influence on the viscous behavior of the fluid.

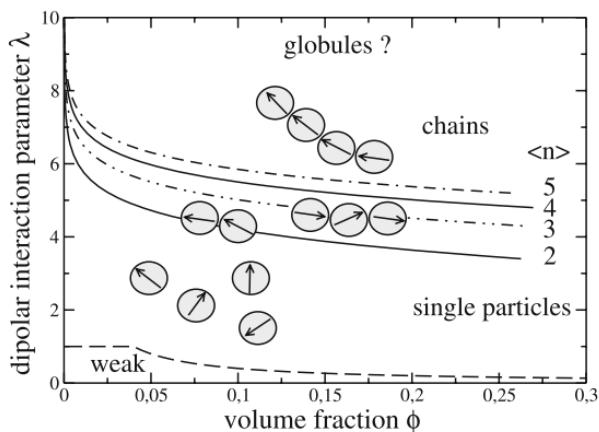


Fig. 2-21. The figure presents how the chain length is a function of the dipolar interaction parameter and the volume fraction of the fluid. The calculation is done in the absence of a magnetic field. Figure taken from [29]

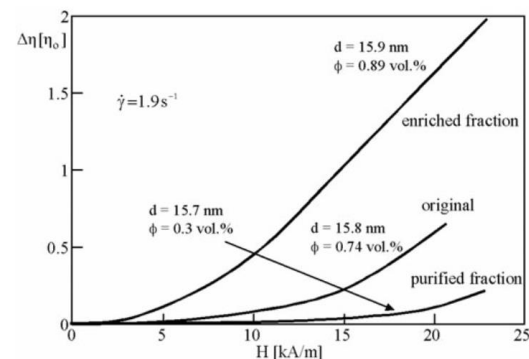


Fig. 2-22. This figure present the viscosity of the fluid as function of the magnetic field for different concentrations of large magnetic particles suspended in the fluid. It can be observed that only a small change in the concentration of large particles has a lot of influence on the viscous behaviour of the fluid. Figure taken from [27]

2.2.4 Rosensweig instability

Ferrofluid subjected to a sufficiently large magnetic field exhibit surface instabilities often referred to as the Rosensweig instability (see Fig. 2-23 and Fig. 2-24)[17]. These shapes form to minimize the total energy of the system. The magnetic energy is minimal for many valleys and peaks while the surface energy is minimal for a completely flat surface. For engineering purposes it might be convenient to not have these instabilities in the system. In this case it is wise to stay under the critical value of magnetic field for the ferrofluid (Fig. 2-25) which can be calculated with the following relation [39]:

$$H_c^2 = \frac{2\mu_r(\mu_r + 1)\sqrt{\rho\sigma g}}{(\mu_r - 1)^2} \tag{2.29}$$

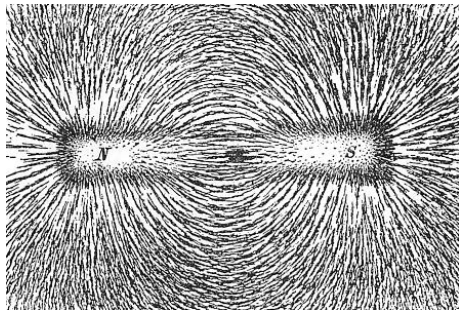


Fig. 2-23. Magnetic particles gathering to resemble field lines flowing from south to north. It can be seen that the concentration of particles is higher near the poles. Figure from [40]

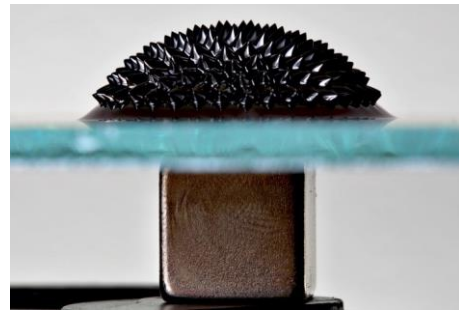


Fig. 2-24. Magnetic fluid on top of a strong magnet. Similarities can be seen between the gathering of iron dust in Fig. 2-23 and the spikes in this picture. Figure from [41]

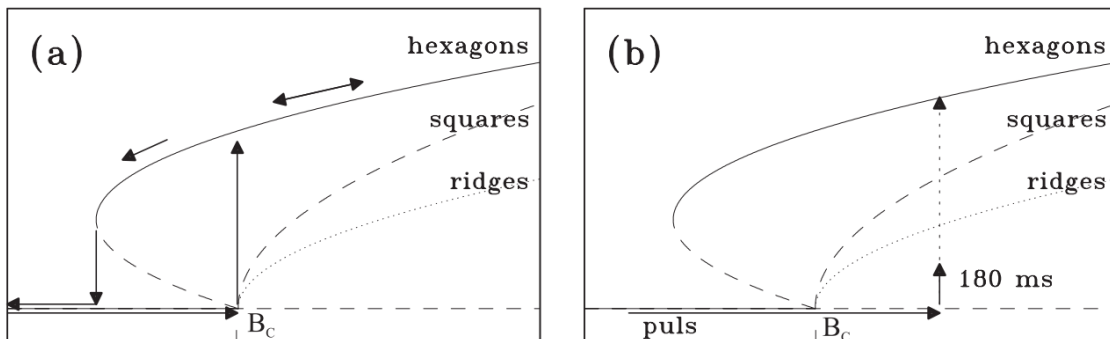


Fig. 2-25. These figures present the bifurcation diagram for a ferrofluid. Figure (a) presents the path that will be travelled if the flux is increased from zero to B_c and from B_c back to zero. It can be seen that the path back is not the same as the path where it came from. Figure (b) shows that a jump like increase results in a jump from no structures to hexagon structures.



Fig. 2-26. The picture presents the Rosensweig instability in a Teflon vessel with a diameter of 12cm . The magnetic field shows to be above the critical value $H > H_c$ since surface instability is observed.

Picture taken at Bayreuth University by B. Reimann.

2.3 Ferrohydrodynamics

2.3.1 Navier-Stokes equation

Navier-Stokes equations for incompressible magnetic flow is given by the following relation at which \underline{M} is assumed to be parallel to \underline{H} . The additional term to this relation compared to the standard Navier-Stokes relation is the magnetic body force. Note that this relation assumes a constant viscosity which is not always valid for a ferrofluid.

$$\rho \frac{\partial \underline{u}}{\partial t} + \rho \underline{u} \cdot \nabla \underline{u} = \underbrace{-\nabla p}_{\text{Pressure Force}} + \underbrace{\eta \nabla^2 \underline{u}}_{\text{Viscous Force}} + \underbrace{\mu_0 \underline{M} \nabla H}_{\text{Magnetic Force}} + \underbrace{\underline{f}}_{\text{Body Force}} \quad (2.30)$$

$$\nabla \cdot \underline{u} = 0$$

This equation fully written out leads to the following relation in Cartesian coordinates:

$$\rho \begin{bmatrix} \frac{\partial u_x}{\partial t} \\ \frac{\partial u_y}{\partial t} \\ \frac{\partial u_z}{\partial t} \end{bmatrix} + \rho \begin{bmatrix} u_x \frac{\partial u_x}{\partial x} + u_y \frac{\partial u_x}{\partial y} + u_z \frac{\partial u_x}{\partial z} \\ u_x \frac{\partial u_y}{\partial x} + u_y \frac{\partial u_y}{\partial y} + u_z \frac{\partial u_y}{\partial z} \\ u_x \frac{\partial u_z}{\partial x} + u_y \frac{\partial u_z}{\partial y} + u_z \frac{\partial u_z}{\partial z} \end{bmatrix} = - \begin{bmatrix} \frac{\partial p}{\partial x} \\ \frac{\partial p}{\partial y} \\ \frac{\partial p}{\partial z} \end{bmatrix} + \eta \begin{bmatrix} \frac{\partial^2 u_x}{\partial x^2} + \frac{\partial^2 u_x}{\partial y^2} + \frac{\partial^2 u_x}{\partial z^2} \\ \frac{\partial^2 u_y}{\partial x^2} + \frac{\partial^2 u_y}{\partial y^2} + \frac{\partial^2 u_y}{\partial z^2} \\ \frac{\partial^2 u_z}{\partial x^2} + \frac{\partial^2 u_z}{\partial y^2} + \frac{\partial^2 u_z}{\partial z^2} \end{bmatrix} + \mu_0 M \begin{bmatrix} \frac{\partial H}{\partial x} \\ \frac{\partial H}{\partial y} \\ \frac{\partial H}{\partial z} \end{bmatrix} + \begin{bmatrix} f_x \\ f_y \\ f_z \end{bmatrix} \quad (2.31)$$

$$\frac{\partial u_x}{\partial x} + \frac{\partial u_y}{\partial y} + \frac{\partial u_z}{\partial z} = 0$$

The same relation can also be written in cylindrical coordinates that has the following form:

$$\rho \begin{bmatrix} \frac{\partial u_r}{\partial t} \\ \frac{\partial u_\theta}{\partial t} \\ \frac{\partial u_z}{\partial t} \end{bmatrix} + \rho \begin{bmatrix} u_r \frac{\partial u_r}{\partial r} + \frac{u_\theta}{r} \frac{\partial u_r}{\partial \theta} - \frac{u_\theta^2}{r} + u_z \frac{\partial u_r}{\partial z} \\ u_r \frac{\partial u_\theta}{\partial r} + \frac{u_\theta}{r} \frac{\partial u_\theta}{\partial \theta} - \frac{u_\theta u_r}{r} + u_z \frac{\partial u_\theta}{\partial z} \\ \frac{\partial u_z}{\partial t} + u_r \frac{\partial u_z}{\partial r} + \frac{u_\theta}{r} \frac{\partial u_z}{\partial \theta} + u_z \frac{\partial u_z}{\partial z} \end{bmatrix} = - \begin{bmatrix} \frac{\partial p}{\partial r} \\ \frac{1}{r} \frac{\partial p}{\partial \theta} \\ \frac{\partial p}{\partial z} \end{bmatrix} + \eta \begin{bmatrix} \frac{1}{r} \frac{\partial}{\partial r} \left(r \frac{\partial u_r}{\partial r} \right) - \frac{u_r}{r^2} + \frac{1}{r^2} \frac{\partial^2 u_r}{\partial \theta^2} - \frac{2}{r^2} \frac{\partial u_\theta}{\partial \theta} + \frac{\partial^2 u_r}{\partial z^2} \\ \frac{1}{r} \frac{\partial}{\partial r} \left(r \frac{\partial u_\theta}{\partial r} \right) - \frac{u_\theta}{r^2} + \frac{1}{r^2} \frac{\partial^2 u_\theta}{\partial \theta^2} + \frac{2}{r^2} \frac{\partial u_r}{\partial \theta} + \frac{\partial^2 u_\theta}{\partial z^2} \\ \frac{1}{r} \frac{\partial}{\partial r} \left(r \frac{\partial u_z}{\partial r} \right) + \frac{1}{r^2} \frac{\partial^2 u_z}{\partial \theta^2} + \frac{\partial^2 u_z}{\partial z^2} \end{bmatrix} + \mu_0 M \begin{bmatrix} \frac{\partial H}{\partial r} \\ \frac{1}{r} \frac{\partial H}{\partial \theta} \\ \frac{\partial H}{\partial z} \end{bmatrix} + \begin{bmatrix} f_r \\ f_\theta \\ f_z \end{bmatrix} \quad (2.32)$$

$$\frac{1}{r} \frac{\partial}{\partial r} (r u_r) + \frac{1}{r} \frac{\partial u_\theta}{\partial \theta} + \frac{\partial u_z}{\partial z} = 0$$

Bearing system can in general be well modelled with a low Reynolds numbers flow. A relation for this can be derived by neglecting the two left terms from relation. This writes to the following relation.

$$\nabla p = \eta \nabla^2 \underline{u} + \mu_0 \underline{M} \nabla H + \underline{f} \quad (2.33)$$

$$\nabla \cdot \underline{u} = 0$$

2.3.2 Bernoulli equation

For some situations it is convenient to use the Bernoulli equation to model the behaviour of the flow. The derivation for this starts from the Navier-Stokes equation presented with relation (2.30), by assuming a stationary ($\partial \underline{u} / \partial t = 0$) and curl free/inviscid ($\nabla \times \underline{u} = 0$) flow, this writes to [42]:

$$\rho \underline{u} \cdot \nabla \underline{u} + \nabla p - \mu_0 M \nabla H - \nabla(-\rho \underline{g} z) = 0 \quad (2.34)$$

Recall the following identity:

$$\nabla(\underline{u} \cdot \underline{v}) = (\underline{u} \cdot \nabla) \underline{v} + (\underline{v} \cdot \nabla) \underline{u} + \underline{u} \times (\nabla \times \underline{v}) + \underline{v} \times (\nabla \times \underline{u}) \quad (2.35)$$

Assuming no curl in the fluid and $\underline{v} = \underline{u}$, this becomes:

$$\underline{u} \cdot \nabla \underline{u} = \nabla \left(\frac{\underline{u} \cdot \underline{u}}{2} \right) \quad (2.36)$$

Now equation (2.34) can be written as:

$$\nabla \left(\rho \frac{\underline{u} \cdot \underline{u}}{2} \right) + \nabla p - \mu_0 M \nabla H - \nabla(-\rho \underline{g} z) = 0 \quad (2.37)$$

Assume that the magnetization of the fluid M is not saturated.

$$M = \chi H \quad (2.38)$$

$$\mu_0 M \nabla H = \mu_0 \chi H \nabla H = \mu_0 \chi \nabla \left(\frac{H H}{2} \right) \quad (2.39)$$

Assume no curl in the magnetic field:

$$\nabla \left(\rho \frac{\underline{u} \cdot \underline{u}}{2} \right) + \nabla p - \nabla \left(\frac{\mu_0 \chi}{2} H^2 \right) - \nabla(-\rho \underline{g} z) = 0 \quad (2.40)$$

This can be written to the following relation that is constant along the streamline of a flow.

$$\frac{1}{2} \rho \underline{u}^2 + p - \frac{1}{2} \mu_0 \chi H^2 + |\rho \underline{g} z| = C \quad (2.41)$$

If the magnetization of the fluid M is not assumed to be fully saturated, this can be written as:

$$\frac{1}{2} \rho \underline{u}^2 + p - \frac{1}{2} M_{sat} |\underline{H}| + |\rho \underline{g} z| = C \quad (2.42)$$

These last two relations can be seen as the Bernoulli equation for incompressible magnetic fluids. The first relation is applicable for fluids that are not yet fully saturated and the bottom one is applicable for fluids that are fully saturated. Note that this relation assumes that the fluid is inviscid which is not applicable for bearing system.

3 Planar ferrofluid bearings in literature

Magnetic fluids have found their way in many applications and publications, though only few of them are dedicated to planar bearings [12], [16], [25], [26], [43]–[52]. From a collection of about 15 review papers discussing applications of magnetic fluids, only two of them discuss a bearing system as an interesting application. From this it seems that the bearing system is not really seen as an interesting application. This chapter discusses the different systems containing a planar ferrofluid bearing published in literature. The goal of this is to get an overview of the advantages and disadvantages of using such a bearing in a system. Furthermore it is investigated what is and what is not already known about the behaviour of these bearings in a system. The focus will be on finding models for interesting parameters like load, stiffness, friction, damping, (non)-linearity, wetting and durability. The focus of the research is on pressure based bearings, viscosity based bearings also exist but are not discussed here.

3.1 Bearing systems found in literature

This section contains an overview of all systems using a ferrofluid bearing published in literature. The different publications are arranged chronologically.

3.1.1 1971: Bearing arrangement with magnetic fluid defining bearing pads

The first application of a ferrofluid bearing using solely pressure induced directly by a magnetic field is from Rosensweig in 1971 [22]. The invention uses a ferrofluid seal that encapsulates a pocket of volume for carrying the load (see Fig. 3-1). Interesting of this application was that it has low stick-slip at low or zero surface velocity while the system is completely passive. This patent can be seen as the first application of a ferrofluid in a planar bearing system.

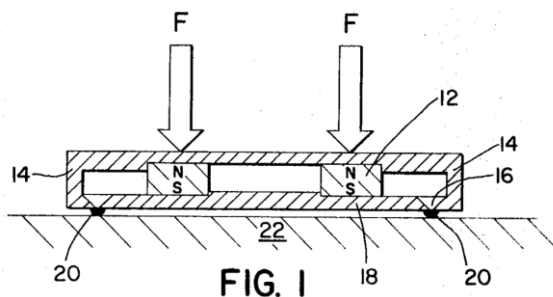


Fig. 3-1. Bearing arrangement with magnetic fluid defining bearing pads. Picture from [22]

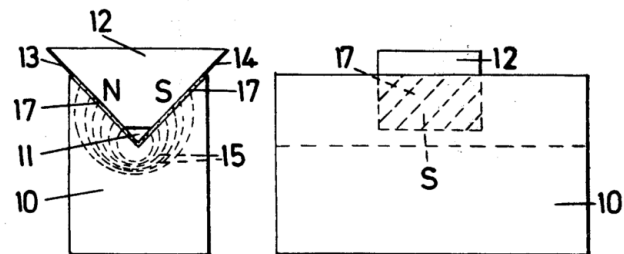


Fig. 3-2. A linear ferrofluid bearing for parallel tracking arm of a gramophone. Picture from [53]

3.1.2 1977: Linear bearing for parallel tracking arm

In 1977 the invention was patented [53] to use a planar ferrofluid bearing in a parallel tracking pick-up arm of a gramophone. The tracking arm has as function to stay at the right radial position of the disc which is either with a rotational or a translational motion. In the case of a translational motion, the ferrofluid bearing appeared to be interesting due to its low friction and passive working principle. The bearing uses a v-shaped groove to move freely in one degree of freedom (Fig. 3-2). One of the sides is magnetized and a magnetic fluid added between the bearing surfaces to create a lift force.

3.1.3 2005: Magnetic fluid devices for driving micro machines

Sudo et al. presented in 2005 a micro actuator system at which the actuator and bearing are integrated into one system [54]. The bearing system is created with the levitating force of a magnet completely surrounded by ferrofluid as can be seen in Fig. 2-15. The same magnet is also actuated by an external magnetic field; the interaction between the two fields causes a force that causes a displacement.

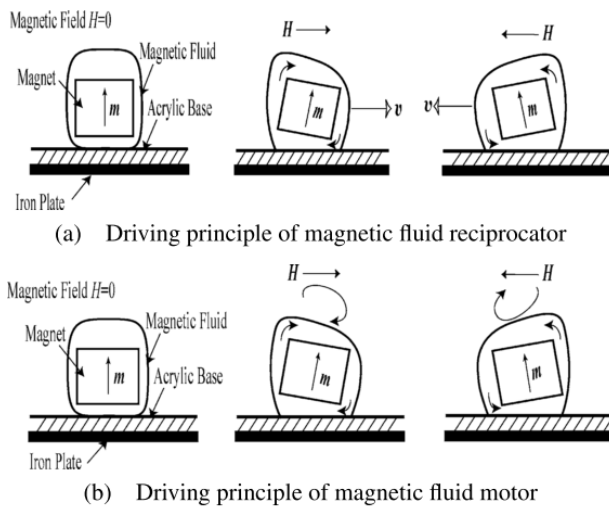


Fig. 3-3. Different driving principles of system. Figure from [54]

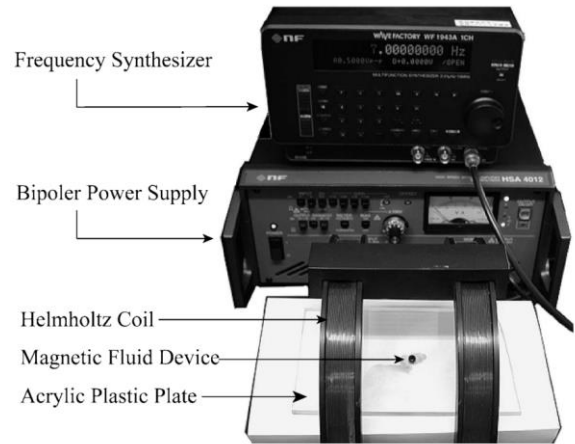


Fig. 3-4. Overview of the complete system built by Sudo et al. Figure from [54]

3.1.4 2006: Development of bearings and a damper based on magnetically controllable fluids

Guldbakke and Hesselbach published in 2006 a system that was similar to the system published by Uhlmann and Bayet [55]. The bearing systems consist of an electromagnetic coil to create a levitating force and a gap completely filled with ferrofluid. The system built is measured to have a distributed load capacity of 0.16bar .

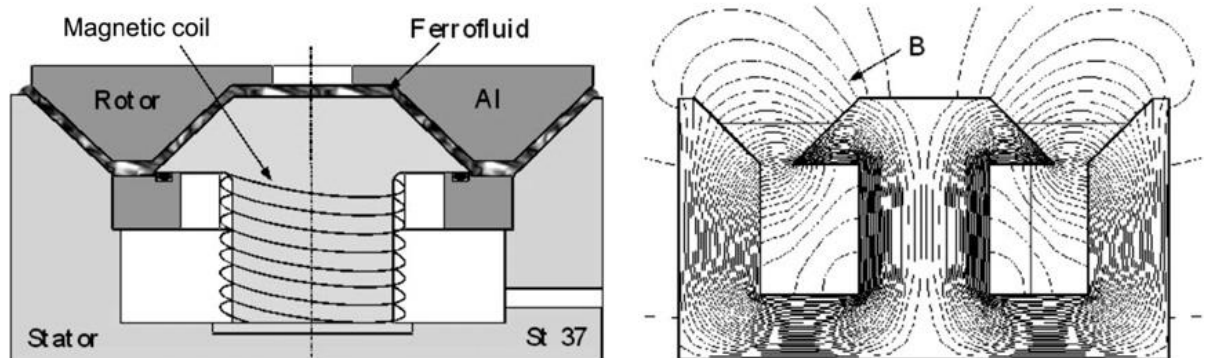


Fig. 3-5. The left picture presents a cross section of the bearing system and the right picture presents the magnetic field in the bearing system. The different liners at the flux paths of the magnetic field. Figure adopted from [55].

3.1.5 2006: High precision positioning with ferrofluids as an active medium

Uhlmann and Bayet published in 2006 multiple ferrofluid based position systems designed to position with high accuracy [56]. They started with a system with one degree of freedom in which they investigated the performance of different kinds of ferrofluid, the two system investigated are presented in Fig. 3-6 and Fig. 3-7. The system reached a stiffness of about 10^3N/m with a maximum load of about 3N . They also built an multi axis positioning systems which is presented in Fig. 3-8, the performance of the system is given by Fig. 3-9.

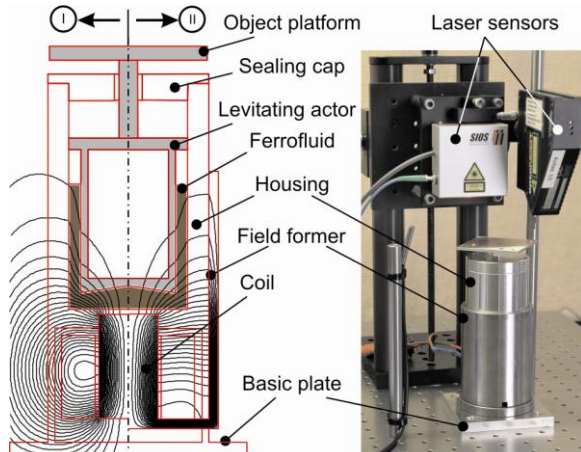


Fig. 3-6. Maximum stiffness is about 10^3N/m with a maximum load of about 3N , an accuracy of $2\mu\text{m}$ was achieved. Figure from [56]

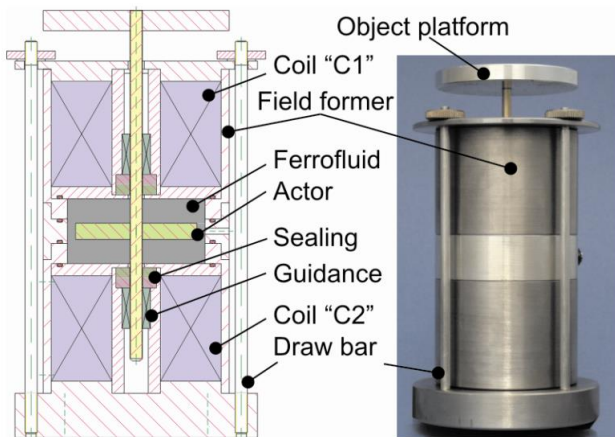


Fig. 3-7. The system presented in this figure is an optimization of the system presented Fig. 3-6. Figure taken from [56]

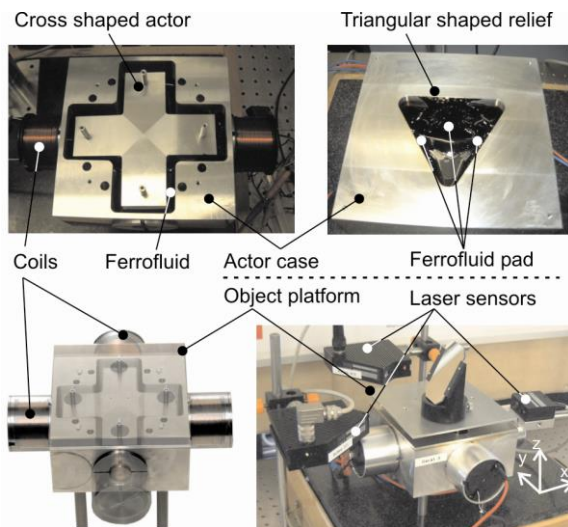


Fig. 3-8. Multi axis positioning system built by Uhlmann and Bayet. Figure from [56]

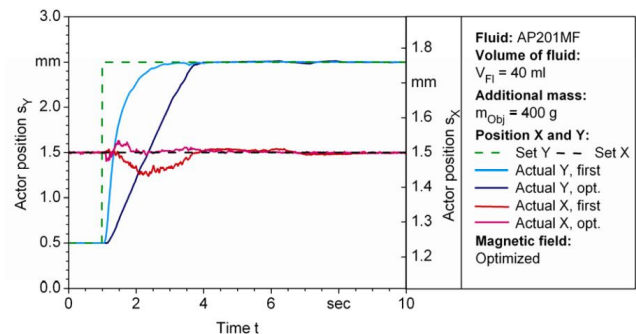


Fig. 3-9. The figure presents the transient behaviour of the multi axis positioning system presented in Fig. 3-8. The performance before and after an optimization step is given. From the data can be seen that the system can position with a relative high accuracy, but the settling time is rather long. Figure from [56]

3.1.6 2006: Design of a 3 DOF displacement stage based on ferrofluids

Millet and Hubert presented in 2006 a 3 DOF displacement stage using a ferrofluid as an bearing and actuation system [57]. The moving part of the stage is floating on three bubbles of ferrofluid that are held in place by permanent magnets in the corners of the stage (see Fig. 3-10 and Fig. 3-11). The movement of the stage is controlled by changing the internal pressure of the ferrofluid with coils in the corner of the stage. The static stiffness of the stage in z-direction is measured be about 300N/m . The planar actuation precision is about 50nm . The stage is working

with only open loop control and in an uncontrolled environment; performance could be increased by improving these two things.

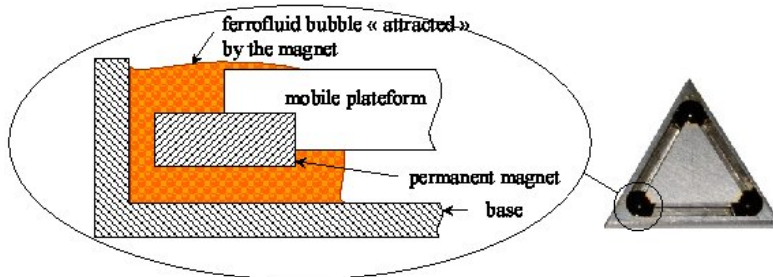


Fig. 3-10 Platform floating in a volume of ferrofluid. The schematic drawing at the left presents the real system at the right. Figure taken from [57].

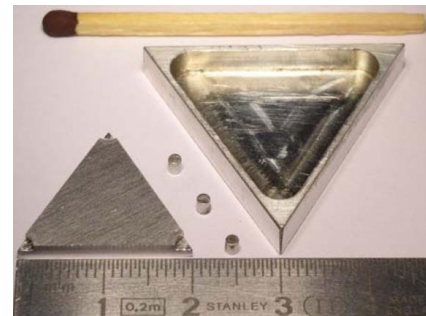


Fig. 3-11. The figure shows the different parts used in the assembly Figure from [57]

3.1.7 2013: Planar ferrofluid bearings for precision stages

Van Veen built in 2013 the system shown in Fig. 3-12 and Fig. 3-13 and discussed in [4], [5]. The stage in this system is constrained to one degree of freedom by using multiple ferrofluid bearings. The system is built to investigate the potential of using a ferrofluid bearing in a precision motion system. It showed that the system had viscous friction only and a complete absence of stick-slip. A bearing concept was chosen that uses solely the pressure induced by the magnetic field, so no pocket of air was encapsulated. This choice was made to have a higher reproducibility of height since preliminary experiments showed problems with air escaping from the seal causing a permanent change in flight height which was assumed to be unacceptable for a precision positioning system. The lowering of the stage caused furthermore a significant increase in friction which was undesirable. Taking away the pocket of air did not completely solve the poor repeatability of the bearing since there was still some so-called trail formation present. Moving the bearing leaves behind a layer, i.e. trail, of ferrofluid that causes some unknown nonlinear effects that cause for example a change in the distance between the bearing faces. The problem was mitigated by first implementing a wetting stroke before taking the system in operation.

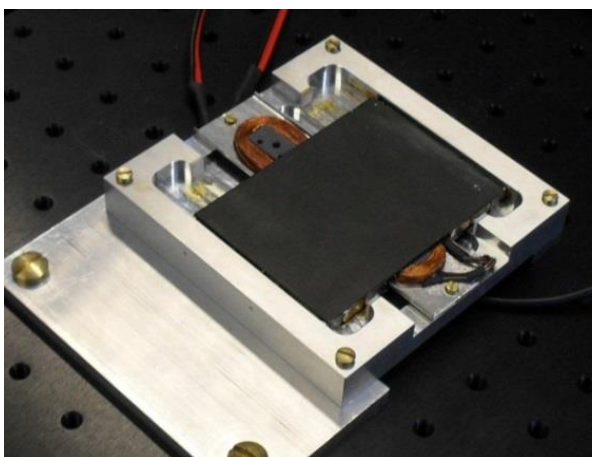


Fig. 3-12. An overview of the 1DOF position stage developed by van Veen. Figure from [5]

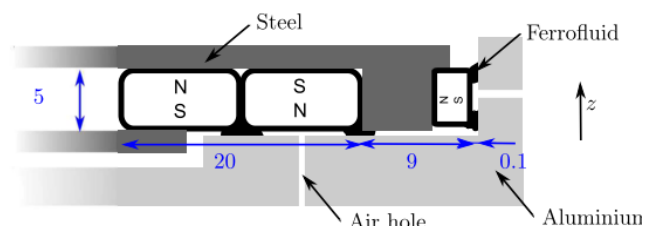


Fig. 3-13. A cross section of the bearing concept developed by van Veen. The ferrofluid used in the system is attracted to the corners of the magnet due to the high magnetic field intensity there. The bearing has a length of 60mm. The pocket of air under the bearing is connected via a hole to ambient conditions. Figure from [5]

The final system had a stiffness of $1.7 \times 10^4 \text{ N/m}$ with a load of 0.5 N which results in a specific load of about 800 Pa . The stiffness of the air pocket bearing was measured to be $1.1 \times 10^4 \text{ N/m}$. This is a lower value than the value with the open pocket since the surface area of the bearing is four times as small. The fundamental mechanism behind this was unclear to van Veen. It is seen that the friction of the stage is not constant but dependent on the stroke length and the velocity. The damping coefficient of the friction of the system is about 36 Ns/m , which was about a factor 4 off from the theoretical model proposed. Finally a bandwidth of 300 Hz is achieved with the system that has a load capacity of 0.3 kg and precision of 10 nm over a range of 2 cm .

3.1.8 2014: Nanometer precision six degrees of freedom planar motion stage with ferrofluid bearings

Café proved in 2014 that a magnetohydrostatic bearing is an interesting concept to be used in high precision positioning systems [58], [59]. The system build is capable of delivering a planar precision of 10 nm (3σ) in a range of $10 \text{ mm} \times 10 \text{ mm}$ and a vertical precision of 3.3 nm [3σ] in a range of 0.2 mm . Café claims that the bearing is not limiting the precision of the system; the planar precision of the system is fully limited by the resolution of the interferometers and the vertical precision is mainly limited by the capacitive sensors and the mechanical resonances. Though, when we have a closer look at these mechanical resonances, it can be seen that these are caused by the limited stiffness of the bearing. The stiffness of the bearing system is measured to be $6.5 \times 10^3 \text{ N/m}$. The system owes its high precision to the actuation and measurement of all the degrees of freedom. This makes the system relatively complex and expensive taking away a big advantage of the bearing: cheap and simple. The actuators in z-direction are necessary to compensate for the nonlinearities of the ferrofluid bearing. Moving the stage causes a trail of ferrofluid to form that causes a change in flight height. This can be compensated by applying a variable lifting force in z-direction. The stage has a $2 \mu\text{m}$ decrease in height per 1 mm displacement.

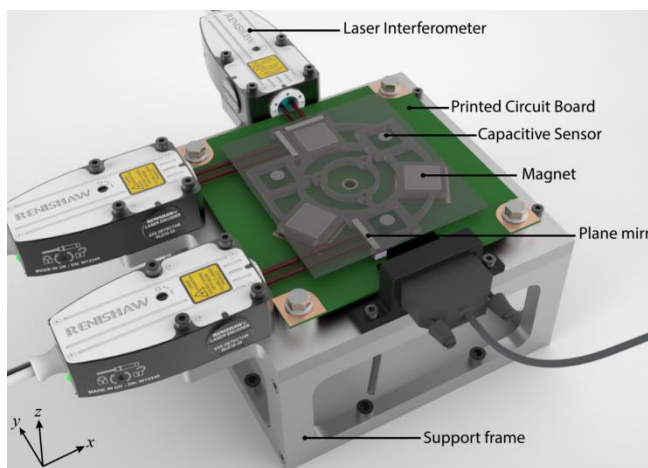


Fig. 3-14. The bearing used in the system build by Café has a measured stiffness of $6.5 \times 10^3 \text{ N/m}$. Figure taken from [58].

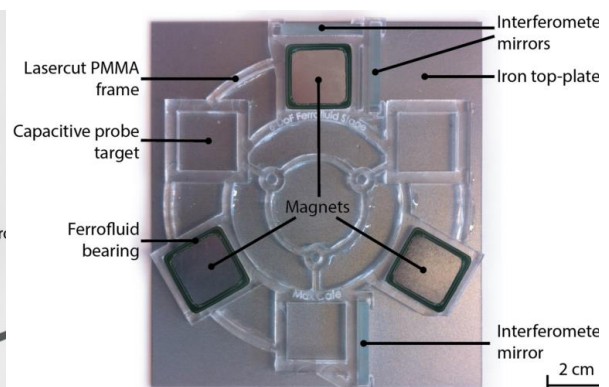


Fig. 3-15. The permanent magnets are located at the moving part of the actuator which is presented in the figure. The coils are placed in the static part to have no moving wires in the system. Figure taken from [58].

3.1.9 2014: Ferrofluid-assisted levitation mechanism for micromotor applications

Assadsangabi et al. published in 2014 the micro sized actuator shown in Fig. 3-16 and Fig. 3-17 and discussed in [60]. The system consists of a permanent magnet floating in a volume of ferrofluid on top of a surface filled with coils. The permanent magnet itself functions as the

moving part of the actuator and has the combined function of delivering the magnetic field for the Lorenz actuation and the ferrofluid lubrication. The measurements of the system show a maximum force of 30mN which results in a specific load of 12kPa. The displacement for the maximum force has a value of 400µm resulting in a stiffness of 75N/m.

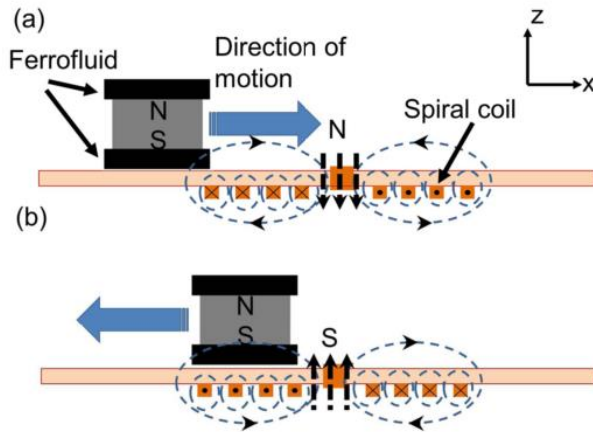


Fig. 3-16. The magnet moves due to the interaction of its own magnetic field with the magnetic field generated in the coils of the stator. Different coils are placed after each other to produce a long stroke. Figure from [60]

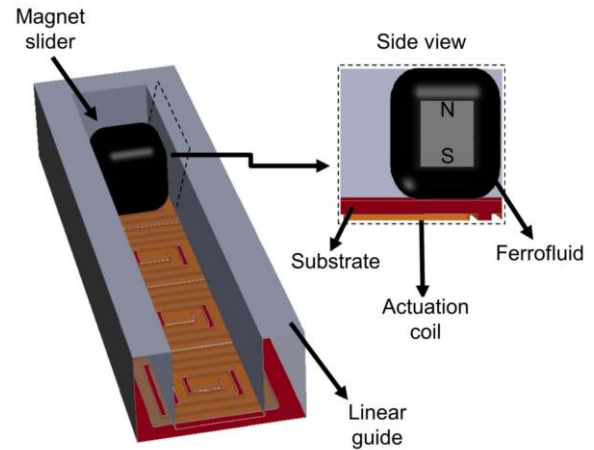


Fig. 3-17. The magnet used in the system is square with a length of 1.6mm. The actuation system is built to have one DOF. Figure taken from [60].

3.1.10 2015: The design of a planar precision stage using cost effective optical mouse sensors

Mok researched in 2015 the possibilities to decrease the cost of precision stages, mainly focusing on the measurement system [61]. To show the potential of an optical mouse sensor in such a system a demonstrator stage was built using a ferrofluid bearing (see Fig. 3-18). The ferrofluid bearing was chosen for its simple design, low (viscous) friction and absence of stick-slip. Like in the system of van Veen, trail formation caused a problem with the repeatability in height.

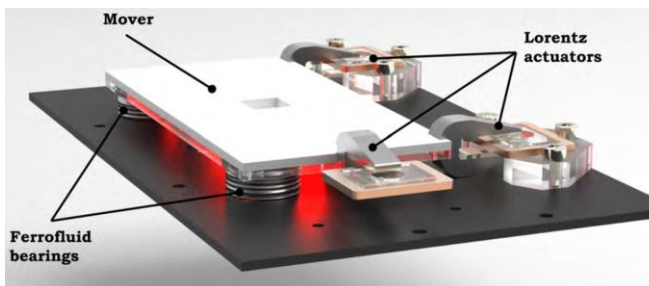


Fig. 3-18. Overview of the system designed by Mok. The system consists of three planar bearing and three actuators. The third actuator is needed to constrain the rotational degree of freedom that is not constrained by the bearing. Figure from [61]

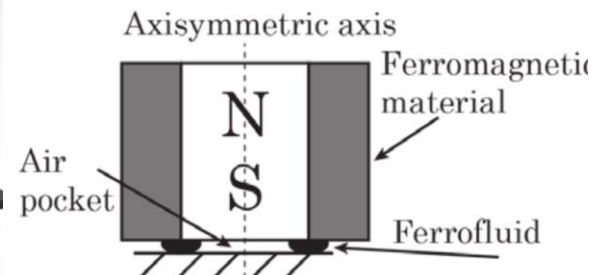


Fig. 3-19. Schematic overview of the bearing system used by Mok. The ferrofluid encapsulates a pocket of air that is carrying the load. The ferromagnetic material is placed around the magnetic to increase the magnetic field intensity and gradient in the ferrofluid. Figure from [61]

3.1.11 2015: Design of a three DOF planar precision stage using a single Position Sensitive Detector

Habib presented in 2015 a three DOF planar precision stage using containing a ferrofluid bearing [62]. The bearing used for this system is given in Fig. 3-21 from which can be seen that a sandwich like structure is applied. The magnets of the bearing function also as magnets for the Lorentz actuators realizing an integrated system. A ferrofluid bearing was chosen for this design to have a simple solution that has complete absence of stick-slip. It provided in the meanwhile magnets that could be used for Lorentz actuation.

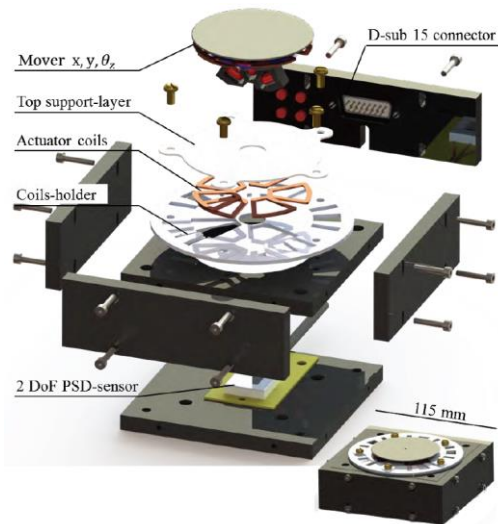


Fig. 3-20. Exploded view of the setup built by Habib. Figure from [62]

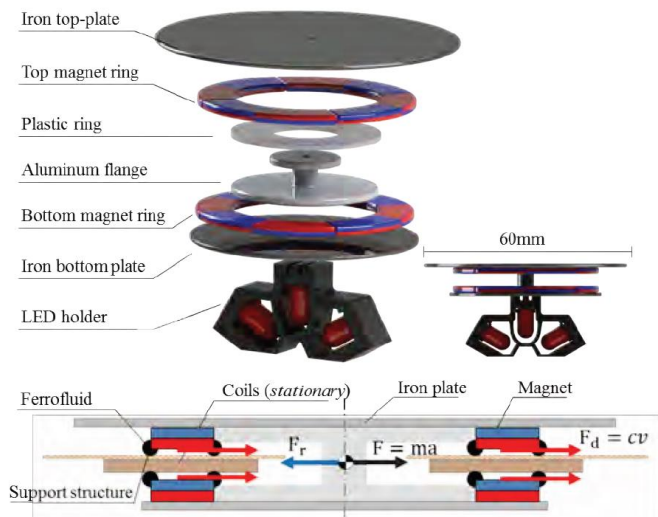


Fig. 3-21. Exploded view of the actuator and sensor system built by Habib. The ferrofluid encapsulates a pocket of air for carrying the load. Figure from [62]

3.2 Conclusion

Looking at all the systems discussed in this chapter it can be said that almost all systems are used for applications in precise positioning. Its simple configuration, low viscous friction and absence of stick slip make the bearing interesting to be used where small and precise displacement are important. In all systems presented the concepts are tested, but failed to link the actual performance to a theoretical model. The only theoretical models that are described are considering only the pressure induced in the ferrofluid due to the magnetic field without taking into account the interface between ferrofluid and air. This demonstrates that if one is interested in designing a bearing on the basis of this concept, one has no information at all on how to configure the system to meet desired specifications. It can be observed that many systems combined the bearing and actuation system in one by using a permanent magnet for ferrofluid lubrication and Lorentz actuation. The systems where the repeatability in flight height was important all struggled with meeting the desired specifications due to the trail formation of the bearing. The bearing concept used can be divided into two different families, one family that uses solely the magnetic pressure and one family that uses the pressure generated by encapsulating a pocket of nonmagnetic fluid. The systems demonstrated in literature showed a maximum stiffness in the order of 10^4 N/m and a maximum specific load in the order of 0.12 bar .

4 Load & Stiffness of a Planar Ferrofluid Pocket Bearing

Stefan G.E. Lampaert¹, Jo W. Spronck¹, Ron A.J. van Ostayen¹

¹Department of Precision and Microsystems Engineering, Delft University of Technology, Delft, The Netherlands

A ferrofluid pocket bearing is a type of hydrostatic bearing that uses a ferrofluid seal to encapsulate a pocket of air to carry a load. Their nature of having a high stiffness, low (viscous) friction and absence of stick-slip make them interesting for applications that require fast and high precision positioning. Knowledge on the exact performance of these types of bearings is up to now not available. This paper presents a method to describe the out-of-plane load and stiffness characteristics of this type of bearings. The method is experimentally validated by comparing the results of a model with the results of experiments. On the basis of new insight developed by this work, a concept is proposed that uses a sandwich like structure to achieve a higher stiffness and a higher repeatability. The mathematical model of this bearing is experimentally validated and it was shown that the performance can be described completely analytically. The proposed method is shown to be correct for describing the load and stiffness characteristic of any shape of ferrofluid pocket bearing.

Index Terms— Ferrofluid, Pocket bearing, Magnetics, Planar bearing, Precision engineering

4.1 Introduction

As man began to explore space, it became relevant to develop efficient techniques to use and store rocket engine propellants under zero gravity conditions. For this reason the NASA Research Center developed in the 1960s a kerosene based magnetic fluid that could be collected at some desired location by the use of a magnetic field [6]. This magnetic fluid consisted of a stable colloidal suspension of tiny magnetic particles ($\sim 10\text{nm}$) giving the fluid paramagnetic properties [7]. Rosensweig continued the research into these so-called ferrofluid and showed in the early 1970s that these fluids might also be interesting for the usage in seals and bearings [21], [22]. Pressure builds up in the fluid because the magnetic particles are attracted by a magnetic field. This pressure can be used to develop a force that is capable of delivering a force that can be used for carrying a load or for sealing a volume of nonmagnetic fluid. Compared to other bearing concepts, the ferrofluid bearings are a cheap solution to create low friction that is free of stick-slip. The bearing is furthermore inherently stable due to the use of permanent magnets. These can additionally be used to develop a field for a Lorentz actuator [4], [5], [58]–[60], [63]. The overall specifications of the bearing show that the bearing is particularly interesting for low load applications that require fast and high precision positioning. Examples of applications that can be thought of are microscopy, wafer/chip inspection and pick and place machines. This type of bearing can also be applied in a zero gravity environment, where the magnetic field keeps the ferrofluid in place.

In this paper we will be focusing on the planar sliding bearing, viz. a bearing with can slide and rotate in a plane and carry a load normal to this

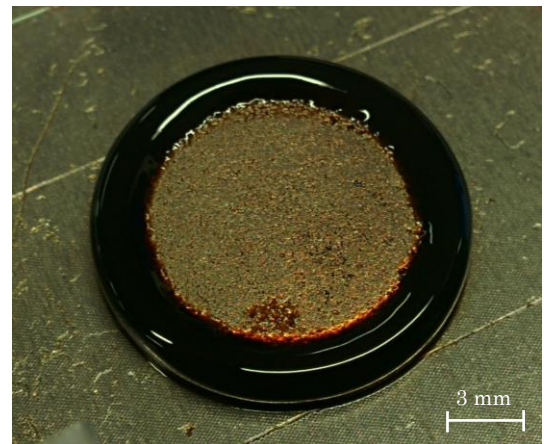


Fig. 4-1. The figure presents a disk shaped magnet with the magnetization axially. The ferrofluid collects at the sides of the magnets since the magnetic field strength is highest there. A bearing is made by placing a surface on top of this configuration such that a pocket of air is encapsulated. The ring of ferrofluid functions then as a seal to keep the air inside. The magnetic field of this magnetic is given in Fig. 4-2.

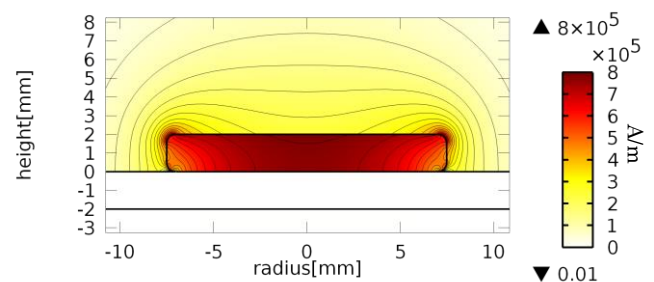


Fig. 4-2. The figure presents the magnetic field developed by the configuration presented in Fig. 4-1. From the picture can be seen that there is a higher magnetic field at the corner of the magnet which causes the ferrofluid to collect there. The calculation is done with a remanent flux density of the magnet of $B_r = 1.3\text{T}$ and a relative permeability of the iron of $\mu_r = 4000$

plane. Basically two different types of these bearings using ferrofluid can be identified. The first category is a ferrofluid pressure bearing that uses solely the magnetic pressure to float a nonmagnetic material on top a layer of ferrofluid that is kept in place by the field of a magnet [53]. The load capability and the stiffness of the bearing are defined by the magnitude and shape of the magnetic field. The second category is a ferrofluid pocket bearing that adds the load carrying capacity of an air pocket (or any other non-magnetic fluid), which is encapsulated and pressurized by a surrounding ferrofluid seal [22]. A simple pocket bearing of this type can be made by taking a disc shaped magnet with axial magnetization. The shape of the magnetic field is such that the magnetic fluid collects at the corner of the magnet as can be seen from Fig. 4-1 and Fig. 4-2. A pocket of air can now be encapsulated by putting a plate on top of the ferrofluid. The load is determined by the pressure in the pocket of air which is determined by the pressure across the magnetic fluid seal.

A problem of this bearing is the repeatability in flight height [4], [5]. Moving the bearing leaves behind a trail of ferrofluid that causes less fluid to be available for carrying load. In the case of a pocket bearing this might cause air to escape from the seal resulting in a permanent change in flight height. Due to the absence of models of this effect, [58], [59] started to mitigate this by adding a control loop that controls the flight height of the bearing with the use of a Lorentz actuator. This decision introduces extra actuators, sensors and complexity in the system which takes away the benefit of being low cost and simple.

Another problem of this bearing is that no method exists on how to describe the load and stiffness characteristic of this bearing. All literature describing these types of bearings, fail to link the measured performance with a theoretical model (chapter 3).

In this paper a method will be presented for predicting the load and stiffness characteristic of a ferrofluid pocket bearing. The method will be used to derive a model that is then experimentally validated. Furthermore a sandwich concept is developed that has a higher stiffness and repeatability. Also for this a model is made by using the proposed method which is then also experimentally validated. This last concept has an additional value in that it demonstrates how the method can be used in a design. These models are relevant since they give a better understanding on how a reduction of ferrofluid due to the trail formation influences the load capacity and stiffness of the bearing.

The paper is structured in the following way. Section 4.2 presents the proposed method to describe the load and stiffness characteristics of a ferrofluid bearing. The derived model and the measurements

conducted for validation are described in section 4.3. Section 4.4 discusses the sandwich structure and section 4.5 gives a summary and conclusion of the paper.

4.2 Method

The following section derives and explains the method to calculate the load and stiffness specifications of a ferrofluid bearing. It presents in a theoretical way how the different parameters contribute to the final specifications. The derivation starts from the Navier-Stokes equations for incompressible magnetic fluids[42]. Note that this also assumes a constant viscosity which is not necessarily true for a ferrofluid.

$$\rho \left(\frac{\partial \underline{u}}{\partial t} + \underline{u} \cdot \nabla \underline{u} \right) = -\nabla p + \mu \nabla^2 \underline{u} + \underline{f} + \mu_0 M \nabla H \quad (4.1)$$

$$\nabla \cdot \underline{u} = 0$$

Assume the fluid velocity component \underline{u} of the bearing will be such that it is of negligible influence on the pressure distribution in the liquid. Furthermore assume that there are no other body forces except the one induced by the magnetic field. Relation (4.1) can then be reduced to the following:

$$\nabla p = \mu_0 M \nabla H \quad (4.2)$$

The magnetization of the fluid is a function of the magnetic field, but since the saturation of the fluid is low, it is safe to assume that the magnetic fluid is saturated immediately. Typical magnetic fluids have a relative permeability μ_r of around 2 with a saturation magnetization of around $M_s = 30 \text{ kA/m}$ or 0.1 T .

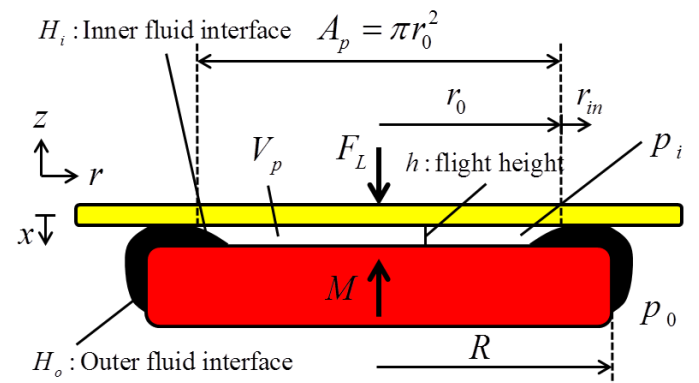


Fig. 4-3. The figure presents a cross section of a disk shaped magnet to define the different parameters used in this paper. The inner fluid interface defines H_i and the outer fluid interface defines H_o . The x- and z- direction are opposite to achieve a positive stiffness in the derivations.

In the case of a bearing that uses a pocket, only the pressure across the seal $p_i - p_o$ is important for calculating the total load. This pressure difference can be calculated from relation (4.2) with the use of the

fundamental theorem of calculus. Integrating along the length of the seal results in:

$$p_i - p_o = \int_C \nabla p \cdot d\vec{r} = \mu_0 M_s \int_C \nabla H \cdot d\vec{r} = \mu_0 M_s (H_i - H_o) \quad (4.3)$$

The magnetic field at the inner fluid interface is equal to H_i and the magnetic field at the outer fluid interface is equal to H_o . From the relation follows that only the magnetic field strength at the fluid-air interfaces will determine the pressure increase in the pocket. The load capacity F_L can be approximated by integrating the pressure difference over the force carrying surface area of the pocket A_p . This can be modelled with relation (4.4) that assumes that the load carrying capacity of the ferrofluid ring itself is negligible. A illustration of the force relation is given in Fig. 4-4.

$$F_L = \int_S (p_i - p_o) dA_p = \mu_0 M (H_i - H_o) A_p \quad (4.4)$$

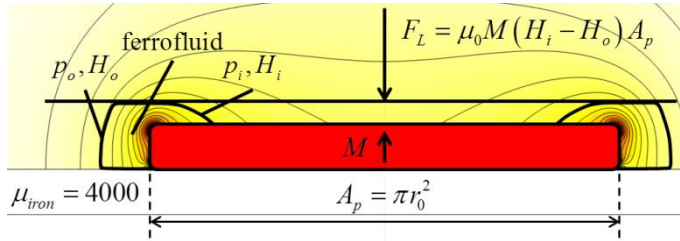


Fig. 4-4. The figure gives a graphical representation of the force development in a pocket bearing. The figure contains a magnet that is placed on an iron plate. The contour plot on the background presents the magnetic field intensity. Ferrofluid is added and attracted to the corners since the field intensity is highest there. A plate is placed on top of the bearing to seal off a volume of air. The pressure across the ferrofluid seal is defined by the difference in magnetic field intensity across the seal. This difference defines the load capacity of the bearing. The figure furthermore shows that the contour lines of the magnetic field intensity are also the contour lines of the pressure distribution.

The stiffness of the bearing can be calculated by taking the derivative of the force over the displacement. In the case of this concept, a change in force will cause the ferrofluid interfaces to move causing a different counteracting pressure across the seal and a different surface area for the force.

$$k_{ff} = \frac{dF_L}{dx} = A_p \frac{d(p_i - p_o)}{dx} + (p_i - p_o) \frac{dA_p}{dx} \quad (4.5)$$

In general the bearings are fairly flat meaning that the change of surface area of the pocket dA_p/dx is of negligible influence on the stiffness of the bearing. Combining relation (4.5) with (4.3) yields:

$$k_{ff} = \mu_0 M A_p \frac{d(H_i - H_o)}{dx} \quad (4.6)$$

The magnetic field is a function of the fluid-air interface r which is related to the change in gap height. The chain rule can be used to incorporate this relation.

$$k_{ff} = \mu_0 M A_p \frac{d(H_i - H_o)}{dr_{in}} \frac{dr_{in}}{dx} \quad (4.7)$$

The relation dr_{in}/dx can be seen as a pneumatic leverage at which a small change of bearing height will result in a large displacement in fluid interface (Fig. 4-5). The two parameters are coupled via the volume of the pocket of air V_p .

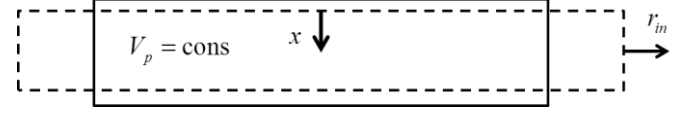


Fig. 4-5. The figure presents a graphical representation of the pneumatic leverage. The figure shows that a small displacement of x results in a large displacement in r_{in} . The relation between these two dr_{in}/dx can be calculated by assuming a constant volume of the pocket of air V_p which is reasonable for small displacements.

The relation in the case of a cylindrical shaped pocket is given by relation (4.8). Fig. 4-6 shows the pneumatic leverage values for some pocket volumes and fixed bearing radii.

$$V_p = (h - x) \pi (r_0 + r_{in})^2$$

$$\frac{dr_{in}}{dx} = \frac{d}{dx} \left(\sqrt{\frac{V_p}{\pi(h-x)}} - r_0 \right) = \sqrt{\frac{V_p}{4\pi(h-x)^3}} \quad (4.8)$$

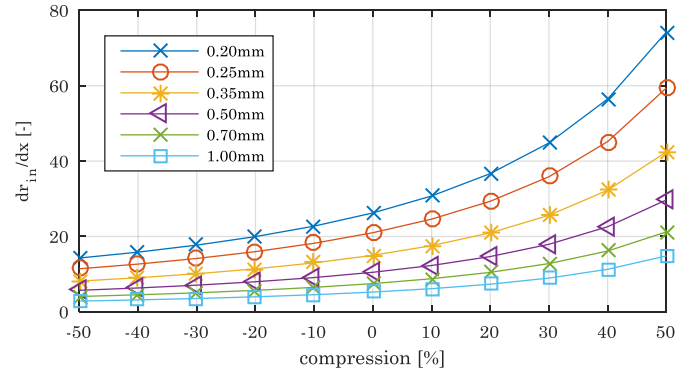


Fig. 4-6. The figure presents the modelled pneumatic leverage for different initial gap heights and a fixed radius of $r_0 = 10.5\text{mm}$. The compression is a measure for how much the height is decreased for achieving the pneumatic leverage. A positive compression means a decrease in flight height.

The stiffness of the air encapsulated by the ring of magnetic fluid can in some situations have the same order of magnitude as the seal stiffness. This additional stiffness component can be incorporated by modelling it as a stiffness of a pneumatic cylinder that is placed in series with the seal stiffness.

Fig. 4-7 and Fig. 4-8 give some examples of the stiffness values for some different bearing geometries. From the graph can be seen that the stiffness increases for smaller gap heights. The figures also illustrate that the stiffness of the bearing is dependent on whether there is an adiabatic or isothermal atmosphere. The relation for the air stiffness is given by the following relation of which the

derivation is presented in appendix H.

$$k_{air} = \left(\frac{V_i}{V_x} \right)^\gamma p_i \gamma \frac{A_p}{h-x} = \left(\frac{h}{h-x} \right)^\gamma p_i \gamma \frac{A_p}{h-x} \quad (4.9)$$

$$k_{total} = \frac{k_{ff} k_{air}}{k_{ff} + k_{air}} \quad (4.10)$$

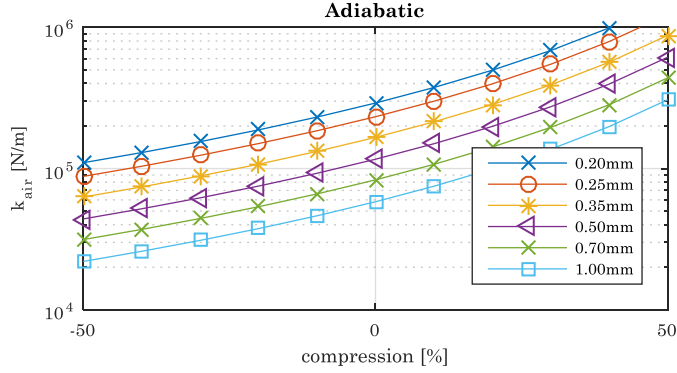


Fig. 4-7. The figure presents the modelled adiabatic stiffness of an air filled cylinder with different initial gap heights and a fixed radius of $r_0 = 10.5\text{mm}$. From the figure can be seen that the air pocket becomes stiffer for decreasing flight height. At no compression there is a pressure condition of $p_i = p_0$.

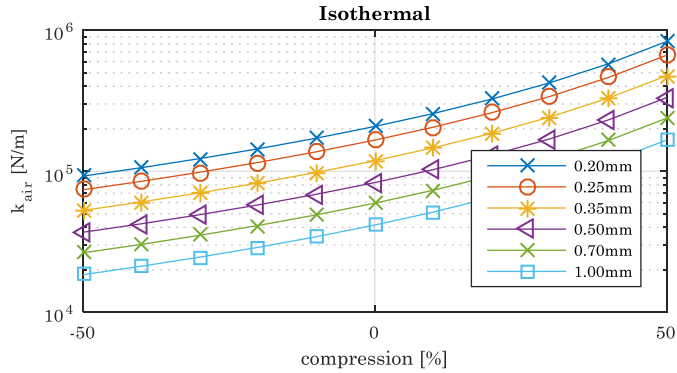


Fig. 4-8. The figure presents the modelled isothermal stiffness of an air filled cylinder with different initial gap heights and a fixed radius $r_0 = 10.5\text{mm}$. From the figure can be seen that the air pocket becomes stiffer for decreasing flight height. At no compression there is a pressure condition of $p_i = p_0$.

For engineering purposes it is convenient to have the Young's modulus of the bearing. Since the stiffness is not necessarily constant, the Young's modulus is not either. A linearized quantity of this value can be derived in the following way:

$$E_{lin} = \frac{\sigma}{\varepsilon} = \frac{F_L h}{A_p x} = \frac{k_{ff} h}{A_p} = \mu_0 M h \frac{d(H_i - H_o)}{dr_{in}} \frac{dr_{in}}{dx} \quad (4.11)$$

This parameter can now be used to calculate the bending stiffness of the bearing in the following way:

$$k_{rot} = \frac{dM}{d\theta} = \frac{EI}{h} = \mu_0 M \frac{d(H_i - H_o)}{dr_{in}} \frac{dr_{in}}{dx} I \quad (4.12)$$

4.3 Ring magnet pocket experiment

A case study is done on a ring shaped neodymium magnet with the magnetization in axial direction. The goal was to show that the load and stiffness characteristics of this bearing could be described by

using the proposed method. The inputs needed for this are the dimensions of the setup and the shape of the magnetic field. The setup is presented in Fig. 4-9 and Fig. 4-10. The magnetic field is derived by using a FE analysis that is shown in Fig. 4-10 and Fig. 4-11. Comparing Fig. 4-9 and Fig. 4-10 nicely shows the ferrofluid shapes along the contours of the magnetic field.

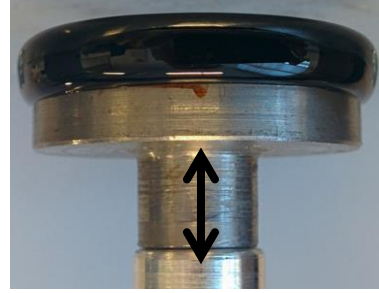


Fig. 4-9. The magnet is placed on an iron adapter and magnetic fluid is added to the configuration. The core of the magnet is filled with an aluminium disc to reduce the volume of the air pocket. A tensile testing machine is used to measure the force-displacement curve by pressing this configuration on a surface. The stiffness of the setup is about $k_{setup} = 3 \times 10^6 \text{N/m}$

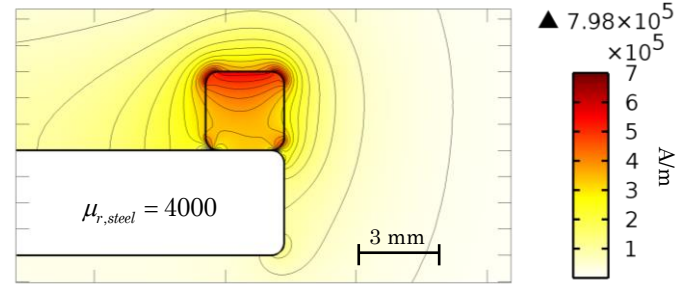


Fig. 4-10. This figure presents the modelled magnetic field of the bearing configuration used in the pocket bearing experiment. The bearing is placed on top of an iron body with a relative permeability of $\mu_{r,steel} = 4000$. The dimensions presented are in mm.

The centre of the ring is filled with aluminium and is not presented in the figure since it has no influence on the magnetic field. The ring magnet used is the KHCM 9963-433 with an outer radius of $R = 12.25\text{mm}$.

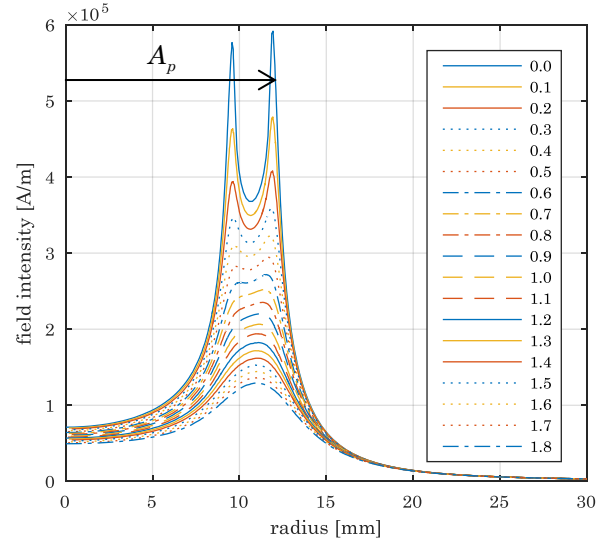


Fig. 4-11. This figure presents the modelled magnetic field intensity at different flight heights (in mm) for a bearing with the dimensions of $[24.5 \times 18.5 \times 3]\text{mm}$ and a remanent flux density of $B_r = 1.17\text{T}$ as function of the bearing radius. The outer peak of the magnetic field is defining the relevant magnetic field for the load capacity since this has the highest magnitude.

4.3.1 Maximum load capacity

The validity of relation (4.4) is first measured by measuring the maximum load curve of the bearing. The measurement is performed by measuring the force from no contact at all to full compression of the bearing. The results of the measurements are presented in Fig. 4-12.

This same performance can be modelled with the use of relation (4.4), by deriving the magnetic field intensities across the fluid interfaces. The measurements show a small ripple caused by air escaping from the chamber. This means that the inner fluid interface is located at a peak of magnetic field intensity along the whole line of the measurement. The values of this peak can be read from Fig. 4-11 that presents the field intensity in function of the radius for different flight heights. The field intensity at the outer fluid interface is measured to have an initial value of $H_0 = 1.3 \times 10^5 \text{ A/m}$. This value is derived by measuring the location of the outer fluid interface with the isolines of Fig. 4-10. During the measurements it is observed that the outer fluid interface moves to a location where the magnetic field intensity has a value of $H_0 = 1.0 \times 10^5 \text{ A/m}$ according to Fig. 4-10 when the bearing faces are touching. This is taken into account by the model, by a linear interpolation of these two values.

The direct load contribution of the seal itself is also taken into account in the model. This is done by averaging the magnetic field intensity over the surface area of the seal.

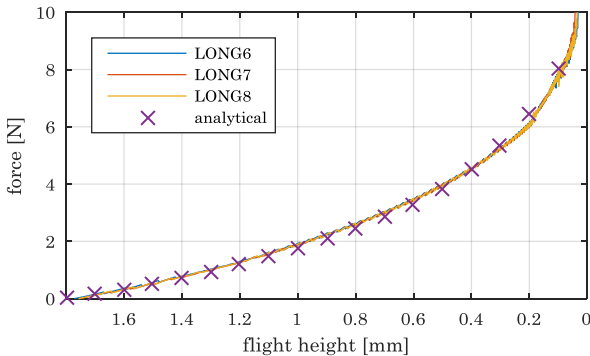


Fig. 4-12. This figure presents the maximum load curve of the bearing. Compressing the bearing will cause air to escape from the seal because the pressure in the pocket of air becomes larger than the pressure that can be counteracted by the seal. The first three datasets in the figure are three different measurements that show that the maximum load curve of the bearing has a high repeatability. The fourth dataset is the result from the theoretical model of this process presented in relation (4.13). The figure shows that the model fits the measurements well.

These steps lead, with the use of relation (4.4), to relation (4.13) that is plotted in Fig. 4-12. It shows that the theoretical model fits the measurements well. This furthermore shows that the load capacity is mainly defined by the pressure across the seal and

only partly defined by the contribution of the pressure of the seal itself.

$$F_L = \mu_0 M (H_i - H_o) \left(A_p + \frac{A_s}{3} \right) \quad (4.13)$$

4.3.2 Load curve

The validity of relation (4.7) is demonstrated by analyzing the load curve of the bearing. The measurements are performed by increasing the force up to a value of $F_L = 5 \text{ N}$ or $p_i = 0.13 \text{ bar}$. The force is then decreased to a negative value to demonstrate that the bearing is also capable to deliver a tension force. The exact force curve that is applied over time is presented in Fig. 4-14. The force in function of the flight height is presented in Fig. 4-15. The graph shows hysteresis that can be explained by the inner peak in magnetic field intensity. The location of this peak is further referred to as “knee point” since it causes a knee shape in the curve (Fig. 4-16). This knee point occurs when the inner fluid interface is at the inner peak of magnetic field strength. The peak itself is not visual in the curve since fluid sticks behind there, as can be seen in Fig. 4-13.

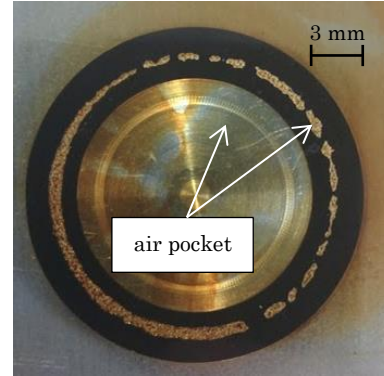


Fig. 4-13. This figure presents the ferrofluid pocket bearing used for the experiment discussed in this section. To be able to visualize what is happening in the pocket of the bearing, a glass plate is used as a surface. This makes it possible to see two seals that have a capillary connection between them. The magnet used is the KHCM 9963-433.

The validation of relation (4.7) continues by first calculating the location of the knee point which is then used to calculate the stiffness.

The location of the knee point is calculated by first considering the magnetic field at point A in Fig. 4-16. This point presents a maximum load condition which means that at that point, the inner fluid interface is located at a peak of magnetic field intensity. Fig. 4-17 presents that this is the case for a radial position of $r_A = 11.8 \text{ mm}$ with a flight height of $h_A = 0.235 \text{ mm}$. Decompressing the bearing must cause the inner fluid interface to move inwards towards point B in Fig. 4-16. These values can be used to calculate the volume of the pocket. This volume is assumed to be constant which is reasonable due to the minor change in pressure. The location of point B can now be calculated with the following relation.

$$r_B = \sqrt{\frac{h_A}{h_B}} r_A = \sqrt{\frac{0.235}{0.28}} 11.8^2 = 10.8 \text{ mm} \quad (4.14)$$

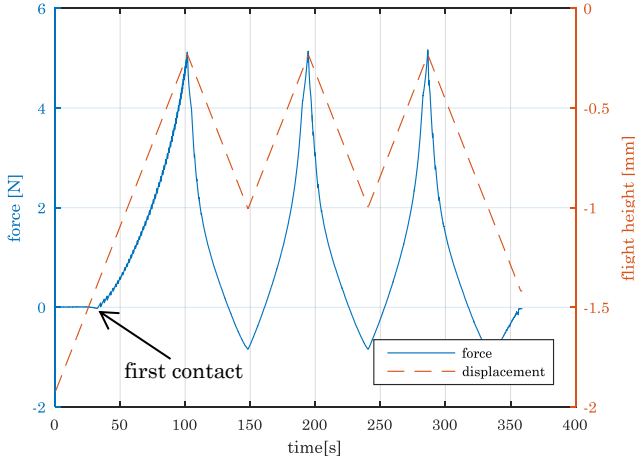


Fig. 4-14. This figure presents the measured force and flight height of the bearing over time. The measurement starts with no contact between the bearing and the surface. The measurement is done multiple times to measure the hysteresis of the bearing.

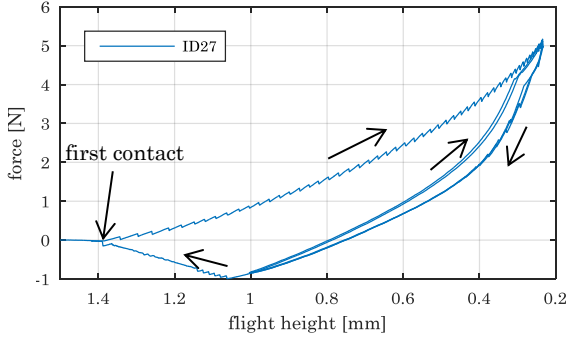


Fig. 4-15. This figure presents the measured force of the bearing as function of its flight height. In the initial part, some force ripple can be observed that is caused by air escaping from the pocket. The repeated part of the graph shows two different stiffness values that are caused by the shape of the magnetic field. The hysteresis is mainly caused by the air transport across the inner ferrofluid seal.

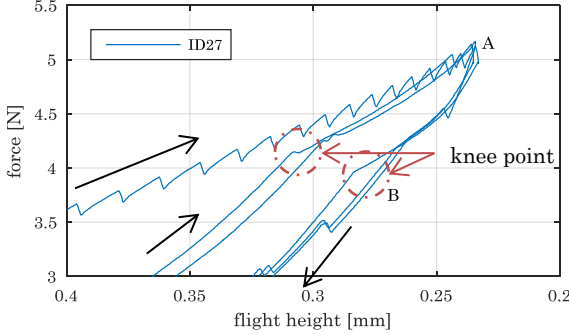


Fig. 4-16. This figure presents a zoomed-in part of Fig. 4-15. It can be seen that the curve shows some hysteresis.

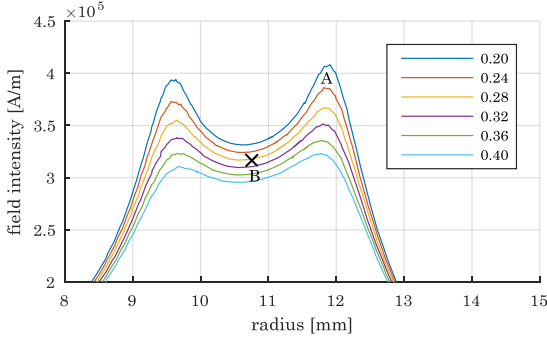


Fig. 4-17. This figure presents the modelled magnetic field intensity as function of the radial position for different flight heights presented in mm. The point A presents a position of $h_A = 0.235\text{mm}$ and the point B presents a position of $h_B = 0.28\text{mm}$.

Comparing this value with Fig. 4-17 shows that this value is right in-between the two peaks of magnetic field intensity. Decreasing the compression even more makes the inner fluid interface to jump over this peak to continue back down at the other side of the inner peak. The inner fluid interface is able to jump over this peak due to the fluid that sticks behind as can be seen from Fig. 4-13. Fluid sticks behind due to the attracting force of the inner peak in magnetic field.

This inner peak also causes ripple in the load curve due to air escaping from the outer chamber into the inner chamber. This introduces a hysteresis like behaviour that is clearly visual in the shape of the curve presented in Fig. 4-15. The hysteresis decreases for increasing flight height due to the decreasing contribution of the inner peak as can be seen from Fig. 4-18.

The stiffness of the bearing can now be validated by comparing the measured stiffness with the stiffness that is described with relation (4.7). The location of the knee point is now used to calculate the average measured stiffness between point A and B in Fig. 4-16. This has the following value:

$$k_{AB,mes} = \frac{F_2 - F_1}{x_2 - x_1} = \frac{5.1 - 4}{(0.235 - 0.28) \times 10^{-3}} = 2.4 \times 10^4 \text{ N/m} \quad (4.15)$$

The theoretical stiffness can be calculated from the magnetic field presented in Fig. 4-17.

$$\begin{aligned} k_{AB,mod} &= \mu_0 MA \frac{\Delta H_{r=11.8} - \Delta H_{r=10.6}}{x_2 - x_1} \\ &= 4\pi \times 10^{-7} \times 32 \times 10^3 \times \pi 0.0118^2 \frac{0.6 \times 10^5}{45 \times 10^{-6}} \quad (4.16) \\ &= 2.3 \times 10^4 \text{ N/m} \end{aligned}$$

The theoretical stiffness can also be calculated by using the pneumatic leverage. This method requires only knowledge on the shape of the magnetic field and the change in flight height. The location of the inner fluid interfaces falls out of the relation.

$$\begin{aligned} \frac{dr_{in}}{dx} &= \sqrt{\frac{V_{pocket}}{4\pi(h-x)^3}} = \sqrt{\frac{\pi 0.0118^2 \times 0.235 \times 10^{-3}}{4\pi(0.2575 \times 10^{-3})^3}} \quad (4.17) \\ &= 21.9 \end{aligned}$$

$$\begin{aligned} k_{AB,mod} &= \mu_0 MA_p \frac{d(H_{in} - H_{out})}{dr} \sqrt{\frac{V_{pocket}}{4\pi(h-x)^3}} \\ &= 4\pi \times 10^{-7} \times 32 \times 10^3 \times \pi 0.0118^2 \frac{0.6 \times 10^5}{1 \times 10^{-3}} 21.9 \\ &= 2.3 \times 10^4 \text{ N/m} \quad (4.18) \end{aligned}$$

The three calculated stiffness's have a value of around $2.3 \times 10^4 \text{ N/m}$ which shows that the theoretical model fits the experimental results well. This furthermore justifies the assumption of the air to be incompressible for small displacements;

Fig. 4-7 shows that the stiffness of the pocket is about a factor of ten higher than the stiffness of the seal itself. The contribution of the pressure of the

ferrofluid to the stiffness is not taken into account here which means that the theoretical model is actually slightly overestimating the real system.

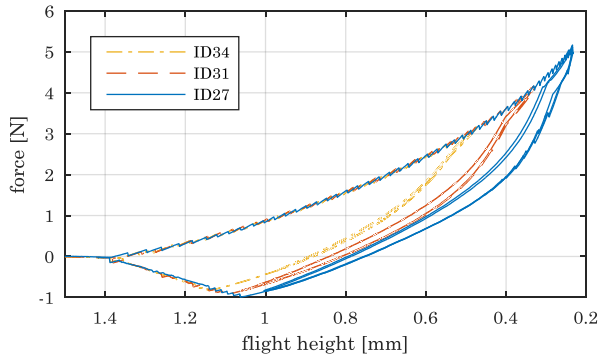


Fig. 4-18. This figure presents the stiffness of the bearing for different pocket volumes. It can be seen that the stiffness becomes larger for smaller pocket volumes.

4.3.3 Conclusion

The theoretical model for the maximum load capacity and the stiffness is in good accordance with the experimental results which means that the proposed method is valid for describing the load capacity and the stiffness of a ferrofluid pocket bearing. This shows that the load characteristics can be directly calculated from the shape of the magnetic field and the geometry of the bearing. Comparing the theoretical model with the measurements shows the load and stiffness of the bearing is mainly determined by the sealing capacity of the seal and only partly determined by the pressure of the ferrofluid itself. The results furthermore show that having two radially distributed peaks in magnetic field intensity introduces some hysteresis in the system that might be undesirable.

4.4 Sandwich structure

Section 4.3 gives a lot of insight in how the different parameters lead to the final load and stiffness performance of a ferrofluid bearing. Section 5.6 presents that the trail formation of a ferrofluid bearing cause problems with the repeatability in height. This section presents a concept that achieves an improved out-of-plane stiffness and repeatability using the same magnets as in the previous section but in another configuration. The goal is furthermore to demonstrate how the proposed method can be used in the design of a ferrofluid pocket bearing. After a general introduction of this new concept, a theoretical model is developed to describe the performance. Finally this model is experimentally validated.

4.4.1 Concept derivation

The decrease in flight height can be minimized by taking a pocket bearing concept and locating the outer fluid interface at such a location that a change in

bearing fluid volume has minimal influence on the magnetic field difference across the seal. This can be achieved by placing a fluid reservoir at the outside of the bearing and by placing the outer fluid interface at a location with a small magnetic field gradient, an example if this is presented in Fig. 4-19 and Fig. 4-20.

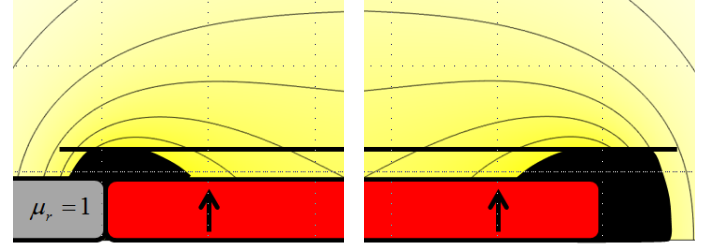


Fig. 4-19. The outer fluid interface of this configuration will change its location a lot due to trail formation because of the minimum amount of available fluid and the high magnetic field gradient at which it is located.

Fig. 4-20. The outer fluid interfaces of this configuration will change its location minimally due to trail formation because of a large amount of available fluid and a low magnetic field gradient at which it is located.

Another way to decrease this effect is to use a sandwich like structure presented in Fig. 4-21. This configuration consists of a plate that is constrained between two facing pocket bearings using an axially magnetized ring magnet. The rings are placed in an attracting configuration to achieve a strong magnetic field within the slot. The pressure in the lower and upper pocket is equal when there is no force applied on the plate, assuming equal volumes of ferrofluid above and below, and equal volumes of enclosed air above and below. The plate is also exactly in the middle in this situation. Moving the plate downwards results in an increase in pressure in the lower pocket and a decreasing pressure in the upper pocket causing a counteracting force (Fig. 4-22).

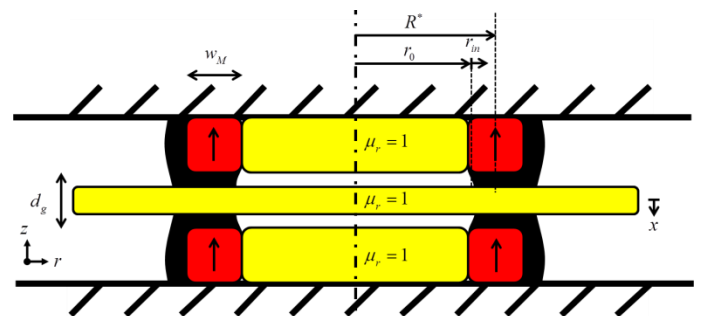


Fig. 4-21. The figure presents a cross section of the sandwich bearing concept consisting of two axially magnetized ring magnets placed in-line on top of each other. The plate is constrained between the magnets and the core of the ring is made out of nonmagnetic material. The magnets are placed on a ferromagnetic material. Note that x here is opposite to z to obtain a positive stiffness value from the model for a positive stiffness value of the bearing.

Moving the plate will cause both fluid interfaces to trail at the top and at the bottom resulting in a smaller change in flight height compared to a single sided bearing. This concept can be combined with the

fluid reservoir to minimize the effects even more, but the cost paid for this is that the outer interface cannot contribute to the stiffness of the bearing anymore. The concept studied in this section does have a fluid reservoir located at the outside of the bearing.

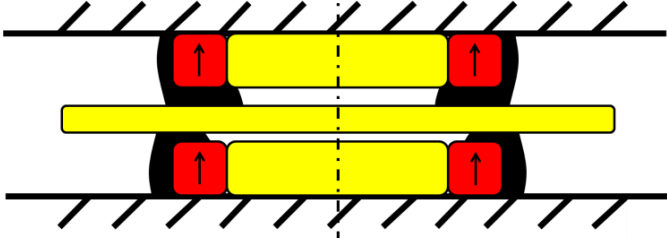


Fig. 4-22. The cross section in the figure presents the fluid interfaces at a deformed configuration. It can be seen that there is a slight movement at the outer interfaces, but this influence is minimal since they are located at a position with low magnetic field gradient.

4.4.2 Magnetic field model

The magnetic field should be known to be able to describe the performance of the bearing. A visualization of the magnetic field caused by the two stacked magnets is presented in Fig. 4-23. The field is simplified with the following relation that approximates the field in-between the two magnets with the product of two quadratic functions forming a saddle point in the middle of the gap.

$$H(r, z) = H_{\max} \left(1 - \left(\frac{r}{f_{fit,r} w_m} \right)^2 \right) \left(1 + \left(\frac{z}{f_{fit,z} d_g} \right)^2 \right) \quad (4.19)$$

$$\approx H_{\max} \left(1 - \left(\frac{r}{f_{fit,r} w_m} \right)^2 \right)$$

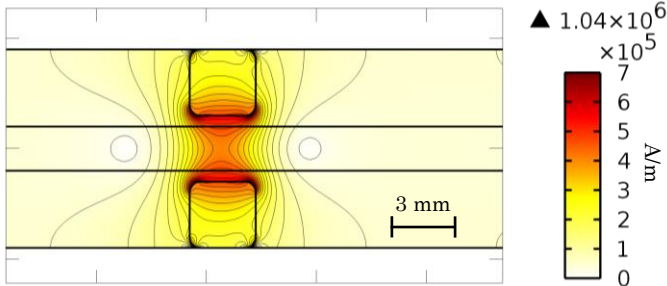


Fig. 4-23. This figure presents the magnetic field developed by the sandwich configuration. It can be seen that there is a strong field in-between the magnets and a relative weak field far apart from that.

The influence of the gradient in r-direction is in general dominant to the influence of gradient in z-direction and is therefore neglected. The shape of the magnetic field calculated by using finite element analyses calculations is presented in Fig. 4-24, the fitted function to that shape is presented in Fig. 4-25.

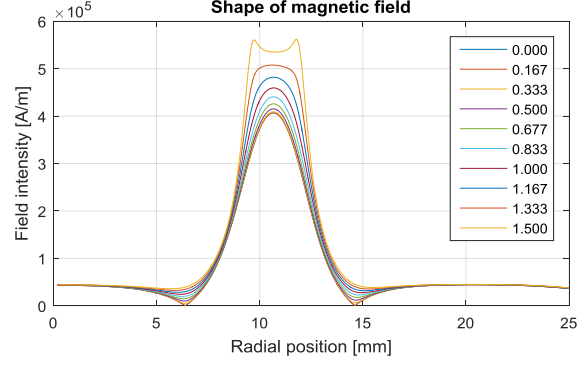


Fig. 4-24. This figure presents the magnetic field intensity as function of the radius for different distances from the centre in z-direction. The centre is defined by the plane in the middle of the two bearing surfaces. The field is modelled by using finite element analyses. The graph is calculated by using the model presented in Fig. 4-23

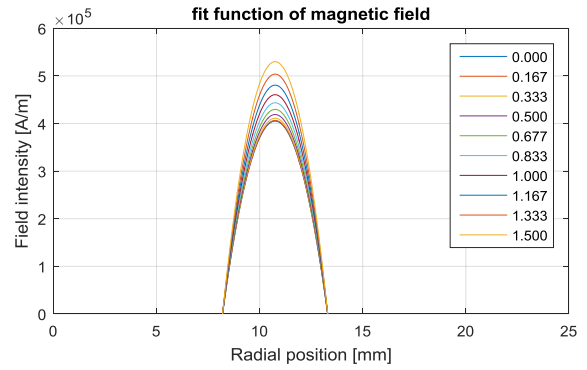


Fig. 4-25. This figure presents the magnetic field intensity calculated with the analytical approximation at different heights. The graph is made by assuming a fit constant of $f_{fit,x} = 0.85$

4.4.3 Force and stiffness model

The difference in pressure between the upper pocket and lower pocket develops a force counteracting the displacement of the mover between the magnets. The total force can be seen as the summation of the force of the bottom pocket F_B and the force of the upper pocket F_T .

$$F_L = F_B - F_T \quad (4.20)$$

$$= \mu_0 M (H_{i,B} - H_{o,B} - H_{i,T} + H_{o,T}) A_p$$

Now assume that such amount of ferrofluid is added that the outer fluid interface is located far from the magnet at a location that has a low gradient in magnetic field. The load capacity for this situation is now only defined by the relative difference of magnetic field intensity at the inner fluid interfaces.

$$F_L = \mu_0 M (H_{i,B} - H_{i,T}) A_p \quad (4.21)$$

The approximation of the magnetic field given by relation (4.19) can now be incorporated with the force equation given by relation (4.21) to describe the load capacity as function of the shape of the magnetic field.

The relation $r = r_0 + r_{in} - R^*$ is substituted into the relation to include the location of the inner fluid interface $r_0 + r_{in}$. The parameter r_0 describes the

location of the interface at no load and the parameter r_{in} describes the displacement of that interface.

$$F_L = \mu_0 MH_{\max} \left(\left(\frac{r_0 + r_{in,top} - R^*}{f_{fit,x} w_m} \right)^2 - \left(\frac{r_0 + r_{in,bot} - R^*}{f_{fit,x} w_m} \right)^2 \right) A_p \quad (4.22)$$

A displacement in the out-of-plane direction z causes the position of the inner fluid interfaces to change. The pneumatic leverage can be used to relate these values with the displacement z of the system. This first involves relating the inner fluid interface to the volume of the pocket by assuming the inner fluid interface to be vertical. This leads to the following relation:

$$V_{pocket} = (h+x)\pi(r_0 + r_{in,top})^2 = (h-x)\pi(r_0 + r_{in,bot})^2 \quad (4.23)$$

By using these relations the pneumatic leverages can be expressed with the following relations.

$$\begin{aligned} \frac{dr_{in,bot}}{dx} &= \frac{d}{dx} \left(\sqrt{\frac{V_{pocket}}{\pi(h-x)}} - r_0 \right) = \sqrt{\frac{V_{pocket}}{4\pi(h-x)^3}} \\ \frac{dr_{in,top}}{dx} &= \frac{d}{dx} \left(\sqrt{\frac{V_{pocket}}{\pi(h+x)}} - r_0 \right) = \sqrt{\frac{V_{pocket}}{4\pi(h+x)^3}} \end{aligned} \quad (4.24)$$

Assuming only small displacements it is reasonable to linearize the system by using the pneumatic leverage in the following way:

$$\begin{aligned} r_{in,top} &\approx -\sqrt{\frac{V_{pocket}}{4\pi h^3}} x \approx -\sqrt{\frac{A_p}{4\pi h^2}} x \\ r_{in,bot} &\approx \sqrt{\frac{V_{pocket}}{4\pi h^3}} x \approx \sqrt{\frac{A_p}{4\pi h^2}} x \end{aligned} \quad (4.25)$$

Substituting relation (4.25) into relation (4.22) leads to the following relation:

$$F_L = \mu_0 MH_{\max} \left(\left(\frac{r_0 - R^* - \sqrt{\frac{A_p}{4\pi h^2}} x}{f_{fit,x} w_m} \right)^2 - \left(\frac{r_0 - R^* + \sqrt{\frac{A_p}{4\pi h^2}} x}{f_{fit,x} w_m} \right)^2 \right) A_p \quad (4.26)$$

This relation can be further simplified by first considering the stiffness of the system.

$$k = \frac{dF_L}{dx} = \mu_0 MH_{\max} \left(-4 \left(\frac{r_0 - R^* + \sqrt{\frac{A_p}{4\pi h^2}} x}{f_{fit,x} w_m} \right) \sqrt{\frac{A_p}{4\pi h^2}} \right) A_p \quad (4.27)$$

By again assuming only small displacements of the system, the relation can be simplified to the following linear stiffness.

$$\begin{aligned} k_{ff} &= 2\mu_0 MH_{\max} \frac{(R^* - r_0) \sqrt{\frac{A_p^3}{\pi h^2}}}{(f_{fit,x} w_m)^2} \\ &= 2\mu_0 MH_{\max} \frac{\pi(R^* - r_0)^3}{(f_{fit,x} w_m)^2 h} \end{aligned} \quad (4.28)$$

The load can now be described by integrating this formula in the region of the linear stiffness.

$$F_L = 2\mu_0 MH_{\max} \frac{\pi(R^* - r_0)^3}{(f_{fit,x} w_m)^2 h} x \quad (4.29)$$

4.4.4 Calculations model

Now the performance of the system can be calculated with the use of the model derived in the previous section. An overview of the system is presented in Fig. 4-26. During the experiments it was measured that air popped out of the seal at a displacement of $x = 0.09mm$. The value for the inner fluid interface at rest can be calculated from this by assuming the volume of the pocket to be incompressible. This is reasonable since we are only considering small displacements.

$$r_0 = \sqrt{\frac{(h-x)r_{\max}^2}{h}} = \sqrt{\frac{(0.4-0.09)10.75^2}{0.4}} = 9.46mm \quad (4.30)$$

The stiffness can now be calculated by using relation (4.28) and substituting the following values. A magnetic field value of $H_{\max} = 4.6 \times 10^5 N/m$ and a fit value of $f_{fit,x} = 0.85$ from Fig. 4-25, the result from relation (4.30), a gap height of $h = 0.4mm$ and the width of the magnets $w_m = 3mm$ from the measurement setup.

$$\begin{aligned} k_{ff} &\approx 2 \times 4\pi \times 10^{-7} \times 32 \times 10^3 \times 4.6 \times 10^5 \frac{\pi(0.00129)0.00946^3}{(0.85 \times 0.003)^2 0.0004} \\ &\approx 4.9 \times 10^4 N/m \end{aligned} \quad (4.31)$$

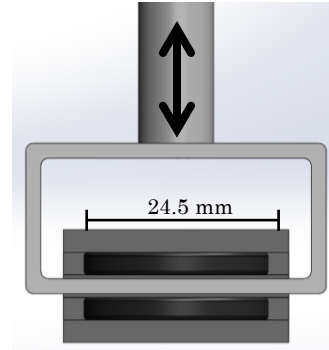


Fig. 4-26. This figure presents a schematic drawing of the setup. The magnets (black) are attached to a fixed frame in-between to iron plates (dark grey) with a distance of $d_g = 2.8mm$ from each other. A load is applied on the bearing via an aluminium construction (light grey) with a thickness of 2mm. The force over the displacement of the system is measured to derive the stiffness of the system. The setup has stiffness of $k_{mes} = 8 \times 10^5 N/m$.

4.4.5 Measurements

Measurements are done with the system presented in Fig. 4-26 to measure the stiffness of the bearing. To make sure that the outer fluid interface is located at a point of low magnetic field gradient, ferrofluid is added first at one of the side of the plate up to a point that there is no change in carrying force measured anymore. Then there is added ferrofluid at the other side of the plate up to a point that the levels are equal. Three measurements are presented in Fig. 4-27 that are measured by applying the force sequence presented in Fig. 4-28. The curve shows no hysteresis, a high repeatability and the following stiffness.

$$F_{mes} = \frac{\Delta F}{\Delta x} = \frac{6.0}{0.14 \times 10^{-3}} = 4.3 \times 10^4 \text{ N/m} \quad (4.32)$$

The measured stiffness should be corrected for the stiffness of the pocket of air and the stiffness of the measurement setup. The correction leads to the following stiffness for the bearing.

$$k_{ff} = \frac{1}{\frac{1}{k_{mes}} + \frac{1}{k_{setup}} + \frac{1}{k_{air}}} = \frac{1}{\frac{1}{4.3 \times 10^4} + \frac{1}{8 \times 10^5} + \frac{1}{4 \times 10^5}} \quad (4.33)$$

$$= 5.1 \times 10^4 \text{ N/m}$$

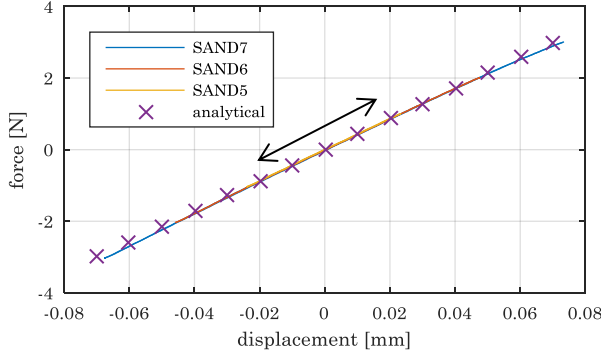


Fig. 4-27. This figure presents the force of the bearing as function of the displacement. Three different measurements are presented from which can be seen that there is no hysteresis and a high repeatability.

The ring of ferrofluid also adds some stiffness to the total systems due to the magnetic field gradient in z -direction. An estimate of this stiffness can be calculated in the following way.

$$k = 2 \frac{\Delta F}{\Delta x} = 2 \mu_0 M A_p \frac{\Delta H}{\Delta x}$$

$$= 8\pi \times 10^{-7} \times 32 \times 10^3$$

$$\times \frac{\pi}{4} (0.0245^2 - 0.0185^2) \frac{1.5 \times 10^4}{1 \times 10^{-4}} \quad (4.34)$$

$$= 2.4 \times 10^3 \text{ N/m}$$

From this value can be seen that the stiffness of the seal is negligible since it is about a factor ten lower than the stiffness of the pocket.

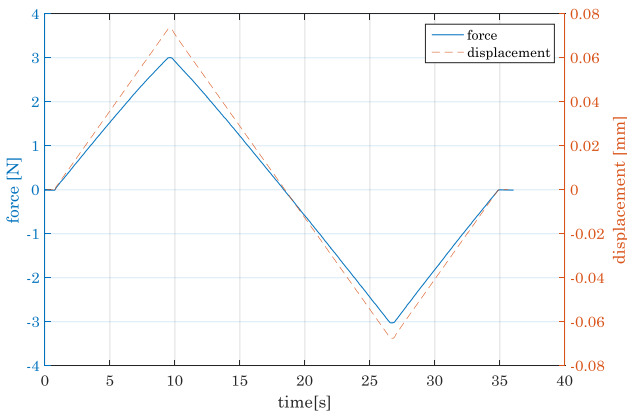


Fig. 4-28. This figure presents the force and displacement over time. The bearing is moved up and down a couple of times to measure the hysteresis.

4.4.6 Discussion model and results

The stiffness calculated with the model has a slightly lower value than the measured stiffness which can be attributed to the assumptions made for the model. The derivation from the fundamental equation of a magnetic fluid up the final stiffness model presented here involves a lot of assumptions. The assumptions that mainly contribute to the difference are the simplification of the magnetic field, the assumption of the ferrofluid ring not contributing to the stiffness and the incompressibility of the air. Despite these assumptions the calculated values are still in good accordance with the measurements and give a lot of insight in how the different parameters influence the behaviour of the bearing.

4.5 Conclusion

The ferrofluid pocket bearing is an interesting concept to be used in systems where precise positioning is required with high precision and velocity. The exact performance of such a bearing is up to now only poorly described in literature. This paper presents a method to describe the load and stiffness specifications of any shape of this type of bearing.

Describing the performance starts with calculating the magnetic field around the magnet, the ferrofluid will locate itself there where the magnetic field intensity is highest, and in balance with the pressure in the air pocket, and the external load on the bearing. The shape of the magnet and the amount of ferrofluid must be such that by placing the contact surface, a volume of air fluid is encapsulated by the ferrofluid. Load is then carried by this pocket and the function of the seal is to keep this fluid inside. The difference in pressure across the seal is defined by the difference in magnetic field intensity across the seal. This results in a stiffness of the seal that is defined by the change of magnetic field intensity with changing seal location. The stiffness is in general defined by the stiffness of the pocket and the stiffness of the seal combined. The pocket has a large surface area with the contact surface and a relative small surface area with the seal, this will result in a sort of pneumatic leverage that results in the situation that a small change in film height causes a large displacement in fluid seal location. Increasing this pneumatic leverage will result in a stiffer bearing. While loading the bearing, it might occur that some air escapes from the seal which will cause the pocket to have other kinematics resulting in different bearing stiffness.

A lateral movement of the bearing results in a trail of fluid which causes the outer fluid interfaces of the bearing to change location which results in a lower film height. Locating the outer interface at a location where there is a low gradient of magnetic field or

building a fluid reservoir might mitigate these effects. Another solution is making a sandwich like structure by placing two pocket bearings mirrored on top of each other. The outer fluid interfaces at the top and the bottom will change with the same amount such that they have minor influence on the load and stiffness of the bearing. This solution can be combined with the previous two solutions to reduce the effect even more.

The load and stiffness are now defined only by the relative difference of the inner fluid interfaces. It has been shown that a bearing with a diameter 24.5mm is capable of carrying a load of around 8N with a stiffness of around $2 \times 10^4 \text{N/m}$. This stiffness can be increased to a value of $5 \times 10^4 \text{N/m}$ by placing the bearings in a sandwich like structure.

5 Friction Behaviour of a Ferrofluid Bearing

Stefan G.E. Lampaert¹, Jo W. Spronck¹, Ron A.J. van Ostayen¹

¹Department of Precision and Microsystems Engineering, Delft University of Technology, Delft, The Netherlands

A ferrofluid is a fluid with paramagnetic properties while having a colloidal stability. This can be used to obtain a hydrostatic type of bearing that distinguishes itself from other bearings by its compactness, inherent stability, low (viscous) friction, absence of pumps and absence of stick-slip. These properties, together with its low price, make the bearing interesting to be used for applications that require fast and precise positioning or applications in the absence of gravity. Knowledge on the exact performance of these types of bearings is up to now not available. This paper presents some models that can be used to understand the friction behaviour of the bearing. The different models that are discussed are for viscosity, translational friction, rotational friction and trail formation. It is showed that the friction can be modelled with the summation of a Couette flow and Poiseuille flow. This results in that the maximum load capacity of the bearing decreases when translating. The trail formation showed to be hard to model since it is a process dependent on patch and time.

Index Terms— Ferrofluid, Planar bearing, Precision engineering, Friction, Trail formation

5.1 Introduction

A ferrofluid bearing is a type of bearing that uses a ferrofluid and a magnetic field to create a load carrying capacity. Advantages over other bearing concepts are price, compactness, inherent stability, low (viscous) friction, absence of pumps and absence of stick-slip. These advantages make the bearing interesting to be used in low load applications that require precise positioning or applications in the absence of gravity.

There are two types of bearings that can be distinguished. The first concept is the ferrofluid pressure bearing that uses solely the magnetic pressure developed by an external magnetic field for creating a load carrying capacity [53]. The second concept is the ferrofluid pocket bearing that encapsulates a pocket of air (or any other nonmagnetic fluid) with a ferrofluid seal [22]. The maximum load capacity of this bearing is determined by the maximum pressure across the seal which has a typical value 0.2bar (chapter 4). The stiffness of the bearing is determined by the stiffness of the pocket and the seal together (section 4).

A problem of this bearing concept in a planar configuration is that it leaves behind a trail of ferrofluid caused by the adhesion of the ferrofluid to the bearing surfaces. The trailing of the ferrofluid reduces the gap between the bearing faces and causes a time and path dependent force between the ferrofluid and the magnet [4], [5]. Due to the absence of models for this effect, [58] and [59] decided to implement a feedback control loop that controls the height of the system since that has the capacity of mitigating unknown factors. A capacitive sensor

measured the height of the stage and a Lorentz actuator compensated the loss in carrying capacity of the bearings due to trail formation. This extra use of an actuator, sensor and controller is undesirable since it takes away the main advantage of the bearing: cheap and simple.

Another problem is that no validated models for the friction exist yet. In [5] a Couette flow model was used to model the friction of a ferrofluid bearing. This model showed a factor 4 difference compared to the measurements. Clearly, a better model needs to be developed.

In this paper, four models are presented that describe the effects seen in the planar movement of the bearing. The first model describes the change of viscosity due to the presence of an external magnetic field. The second and third model describe respectively the translational and rotational friction of a ferrofluid bearing. The fourth model describes the trail formation of a ferrofluid bearing. These four models cover together the main effects seen with ferrofluid bearings.

The paper starts with a general method that is used to derive the different parameters of interest like the flow field and the stresses. A discussion follows on the viscosity of the fluid, and under what conditions this can be assumed to be constant. Then the translational friction, the rotational friction and the trail formation are discussed with the goal to develop understanding of their impact on the performance of the system.

5.2 General method

The relations for the forces that act on the ferrofluid bearing are derived by first calculating the flow field in-between the bearing pads. This flow field is then

used to calculate the stresses in the system which can be related to the forces of interest. The derivations assume the viscosity of the fluid to be constant which is showed to be reasonable according to the discussion in the next section. The magnetization of the fluid is also assumed to be saturated instantly. This assumption is reasonable since the saturation magnetization and relative permeability of the fluid are relatively low (respectively $M_s \sim 3 \times 10^4 \text{ A/m}$ and $\mu_r \sim 2$).

All derivations of the flow field presented in this paper start from the Navier-Stokes equations for incompressible magnetic fluids which is given by the following relation (section 2.3). Note that this relation already assumes a Newtonian fluid which is not always the case for a ferrofluids. Throughout the paper will be assumed that a ferrofluid is used that has negligible change of viscosity during operation.

$$\rho \left(\frac{\partial \underline{u}}{\partial t} + \underline{u} \cdot \nabla \underline{u} \right) = -\nabla p + \eta \nabla^2 \underline{u} + \underline{f} + \mu_0 M \nabla H \quad (5.1)$$

$$\nabla \cdot \underline{u} = 0$$

To simplify this relation it is reasonable to assume a low Reynolds number flow that results in neglecting the inertial term from the Navier-Stokes equations. The Reynolds number for a typical system presented in Table 1 has the following value:

$$\text{Re} = \frac{\rho U L}{\eta} \sim \frac{1380 \times 0.001 \times 0.01}{0.15} = 0.09 \ll 1 \quad (5.2)$$

By assuming the magnetic body force as the only body force, the following relations are derived which are used as a basis for all further derivations concerning the flow field.

$$\nabla p = \eta \nabla^2 \underline{u} + \mu_0 M \nabla H \quad (5.3)$$

$$\nabla \cdot \underline{u} = 0$$

A case study is done throughout this paper to give a comparison of how the different effects relate to each other. The different parameters used for this are presented in Table 1 and are taken from an application that desires precise positioning with a relative low velocity and load.

Table 1: Parameters used for calculations

Parameter	Value	Unit
η	0.15	kg / m s
U	1	mm / s
h	0.2	mm
l_{seal}	3	mm
A_{pocket}	202	mm ²
A_{pres}	471	mm ²
r_o	12.25	mm
r_i	9.25	mm
H_{trail}	1×10^5	A / m
x_{trail}	5	mm

μ_0	$4\pi \times 10^{-7}$	N / A ²
M	32×10^3	A / m
A_{trail}	400	mm ²
ρ	1380	kg / m ³

5.3 Viscosity

The viscosity of a ferrofluid changes when subjected to a magnetic field [18]. This happens due to two different effects: rotational viscosity and particle chain formation. The following section discusses the impact of these effects on a typical bearing system.

5.3.1 Rotational viscosity

The effect of rotational viscosity is caused by the alignment of the particles to the magnetic field. This results in a larger effective viscosity when the vorticity is perpendicular to the magnetic field. The viscosity of the fluid is defined by the following relation [31]:

$$\eta = \eta_c \left(1 + \frac{5}{2} \tilde{\phi} + \frac{3}{2} \tilde{\phi} \frac{\alpha - \tanh \alpha}{\alpha + \tanh \alpha} \sin^2 \beta \right) \quad (5.4)$$

$$\alpha = \frac{\mu_0 m H}{k T} \quad (5.5)$$

The first term of this equation presents the viscosity of the carrier fluid, the second term presents the increase in viscosity due to the suspension of particles and the third term presents the change in viscosity due to the magnetic field. For large values of α this relation has a maximum value of:

$$\eta_{\text{max}} = \eta_c \left(1 + \frac{5}{2} \tilde{\phi} + \frac{3}{2} \tilde{\phi} \right) = \eta_c (1 + 4 \tilde{\phi}) \quad (5.6)$$

Datasheets often give the viscosity of the fluid as the viscosity in the absence of the magnetic field. This basically reduces to the Einstein formula [64]:

$$\eta_0 = \eta_c \left(1 + \frac{5}{2} \tilde{\phi} \right) \quad (5.7)$$

A typical value for the increase in viscosity caused by the effect of rotational viscosity can be calculated by combining relation (5.6) and (5.7) and assuming a typical concentration of about $\phi = 8\% \text{ vol}$.

$$\frac{\eta_{\text{max}}}{\eta_0} = \frac{(1 + 4 \tilde{\phi})}{1 + \frac{5}{2} \tilde{\phi}} = \frac{(1 + 4 \times 0.08)}{1 + \frac{5}{2} \times 0.08} = 1.1 \quad (5.8)$$

This relation shows that the increase in viscosity is only in the order of 10%.

5.3.2 Particle chain formation

The particle chain formation, often referred to as the magnetoviscous effect [30], is the formation of chain like structures in the fluid due to the magnetic interaction between the particles. These structures are more difficult to rotate in the fluid resulting in a larger resistance to shear which results in an increase

in effective viscosity [34]. Applying a magnetic field on the fluid increases the resistance to rotation even more resulting in an even further increase in viscosity. Shear forces in fluid might break the chains in the fluid resulting in a shear thinning effect. The formation of chains can be investigated by analysing the dipolar interaction parameter λ that compares the dipolar energy with the thermal energy. Chain like structures will develop in the fluid when this parameter becomes larger than one. Increasing this parameter results in longer chains in the fluid [36].

$$\lambda = \frac{\mu_0 M_0^2 V}{24 k_B T} = \frac{\mu_0 m^2}{4\pi k_B T d_m^3} \quad (5.9)$$

The formula shows that λ increases with the size of the particles resulting in only the larger particles contributing to the formation of chains. It has been shown that even a small concentration of large particles in the fluid can cause a high increase of viscosity [37]. When this behaviour of the viscosity of the fluid is not desired, it is wise to choose a ferrofluid at which the dipolar interaction parameter is lower than one for all suspended magnetic particles.

5.4 Translational friction

The translational friction of the bearing is an important parameter since it has a lot of influence on the desired actuation force, damping and efficiency of the system. The section starts with a discussion on a friction model found in literature. Then the flow field between the bearing pads is derived, which is used to calculate the resulting friction force.

5.4.1 Literature

The research of [5] presents some work on the friction of a ferrofluid bearing. This friction was modelled using the viscous damping model that assumes a Couette flow (Fig. 5-1) in-between the bearing surfaces defined by the following relation:

$$u_x = \eta \frac{U}{h} z \quad (5.10)$$

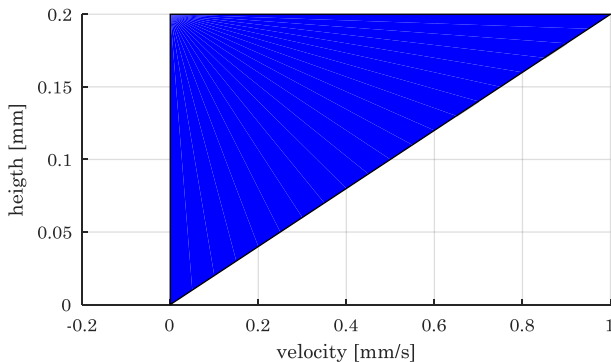


Fig. 5-1. The figure presents a Couette flow. The area of the filled surface is a measure of the fluid transport. Net fluid transport can be concluded from this graph since the area of the surface is nonzero.

The value for the shear stress derived from this assumption is given by the following relation.

$$\tau_{iu} = \eta \frac{\partial u_x}{\partial z} = \eta \frac{U}{h} \quad (5.11)$$

This leads to the following damping coefficient.

$$c_{iu} = \frac{F}{U} = \frac{\tau_{iu} A}{U} = \eta \frac{A}{h} \quad (5.12)$$

A measurement of the damping done by [5] is presented in Fig. 5-2. It shows that the friction model is about a factor four too low. The research fails to explain where this difference comes from. Rotational viscosity is not responsible for this difference since it only gives a typical increase of about 10% according to (2.19). Also particle chain formation cannot be the cause since this would mean that the fit in Fig. 5-2 could not be fitted with one damping constant which appeared to be possible. A constant damping value is not possible due to the shear thinning effect of particle chain formation.

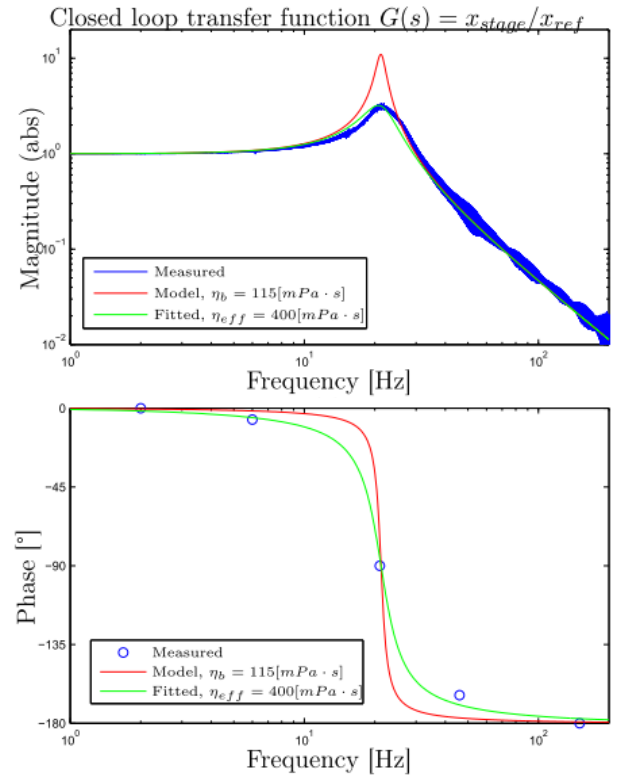


Fig. 5-2. The figure presents the magnitude plot of the data presented by [5]. The blue line in this figure presents the measurement, the red line gives the result of the model and the green line presents the fit of the viscosity. It shows that the viscosity is about a factor of four too high.

The derivation of the flow field given by relation (5.10) result in fluid transport between the bearing pads as can be seen from Fig. 5-1. However, a translation of the bearing shows no fluid transport which means that this assumption is not correct. The fluid under the bearing pads stays under the bearing pads due to the magnetic body force from the permanent magnets. The next section will derive a

new model in which the assumption of no net fluid transport is included. The goal is to find a model that fits the measurements of [5].

5.4.2 Flow field

This section discusses the derivation of the flow field of the flow between two moving plates with no net fluid transport. A relative velocity between the two plates will cause a Couette flow which should be counteracted by a Poiseuille flow developed by the counteracting (magnetic) body force. The derivation continues from (5.3) by assuming a flow with only a component in the r-direction and a magnetic field gradient predominantly in the r-direction. This leads to the following relation:

$$\frac{\partial p}{\partial r} = \eta \frac{\partial^2 u_x}{\partial z^2} + \mu_0 M \frac{\partial H}{\partial r} \quad (5.13)$$

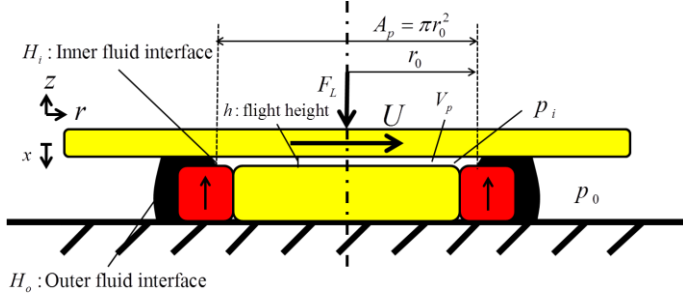


Fig. 5-3. The figure presents a cross section of a pocket bearing consisting of an axially magnetized ring magnet. The plate on top of the magnet and the core of the ring are made out of nonmagnetic material. The material on which the magnets are placed is made out of a ferromagnetic material.

From this relation can be seen that the pressure across the seal that is build up by the magnetic body force is influenced by the viscous effects during translation. For the sake of simplicity, the pressure gradient and magnetic body force are replaced by $\partial p^* / \partial r$.

$$\begin{aligned} \frac{\partial^2 u_x}{\partial z^2} &= \frac{1}{\eta} \frac{\partial}{\partial r} (p - \mu_0 M H) \\ &= \frac{1}{\eta} \frac{\partial p^*}{\partial r} \end{aligned} \quad (5.14)$$

Integrating this relation twice over the flight height leads to the following relation.

$$u_r = \frac{1}{2\eta} \frac{\partial p^*}{\partial r} z^2 + C_1 z + C_2 \quad (5.15)$$

The velocity of the fluid at the static surface should be zero. Applying this no slip boundary condition of $u_r = 0$ at $z = 0$ gives:

$$C_2 = 0 \quad (5.16)$$

The fluid velocity at the moving surface should have the velocity of the moving surface. Applying this no slip boundary condition of $u_r = U$ at $z = h$ gives:

$$\begin{aligned} u_r &= \frac{1}{2\eta} \frac{\partial p^*}{\partial r} h^2 + C_1 h = U \\ C_1 &= \frac{U}{h} - \frac{1}{2\eta} \frac{\partial p^*}{\partial r} h \end{aligned} \quad (5.17)$$

Substituting the values of (5.16) and (5.17) into (5.15) gives the following relation:

$$u_r = \frac{1}{2\eta} \frac{\partial p^*}{\partial r} (z^2 - hz) + \frac{U}{h} z \quad (5.18)$$

Now the value for the magnetic body force is such that there is no net fluid transport under the bearing pads. This means that the value of $\partial p^* / \partial r$ can be calculated by setting the integral of the fluid velocity over the flight height equal to zero.

$$\int_0^h u_r dz = 0 \quad (5.19)$$

The integral can be calculated in the following way:

$$\begin{aligned} \int_0^h \left[\frac{1}{2\eta} \frac{\partial p^*}{\partial r} (z^2 - hz) + \frac{U}{h} z \right] dz &= 0 \\ \left[\frac{1}{2\eta} \frac{\partial p^*}{\partial r} \left(\frac{1}{3} z^3 - \frac{1}{2} h z^2 \right) + \frac{U}{2h} z^2 \right]_0^h &= 0 \\ \frac{1}{2\eta} \frac{\partial p^*}{\partial r} \left(\frac{1}{3} h^3 - \frac{1}{2} h h^2 \right) + \frac{U}{2h} h^2 &= 0 \\ \frac{1}{12\eta} \frac{\partial p^*}{\partial r} h^2 &= \frac{U}{2} \\ \frac{\partial p^*}{\partial r} &= 6 \frac{\eta U}{h^2} \end{aligned} \quad (5.20)$$

Substituting this result in relation (5.17) gives the flow field in-between the two bearing surfaces.

$$\begin{aligned} u_r &= \frac{1}{2\eta} 6 \frac{\eta U}{h^2} (z^2 - hz) + \frac{U}{h} z \\ u_r &= 3 \frac{U}{h} \left(\frac{z^2}{h} - z \right) + 3 \frac{U}{h} \frac{z}{3} \\ u_r &= 3 \frac{U}{h} \left(\frac{z^2}{h} - \frac{2z}{3} \right) \end{aligned} \quad (5.21)$$

From the flow field can be seen that the Couette flow developed by the translation is counteracted by a Poiseuille flow developed by the magnetic body force in such a way that there is no net fluid transport across the bearing length. A graphical representation of the flow field is given in Fig. 5-4.

5.4.3 Friction force

The two forces in the system are the friction force and the magnetic body force. The friction force can be calculated by integrating the shear stress of the fluid over the whole bearing surface. The shear stress in the fluid is defined by the change of velocity of the distance between the bearing surfaces and can be modelled by using the flow field given by relation (5.21). A graphical representation of the shear force in-between the two bearing pads is given by Fig. 5-5.

$$\begin{aligned}\tau_{fric} &= \eta \frac{\partial u_r}{\partial z} = \eta \frac{\partial}{\partial z} 3 \frac{U}{h} \left(\frac{z^2}{h} - \frac{2z}{3} \right) \\ &= 3\eta \frac{U}{h} \left(2 \frac{z}{h} - \frac{2}{3} \right) = 6\eta \frac{U}{h} \left(\frac{z}{h} - \frac{1}{3} \right)\end{aligned}\quad (5.22)$$

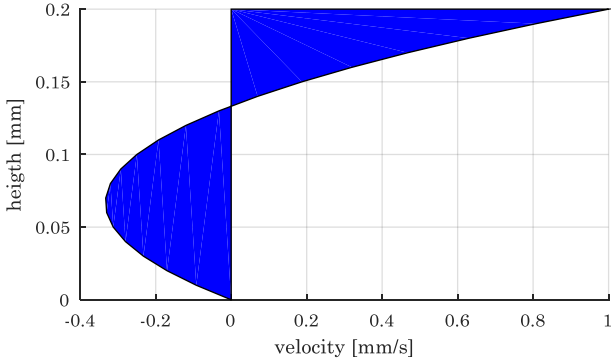


Fig. 5-4. This figure presents the flow field of a ferrofluid bearing during a translational motion. The total area of the surface is zero since the bottom parts is equally large as the upper part which means that there is no net fluid transport.

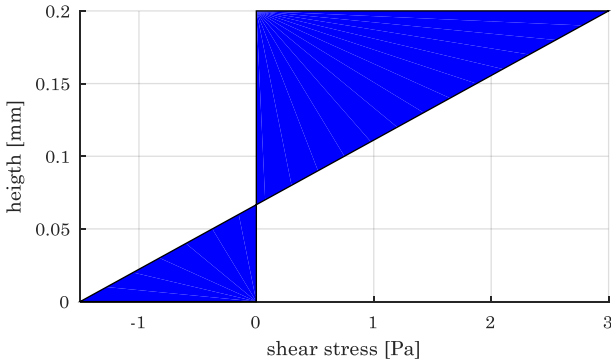


Fig. 5-5. This figure presents the shear stress in-between the two bearing surfaces of a ferrofluid bearing.

The shear force at the surface of the moving bearing is defining the force on the moving surface. The value of this shear force can be calculated for a value of $z = h$.

$$\tau_{fric}(z = h) = 6\eta \frac{U}{h} \left(\frac{h}{h} - \frac{1}{3} \right) = 4\eta \frac{U}{h} \quad (5.23)$$

The friction at the moving surface can be calculated by integrating the shear stress over the area of the bearing surfaces. The shear stress is in this situation not related to the area of the bearing surfaces which means that it can be taken out of the integral.

$$F_{fric} = \int_S \tau_{fric} dA = \tau_{fric} \int_S dA = \tau_{fric} A = 4\eta \frac{U}{h} A \quad (5.24)$$

The damping coefficient in this situation is given by the following relation:

$$c_{trans} = \frac{F}{U} = 4\eta \frac{A}{h} \quad (5.25)$$

With the use of (5.20), the magnetic body force that keeps the fluid on its place can be described with the following relation.

$$F_{body} = \iint_S \frac{\partial P^*}{\partial x} dy dA = 6\eta \frac{U}{h} A \quad (5.26)$$

The balance of the forces is closed with the traction force on the lower surface.

$$F_{trac} = F_{body} - F_{fric} = 2\eta \frac{U}{h} A \quad (5.27)$$

5.4.4 Seal and load capacity with translation

Relation (5.14) showed that the pressure distribution across a seal is influenced by the viscous effect during translation. A model of this effect can be developed by combining this relation with relation (5.20).

$$\frac{\partial}{\partial r} (p - \mu_0 M H) = 6 \frac{\eta U}{h^2} \quad (5.28)$$

Based on the work presented in chapter 4, the pressure across a seal can now be calculated to be:

$$\begin{aligned}\Delta p &= \mu_0 M \Delta H - \int_0^{l_{seal}} 6 \frac{\eta U}{h^2} dr \\ &= \mu_0 M \Delta H - 6 \frac{\eta U}{h^2} l_{seal}\end{aligned}\quad (5.29)$$

In the case of a pocket bearing, the maximum load capacity can be modelled with the following relation:

$$F_L = \mu_0 M \Delta H A_p - 6 \frac{\eta U}{h^2} l_{seal} A_p \quad (5.30)$$

5.4.5 Discussion

The model derived in this paper, using the assumption that there is zero fluid transport out of the fluid seal provides a close correspondence with friction measurements. The damping coefficient derived from this model, given by relation (5.25), seems to be a factor four higher than the damping coefficient given in relation (5.12). This explains that the theoretical prediction of [5] is a factor four off with the measurements. From this can be said that the new model gives an accurate representation of the bearing friction.

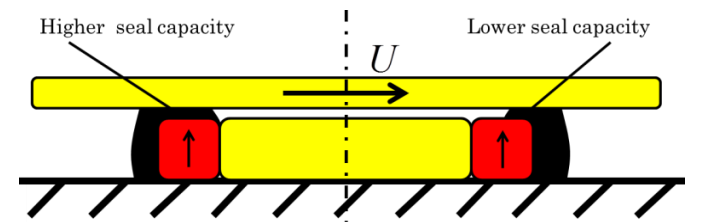


Fig. 5-6. Moving the bearing to the right causes a higher seal capacity at the left and a lower seal capacity at the right. The lowest seal capacity defined the maximum load capacity of the bearing, exceeding this will cause air to escape from the pocket.

The friction model presented in this chapter also shows that the maximum bearing capacity is being reduced by the translational motion of the bearing (see relation (5.30)). The fluid is kept in place by the magnetic body force, but this magnetic body force also provides the load capacity of the bearing. The pressure difference can increase or decrease

depending on the difference in magnetic field and the direction of the translation of the bearing surfaces (Fig. 5-6). When the full potential of the magnetic body force is being utilized for the generation of load, moving the bearing will cause air in the pocket to escape from the seal. In other words, when the seal is already close to escaping translating the bearing will push it over the border of escaping. This also holds for another application which is that of a vacuum throughput using a ferrofluid seal. A translational motion reduces the sealing capacity of the system which may cause air to leak through the seal.

A typical value of the friction force and the pressure across the seal developed by the viscous forces can be calculated with the use of relation (5.20), (5.24) and the parameters presented in Table 1.

$$F_{\text{fric}} = 4 \times 0.15 \frac{0.001}{0.0001} \pi (0.01225^2 - 0.00925^2) = 0.0012 \text{N} \quad (5.31)$$

$$p^* = 6 \frac{0.15 \times 0.001}{0.0002^2} 0.003 = 68 Pa = 0.68 \text{mbar} \quad (5.32)$$

The friction and the pressure difference due to the viscous effects are only small. It is about a factor hundred lower than the pressure difference needed for carrying a load. The viscous effects might become significant when the translational velocity of the bearing is increased.

5.5 Rotational friction

This section discusses the friction when the bearing is being rotated about its central axes due to a torque. First a flow field is derived that is then used for deriving the forces in the system.

5.5.1 Flow field

The derivation continues from (5.3) by assuming a flow with only a component in the tangential direction. It is assumed that the magnetic field has no influence on the flow since pressure could not build up over the tangential contour. It is also assumed that the rotational velocity is low enough to not include the influence of centrifugal forces. Applying these boundary conditions leads to the following equation:

$$\frac{1}{r} \frac{\partial}{\partial r} \left(r \frac{\partial u_\theta}{\partial r} \right) - \frac{u_\theta}{r^2} + \frac{\partial^2 u_\theta}{\partial z^2} = 0 \quad (5.33)$$

By nondimensionalizing the equation it can be seen that the last term of equation (5.33) is the only dominant one since $R^2 \gg Z^2$. The equation now reduces to the following form:

$$\frac{\partial^2 u_\theta}{\partial z^2} = 0 \quad (5.34)$$

By integrating twice, the following relation is obtained:

$$u_\theta = C_1 z + C_2 \quad (5.35)$$

The velocity of the fluid at the static bearing surface should be zero. Applying this no slip boundary condition of $u_\theta = 0$ at $z = 0$ gives:

$$\begin{aligned} u_\theta &= C_1 \cdot 0 + C_2 \\ C_2 &= 0 \end{aligned} \quad (5.36)$$

The fluid velocity at the spinning surface should have the velocity of the moving surface. Applying this no slip boundary condition of $u_\theta = r\omega$ at $z = h$ and substituting the result of equation (5.36) gives:

$$\begin{aligned} u_\theta &= C_1 h = r\omega \\ C_1 &= \frac{r\omega}{h} \end{aligned} \quad (5.37)$$

Relation (5.36) can now be written as:

$$u_\theta = \frac{rz}{h} \omega \quad (5.38)$$

This shows that the flow in-between the two bearing surfaces increases for increasing radius and decreasing spinning height.

5.5.2 Friction torque

The friction torque can be calculated by integrating the shear stress of the fluid over the whole bearing surface. The shear stress in the fluid is defined by the change of velocity over the distance between the bearing surfaces. Relation (5.38) can be used to model the shear with the following relation:

$$\tau = \eta \frac{\partial u_\theta}{\partial z} = \eta \frac{r}{h} \omega \quad (5.39)$$

The torque can be calculated from the shear stress in the following way:

$$\begin{aligned} T &= \iint_S \tau r^2 dr d\theta = \iint_S \eta \frac{r\omega}{h} r^2 dr d\theta = \eta \frac{\omega}{h} \iint_S r^3 dr d\theta \\ &= \eta \frac{\omega}{h} J \end{aligned} \quad (5.40)$$

Using the polar moment of inertia here means that this derivation is also valid for other geometries, as long as the assumptions mentioned earlier are still reasonable. Note that it is important to have a closed loop with near constant radius for this. The damping coefficient for the torque can be expressed with the following formula:

$$c_{\text{rot}} = \frac{T}{\omega} = \eta \frac{J}{h} \quad (5.41)$$

5.5.3 Discussion

The model presented in this section shows that the flow in-between two rotating disks can be described by a Couette flow that increases in magnitude with increasing radius. The model is also suitable for modelling other geometries than a circular ring by using another value for the polar moment of inertia.

Caution must be taken that not all polar moment of inertia shapes are in accordance with the assumptions made. The damping coefficient is a function of only the geometry and the viscosity of the fluid. The flow does not induce any pressure in the fluid which means that it does not influence the load capacity of the bearing. As with the translational friction, the rotational friction of a pressure bearing is higher than that of the pocket bearings, since there is in general a larger surface area of fluid needed to create the same load capacity.

5.6 Trail formation

Moving the bearing leaves behind a trail of ferrofluid that has three effects on the performance of the bearing (Fig. 5-7). The first effect is that the flight height will decrease due to a smaller available amount of fluid for creating lift (see section 4). The flight height has to decrease to keep the same difference in magnetic field across its fluid interfaces. The second effect is that the decrease in flight height will cause an increase in damping since there is a thinner lubrication film present. The third effect is that there is an attracting force between the trail of ferrofluid and the magnet itself which causes a time and path dependent lateral stiffness. These three effects give the bearing a less well defined nonlinear behaviour which is undesirable for controlled systems.

This section presents the flow field of the trail flowing back to the magnet. The section starts with deriving the flow field which will then be used to model the force between the magnet and the trail. A measurement is done on the thickness of the fluid trail to be able to quantify the magnitude of the force and the time constant of the problem.

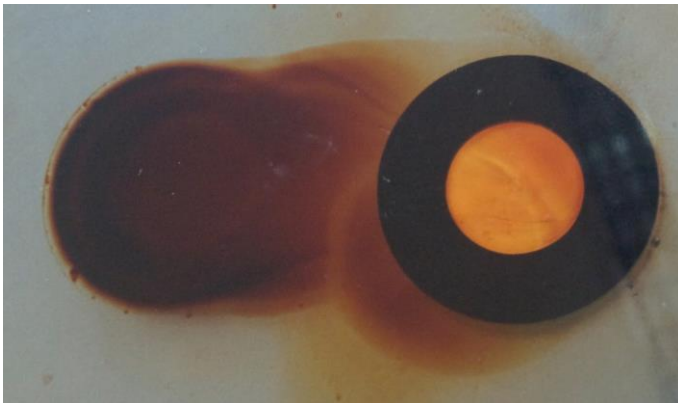


Fig. 5-7. This figure presents the trail formation of a ferrofluid bearing. The picture is made by placing a glass surface on top of this pocket bearing and then displacing it. The picture is taken 20 seconds after the displacement to show that the fluid close to the magnet flows back faster. The bearing is made with the use of an axially magnetized ring magnet.

5.6.1 Flow field

The derivation for the flow field continues from the results presented in relation (5.3). The derivation assumes a flow field with its dominant component in r-direction. Furthermore, it is assumed that the gradient of the magnetic field in r-direction is much larger than the gradient in y- and z-direction. The problem now results in the following relation.

$$\eta \frac{\partial^2 u_r}{\partial z^2} + \mu_0 M \frac{\partial H}{\partial r} = 0 \quad (5.42)$$

Integrating this relation twice gives:

$$u_r = -\frac{1}{2} \frac{\mu_0 M}{\eta} \frac{\partial H}{\partial r} z^2 + C_1 z + C_2 \quad (5.43)$$

There is assumed to be a no slip condition at the static surface, applying this boundary condition of $u_r = 0$ at $z = 0$ results in:

$$0 = -\frac{1}{2} \frac{\mu_0 M}{\eta} \frac{\partial H}{\partial r} 0 + C_1 0 + C_2 \quad (5.44)$$

$$C_2 = 0$$

There is assumed to be a no stress condition at the free surface. Applying this boundary condition of $\partial u_r / \partial z = 0$ at $z = h$ gives the following result:

$$\frac{\partial u_r}{\partial z} = -\frac{\mu_0 M}{\eta} \frac{\partial H}{\partial r} h + C_1 = 0 \quad (5.45)$$

$$C_1 = \frac{\mu_0 M}{\eta} \frac{\partial H}{\partial r} h$$

Substituting the value of (5.44) and (5.45) into (5.43) gives the flow field of the fluid flowing back to the magnet. The profile has the shape of a half Poiseuille flow as can be seen from the visualization presented in Fig. 5-8.

$$u_r = \frac{\mu_0 M}{\eta} \frac{\partial H}{\partial r} \left(hz - \frac{1}{2} z^2 \right) \quad (5.46)$$

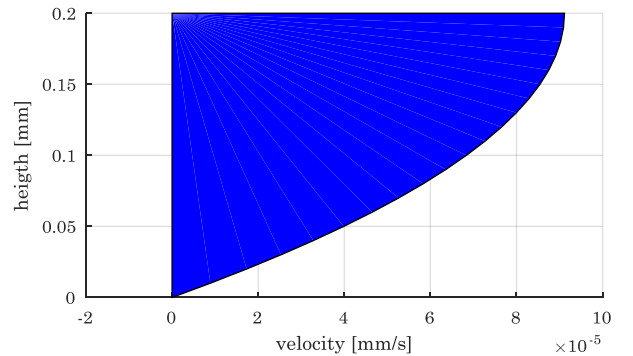


Fig. 5-8. The figure presents the flow profile directly after translating the bearing. The flow presents a half Poiseuille flow such that there is a no stress condition at the free surface and a no slip condition at the bearing surface.

From this a mean velocity of the fluid flowing back can be calculated:

$$\begin{aligned}\bar{u}_r &= \frac{1}{h} \int_0^h u_r dz = \frac{1}{h} \int_0^h \frac{\mu_0 M}{\eta} \frac{\partial H}{\partial r} \left(hz - \frac{1}{2} z^2 \right) dz \\ &= \frac{1}{h} \frac{\mu_0 M}{\eta} \frac{\partial H}{\partial r} \left(\frac{h}{2} z^2 - \frac{1}{2 \cdot 3} z^3 \right) \Big|_0^h \\ &= \frac{1}{h} \frac{\mu_0 M}{\eta} \frac{\partial H}{\partial r} \left(\frac{1}{3} h^3 \right) \\ &= \frac{1}{3} \frac{\mu_0 M}{\eta} \frac{\partial H}{\partial r} h^2\end{aligned}\quad (5.47)$$

Caution must be taken with the fluid height in this formula since it is not constant but dependent on time. The free surface flow causes the fluid height to increase or decrease over time, depending on the shape of the magnetic field. By using conservation of mass, the relation between the flowing back of the fluid and the change in fluid height can be expressed in the following way:

$$\begin{aligned}\frac{\partial u_r}{\partial r} &= -\frac{\partial u_z}{\partial z} \\ \frac{\mu_0 M}{\eta} \frac{\partial^2 H}{\partial r^2} \left(hz - \frac{1}{2} z^2 \right) + \frac{\mu_0 M}{\eta} \frac{\partial H}{\partial r} \frac{\partial h}{\partial r} z &= -\frac{\partial}{\partial z} \frac{\partial h}{\partial t}\end{aligned}\quad (5.48)$$

Nondimensionalizing the terms show that the first and second term are in the same order of magnitude which means that none of them can be neglected. No analytical solution could be found for this problem. A time constant of the problem can be calculated by using the third nondimensionalized term including time.

$$\bar{t} \sim \frac{\eta \bar{r}^2}{\mu_0 M \bar{H} h^2}\quad (5.49)$$

5.6.2 Attracting force

This section discusses the attracting force between the ferrofluid trail and the magnet. This effect causes some undefined behaviour in the system which makes it up to now impossible to use a system without feedback loop. The magnetic field of the magnet induces a body force in the ferrofluid trail such that the magnet and the trail are attracted to each other. The body force can be described with the following relation:

$$f = \mu_0 M \frac{\partial H}{\partial r}\quad (5.50)$$

The actual force can be calculated by integrating the body force over the whole volume of the ferrofluid trail.

$$\begin{aligned}F &= \int_V f dV = \int_{w_1}^{w_2} \int_{r_1}^{r_2} \int_0^h \mu_0 M \frac{\partial H}{\partial x} dy dz \\ &= \int_{w_1}^{w_2} \int_{x_1}^{x_2} \mu_0 M \frac{\partial H}{\partial x} h dx dz\end{aligned}\quad (5.51)$$

5.6.3 Measurement of trail height

This section discusses the measurements done to get an idea of the fluid height of a ferrofluid trail. This is an interesting value since it gives an order of magnitude of the velocity of the fluid flowing back and the force between the magnet and the trail.

The height of the layer of fluid is measured with the setup presented in Fig. 5-9. A glass plate is placed on top of three pocket bearings and a translational movement is performed that creates a square shaped fluid trail. Then the glass plate with the fluid trail is taken from the setup and its weight is measured. The fluid trail causes an increase in weight that can be related to the film height in with the following relation:

$$h = \frac{V}{A} = \frac{m \rho}{A}\quad (5.52)$$

The results of the experiment presented in Fig. 5-10 show the height of the fluid layer to be in the order of $14 \mu\text{m}$.

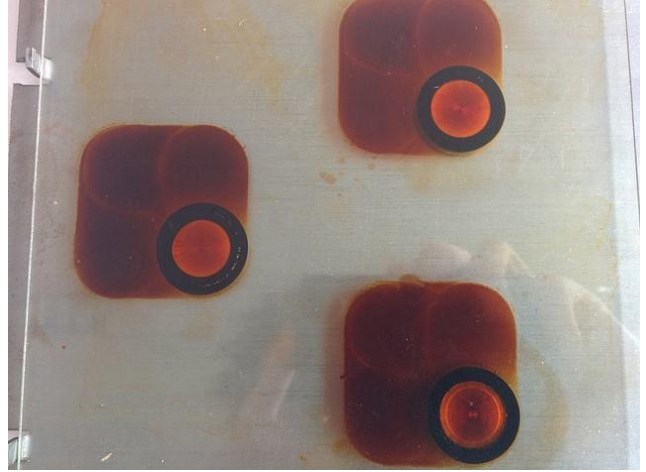


Fig. 5-9. The figure presents a glass plate placed on top of three pocket bearings using the ferrofluid APG513A. Translating the plate causes a trail of ferrofluid. By making the movement sufficiently large (1cm/s in this case) makes a uniform trail. The height of the trail can be measured by weighing the plate with and without ferrofluid trail. New ferrofluid was added to the plate when it was notices that the glass plate began to touch the magnets.

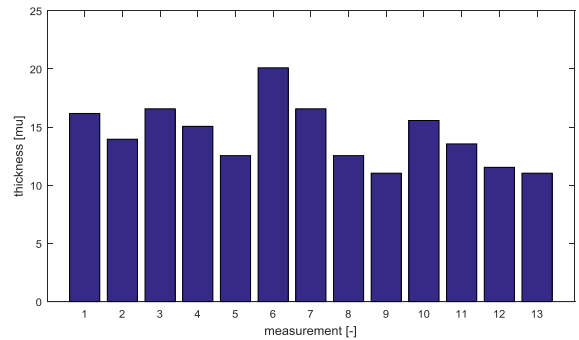


Fig. 5-10. The graph presents the measured height of the experiment. New ferrofluid was added to the magnets in-between experiment 2 and 3, 5 and 6, 9 and 10. The data show the height of the fluid to be in the order of $14 \mu\text{m}$. New ferrofluid was added to prevent the bearing surfaces from touching.

5.6.4 Discussion

The derivation of the flow field shows that the field is dependent on position and time. No general analytical solution could be given for the field. It is possible to describe the flow field just after it is initiated since it has a constant film height at that moment. Calculating the time constant of this problem using relation (5.49) and the data presented in Table 1 gives a value in the order of seconds. This corresponds with observations done during the experiments.

$$\begin{aligned} \bar{t} &\sim \frac{0.15 \times (5 \times 10^{-3})^2}{4\pi \times 10^{-7} \times 32 \times 10^3 \times 1 \times 10^5 \times (15 \times 10^{-6})^2} \\ &\sim 4\text{s} \end{aligned} \quad (5.53)$$

Relation (5.51) shows that there is a path and time dependent force between the trail of ferrofluid and the magnet. This makes it difficult to predict the force during operating which makes it difficult to use this in a system without proper control. The effect can be mitigated by using a (PID based) feedback loop since this has the capacity to handle unknown effects in a system. The force is easier to predict for the moment just after the trail is created since the flow field is precisely known at that moment. This makes it interesting to implement the effect into a feedforward system to reduce the settling time. The effect of flowing back, with its long time constant, could be mitigated by a feedback loop. The trail formation that has a short time constant could be mitigated with a feedforward system. An order of magnitude of the force between the trail and the magnet can be calculated by assuming a magnetic field gradient only in r-direction, a square shaped fluid trail, the fluid height measured in Fig. 5-10 and the data from Table 1.

$$\begin{aligned} F_{\text{trail}} &= \mu_0 M \frac{\partial H}{\partial r} h x w \\ &= 4\pi \times 10^{-7} \times 32 \times 10^3 \frac{1 \times 10^5}{0.005} 14 \times 10^{-6} \times 0.02 \times 0.02 \\ &= 0.0045\text{N} \end{aligned} \quad (5.54)$$

Two different strategies can be chosen to achieve a constant flight height. One possibility is to make a large fluid reservoir to make sure that the trail formation has a negligible effect on the amount of fluid that is available for creating lift. The other possibility is placing the outer fluid interface at a location with a high gradient in magnetic field. The high gradient causes a high body force on the fluid that prevents it from trailing away. Fig. 5-10 gives a demonstration of this effect by showing a reduction in

measured flight height in every series. This decrease can be attributed to the movement of the outer fluid interface towards a region with higher magnetic field gradient.

5.7 Conclusion

The ferrofluid bearing is an interesting component to be used in systems where precise positioning is important. The friction behaviour of this type of bearing was up to now only poorly described and is important since it has a lot of influence on the design of the system. The models presented in this paper help to generate a better understanding on how the different parameters influence the final performance of the system. The presented models describe the viscosity, the translational friction, the rotational friction and the trail formation of the bearing.

It is shown that the influence of rotational viscosity is limited to an increase of around 10%. The effect of particle chain formation is negligible if all suspended particles have a dipolar interaction parameter λ smaller than one. The derivations show that the translational friction can be modelled by the summation of a Couette flow and a Poiseuille that have magnitudes in a way that no net fluid transport occurs along the length of the bearing. As a result the maximum load capacity of a ferrofluid pocket bearing becomes a function of the bearing velocity since a part of the magnetic force is used for keeping the fluid in place. This holds also for the seal capacity of a vacuum throughput. A translational motion lowers the sealing capacity of the system. The load capacity of a pressure bearing is unaffected by the translational motion, since no seals are used there. The friction model also demonstrates that a ferrofluid pressure bearing has a higher friction than a ferrofluid pocket bearing since it has in general a higher fluid surface area. The friction model is not only useful for bearings, but also for other systems like loudspeakers using ferrofluid. The derivation of the rotational friction shows that the maximum load capacity of a ferrofluid pocket bearing is not influenced by the rotational velocity of the bearing. The model of the trail formation demonstrates that this is a process depending on the path that the bearing has travelled and time. The numbers calculated for the friction force and trail formation force show that they are in the same order of magnitude. This demonstrates that both effects should be taken into consideration when designing a ferrofluid bearing.

6 Discussion

6.1 General discussion of results

The research on different bearing concepts discussed in literature showed that a ferrofluid bearing is an interesting concept to use in systems where fast and precise positioning is important (chapter 3). The bearing distinguishes itself from other bearing concepts by its price, compactness, inherent stability, low (viscous) friction, absence of pumps and absence of stick-slip. The magnetic properties make it possible to use hydrostatic and hydrodynamic bearings without the use of pumps or seals and without the risk of leakage. Almost all demonstrators discussed in literature failed to link the actual performance to theoretical models. This demonstrates that if one is interested in designing a bearing on the basis of this concept, one has no information at all on how to configure the system to meet desired specifications. The goal of the research was therefore set to derive methods and models that help to link the expect performance from literature with the observations done in practice. The discussion is split into four different parts that are discussed below.

6.1.1 Ferrofluid properties

A literature research is done to map the different properties of ferrofluids (chapter 2). This shows that a colloidal stability in the fluid can be maintained by making sure that the magnetic energy, the gravitational energy and the dipolar interaction energy stay in the same order of magnitude as the thermal energy. A surfactant is also added to the particles to make sure that no aggregation can happen due to the van der Waals forces (Fig. 6-1). The magnetization of the fluid can be taken as a constant since it has a low relative permeability and a low saturation magnetization (Fig. 6-2). The interaction of the particles with the magnetic field has some influence on the viscosity of the fluid; the effects can be divided in the rotational viscosity and the particle chain formation. The rotational viscosity is in general only small for a ferrofluid ($\sim 10\%$), but the particle chain formation can have a large effect since it has been showed that only a small fraction of larger particles in the fluid can have a large increase in viscosity due to this effect. If this effect is undesirable it is wise to choose a fluid that has complete absence of these large particles.

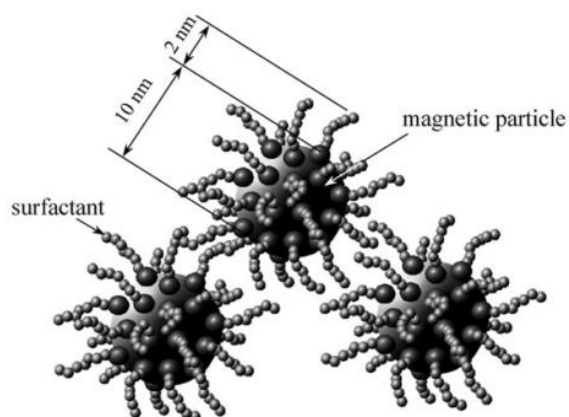


Fig. 6-1: The particles in ferrofluids are coated with a surfactant of long polymer chains to prevent the particles sticking to each other due to van der Waals forces. Figure from [27]

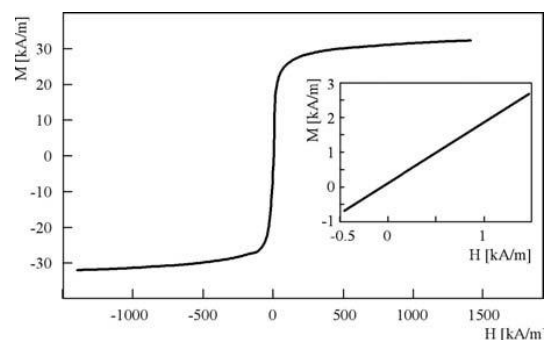


Fig. 6-2. Typical magnetization curve of a ferrofluid. The curve shows that the ferrofluid has a saturation magnetization $M_s \approx 30 \times 10^3 \text{ A/m}$. The box at the bottom right shows a zoomed in part from which the relative permeability can be calculated to be around $\mu_r \approx 2$. Figure from [29]

6.1.2 Load and stiffness

Chapter 4 of the thesis discusses the out-of-plane load and stiffness model of a ferrofluid pocket bearing and a ferrofluid pressure bearing. The main emphasis is put on a ferrofluid pocket bearing since this has a larger load capacity and larger stiffness (Fig. 6-3). A method is derived that is capable of describing the load and stiffness specifications of any shape of ferrofluid bearing. This method is used to derive a model of a ring shape pocket bearing that is validated by experiments (Fig. 6-5). This validation demonstrates the validity of the method that is used for deriving the model. The out-of-plane stiffness of the bearing can be calculated back to a linearized Young's modulus of the bearing which can be used to calculate the rotational stiffness of the bearing.

Based on this new knowledge a sandwich like bearing concept is configured that is particularly interesting because of its higher load, stiffness and repeatability (Fig. 6-4). Again based on the method a model is derived that is validated by experiments. This demonstrates how the method can be used to design a bearing according desired load and stiffness requirements. Also a damping model is derived that models the out-of-plane damping of a ferrofluid bearing (appendix B). This model is not yet validated, but seems valid since it is basically based on the same assumptions as the friction model that is validated in chapter 5.

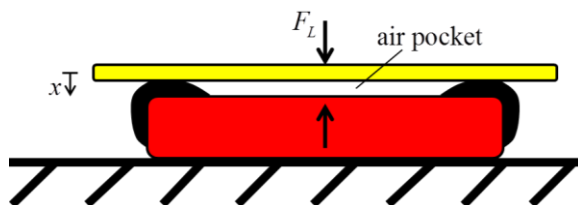


Fig. 6-3. The figure presents a cross section of a disk shaped magnet. The ferrofluid is attracted to the corners of the magnet because the field intensity is highest there. The ferrofluid forms a seal that encapsulates a pocket of air. The air pocket increases the load capacity of the bearing since the pressure is defined by the largest value of magnetic field intensity which is at the corner of the magnet.

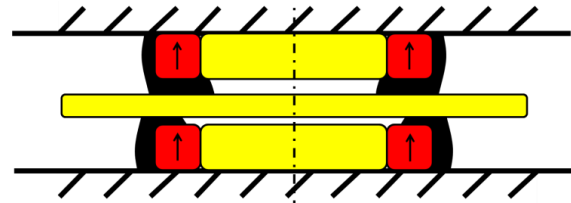


Fig. 6-4. The cross section in the figure presents the fluid interfaces at a deformed configuration. It can be seen that there is a slight movement at the outer interfaces, but this influence is minimal since they are located at a position with low magnetic field gradient. This demonstrates that the load capacity for this concept is predominantly defined by the change of the inner interfaces.

During the experiments it is observed that the magnetization of the fluid changes in time (appendix E). It seems likely that this is caused by a change of concentration in magnetic particles due to diffusion caused by the magnetic field gradient. The observations done during the experiments could not be linked to a theoretical model. The modelled diffusion shows a much higher diffusion than observed in the experiments.

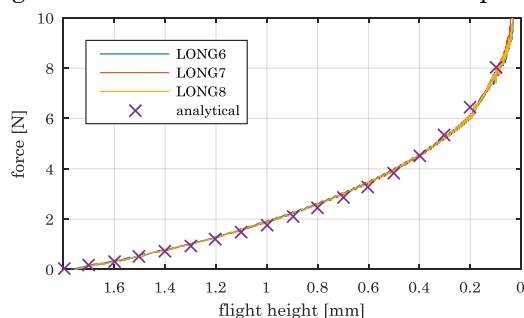


Fig. 6-5. Compressing the bearing will cause air to escape from the seal because the pressure in the pocket of air becomes larger than the pressure that can be counteracted by the seal. The first three datasets in the figure are three different measurements that show that the maximum load curve of the bearing has a high repeatability. The fourth dataset is the result from the theoretical model of this process. The figure shows that the model fits the measurements well.

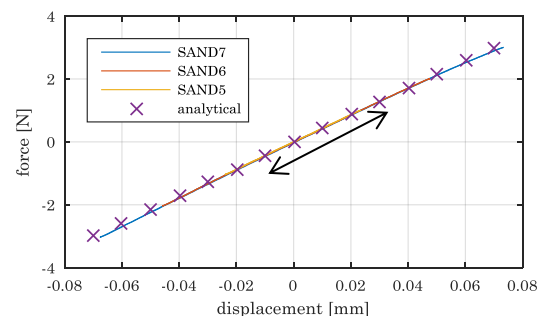


Fig. 6-6. This figure presents the force of the bearing as function of the displacement. Three different measurements are presented from which can be seen that there is no hysteresis and a high repeatability.

6.1.3 Friction

Chapter 5 of this thesis discusses the friction and trail formation of the bearing. In literature it is found that the friction of the bearing is modelled by a viscous damper model that assumes a Couette flow in-between the two bearing pads. The friction values based on this model were about a factor of four off compared to the friction values measured during experiments. In this research it was shown that this difference is caused by a wrong assumption in the flow field. The Couette flow assumes a net fluid transport in-between the bearing pads which is incorrect. A model is derived that shows that the flow is a summation of a Couette flow and a Poiseuille flow, that are such in magnitude, that there is no fluid transport across the length of the bearing. A model is derived that show that the translational friction can be modelled by the summation of a Couette flow and a Poiseuille that have magnitudes in a way that no net fluid transport occurs along the length of the bearing (Fig. 6-7).

This new model is a factor of four off with the old model which means that it is in accordance with the measurements done during experiments. This new model also demonstrates that translating the bearing reduces the load capacity of a ferrofluid pocket bearings since a part of the magnetic body force is used for keeping the fluid on its place (Fig. 6-8).

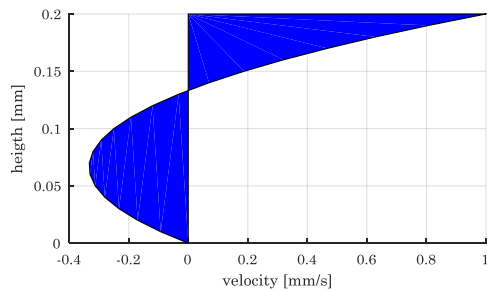


Fig. 6-7. This figure presents the flow field of a ferrofluid bearing during a translational motion. Integrating the blue surface shows a zero net fluid flow that is observed during translation.

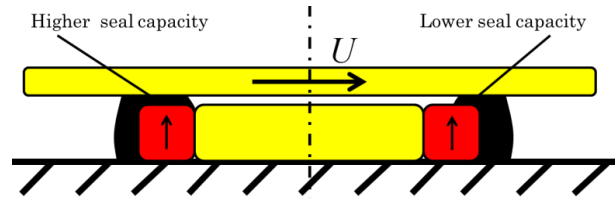


Fig. 6-8. Moving the bearing to the right causes a higher seal capacity at the left and a lower seal capacity at the right. The lowest seal capacity defined the maximum load capacity of the bearing, exceeding this will cause air to escape from the pocket.

Translation of a ferrofluid bearing leaves behind a trail of ferrofluid caused by the adhesive force between the ferrofluid and the moving surface. This trail causes a path and time dependent force in the direction of where it came from. The trail has a thickness of around $\sim 10\mu\text{m}$ from which it can be shown that the force is in the same order of magnitude as the friction force. This means that the force cannot be simply ignored and should be taken into account in the design of the bearing system. The process is hard to describe since it is dependent on the path and time, but the process can be mitigated by a proper designed feedback loop since it has the capacity of handling uncertainties in the system.

6.1.4 Comparison with other bearing concepts

The ideal bearing can be defined by having sufficient load, a maximum out-of-plane stiffness with sufficient damping while having negligible in-plane stiffness and sufficient in-plane damping. Of course no system can meet this, which makes it a challenge to come as close to it as possible. For fast and precise positioning it is desired to have viscous friction only, which means that a bearing concept is preferred that does not show any coulomb friction and stick-slip since these effects are difficult to mitigate [65]. The different concepts, that can be chosen to achieve this, are in general summarized to be air (fluid) bearings and magnetic bearings. A drawback of these systems in general is that they are all relatively expensive. This thesis shows that the ferrofluid bearing is an interesting bearing to add to this list, as being a simple and cheap solution (only magnet and ferrofluid) to achieve complete absence of coulomb friction and stick-slip.

6.2 Discussion on bearing configuration for precise positioning

This section discusses how the new knowledge of this thesis can be used to configure a ferrofluid bearing used for precise positioning. The section is divided in small discussions considering what should be done to get the desired performance on different specifications. The end of the section contains a brief comparison between the two ferrofluid concepts.

6.2.1 Pressure bearing: Load

The pressure bearing gets its load capacity solely from the magnetic fluid that is subjected to a magnetic field. The load can be calculated by integrating the pressure distribution over the carrying surface, which is known for a known magnetic field. The load of a ferrofluid pressure bearing is described by the following relation:

$$F_L = \mu_0 M \int_S H(r) dA \quad (5.55)$$

From this formula can be concluded that high load capacity is generated by having a large fluid contact area at the carrying surface, a large magnetic field strength at the carrying surface and a low magnetic field strength at the outer fluid interfaces.

6.2.2 Pressure bearing: Stiffness

Stiffness is created by the change in magnetic pressure at the load carrying surface, which is defined by the magnetic field gradient in the direction of the displacement and the magnetic field gradient at the outer fluid interface. The stiffness of a ferrofluid pressure bearing is described by the following relation:

$$k_{ff} = \mu_0 M \frac{d}{dx} \int_S H(r) dA \quad (5.56)$$

A high load stiffness can be generated by having a large fluid contact area at the carrying surface, a large magnetic field gradient in the out-of-plane direction at the carrying surface and a large magnetic field gradient in the in-plane direction at the outer fluid interfaces.

6.2.3 Pocket bearing: Load

The pocket bearing gets its load capacity from the pocket of air (or any other nonmagnetic fluid) that is encapsulated by a ring of magnetic fluid. The load is carried by air that transfers the force to the magnetic fluid seal.

$$F_L = (p_i - p_o) A_p = \mu_0 M (H_i - H_o) A_p \quad (5.57)$$

To have a high load capacity it is important to have a high magnetic field strength located at the magnetic fluid seal, and a large surface area of the bearing. A higher magnetic field strength can be obtained by decreasing the flight height since the magnetic field intensity close to the magnet is higher. Caution must be taken when moving the bearing since this motion decreases the maximum load capacity of the bearing. A part of the pressure induced by the magnetic field is needed for keeping the fluid in-between the bearing surfaces. The relation for the reduce in seal capacity is given by the following relation:

$$\Delta p = \mu_0 M \Delta H - 6 \frac{\eta U}{h^2} l_{seal} \quad (5.58)$$

To minimize these effects it is wise to make a short seal length, use a low viscosity fluid, increase the velocity not too much and have a large flight height. Caution must be taken with increasing the flight height since this also decreases the stiffness and load capacity of the system.

6.2.4 Pocket bearing: stiffness

The stiffness of this type of bearing is created by the change in pressure across the ferrofluid seal, which is defined by the magnetic field gradient in the direction of the displacement of this seal. The displacement of this seal is defined by the displacement of the carrying surface that is amplified by using the pocket of air (pneumatic leverage). The stiffness and pneumatic leverage of this bearing are described by the following relations:

$$k_{ff} = \mu_0 M A_p \frac{d(H_i - H_o)}{dr_{in}} \frac{dr_{in}}{dx} \quad (5.59)$$

$$\frac{dr_{in}}{dx} = \sqrt{\frac{V_p}{4\pi(h-x)^3}} \quad (5.60)$$

From these relations it can be concluded that a high bearing stiffness is obtained by having a stiff seal and a high pneumatic leverage. A stiff seal can be created by having a high gradient in magnetic field strength at the location of the seal. A high pneumatic leverage can be obtained by making a pocket that has a large carrying surface and a small flight height. This has as an additional effect that it has a small contact area with the sliding surfaces that causes a relative low in- and out-of-plane damping.

6.2.5 Pocket bearing: pocket volume control

Overloading the bearing may cause air to escape from the bearing which results in a smaller pocket volume. Fig. 4-18 on page 33 presents the stiffness curve for a couple of pockets with the same radius, but different film height. A defined pocket of air and a defined stiffness region can be realized by overloading the bearing with a known force or displacement. This principle can also be used to prevent air escaping by building a physical stop to realize a certain maximum displacement. The load and stiffness may be increased by making multiple sealing steps in the bearing, though caution must be taken to not make any capillary connection between the seals. This connection will cause fluid to flow between the two seals causing only the most inner and outer interface to contribute to the load and stiffness.

6.2.6 Magnetic field

For both concepts it is of importance to know the magnetic field since it has a lot of influence on the final behaviour of the bearing. The shape of the field and the fluid volume will define the shape of the ferrofluid film in-between the two bearing surfaces. In the case of a pressure bearing, there must be a high magnitude and gradient in the magnetic field at the carrying surfaces to achieve a high load capacity and stiffness. In the case of a pocket bearing the shape must be such that a seal can be formed to encapsulate a pocket of air. The magnetic field at the seals must have a high magnitude and a high gradient to achieve a high load and stiffness. This knowledge on the field can be generated with computer calculations or gathered from literature like [66]–[68].

6.2.7 Damping

Appendix C discusses a model for the squeeze film damping of a ferrofluid bearing. When the two bearing surfaces move towards each other, the fluid in-between is squeezed to the outside

causing a reaction force. In the case of round shaped fluid pads, it can be modelled by the following relations.

$$c_{pres} = \frac{F}{u} = -\frac{3\pi\eta R_o^4}{2h^3} \quad (5.61)$$

$$c_{pocket} = \frac{F}{u} = -\frac{3\pi\eta(R_o^4 - R_i^4)}{2h^3} \quad (5.62)$$

The first relation describes the squeeze flow damping of the pressure bearing and the second relation describes the squeeze flow damping of the pressure bearing. The relations show that the damping increases with the bearing radius and the viscosity and decreases with the flight height. The pocket bearing has in general a lower damping since the core of the pockets does not contribute to the damping.

6.2.8 Friction and Trail formation

The friction of a ferrofluid bearing can be modelled by the summation of a Couette flow and a Poiseuille that have magnitudes in a way that no net fluid transport occurs along the length of the bearing. The friction for both the ferrofluid pocket and pressure bearing can be modelled by the following relation:

$$F_{fric} = 4\eta \frac{A}{h} U \quad (5.63)$$

It can be concluded from the relation that the friction force increases with viscosity, surface area and velocity and decreases with the flight height. The ferrofluid pocket bearing will in general have a lower friction value compared to the pressure bearing since it has a lower surface area for the same amount of load carrying capacity.

The trail formation can be mitigated with two different strategies. The first strategy is making the magnetic field gradient at the outer fluid interface such that almost all fluid is pulled back instantly. The second strategy is making a fluid reservoir at the outer fluid interface such that the trail of fluid has a negligible influence on the displacement of the outer fluid interface.

6.2.9 General overview

According to the discussion done in this section, a brief overview can be generated to give a comparison between the performances of the two different concepts in general. The pressure bearing is taken as a benchmark.

Table 2: Comparison pressure bearing and pocket bearing

Specification	Pressure bearing	Pocket bearing
Load	0	+
Stiffness	0	+
Friction	0	+
Trail formation	0	0
Repeatability in height	0	-

7 Conclusion and recommendation

7.1 General conclusions

This thesis discussed different properties of a ferrofluid pocket bearing that are interesting for systems that require precise positioning. A problem of this bearing was that it was unclear how a certain configuration led to the final performance of the bearing. The goal of this research was set to develop more knowledge on this and to come with some recommendations for a good bearing configuration for precise positioning. The sections below present a brief summation of the most important conclusions from the research.

7.1.1 Literature

The main conclusions according to the information found in literature can be summarized by the following bullets:

- C1. The ferrofluid pocket bearing is an interesting application to be used for applications that desire fast and precise positioning.
- C2. A ferrofluid bearing can be seen as a hydrostatic bearing without the need of pumps and seals.
- C3. No stick-slip effects are seen in a ferrofluid bearing.
- C4. No knowledge is available to derive a model that fits experimental results.
- C5. The ferrofluid pocket bearing is an interesting application to be used in bearing systems that have complete absence of gravity.
- C6. The influence of rotational viscosity on the viscosity of the fluid is only small ($\sim \eta_0 \times 0.1$).
- C7. The influence of particle chain formation on the viscosity of the bearing can be large even when the ferrofluid only has a small concentration of large particles in the fluid ($\sim \eta_0 \times 50$).
- C8. A ferrofluid bearing and a Lorenz actuator can be integrated into one system.
- C9. Trail formation has a lot of influence on the height reproducibility.
- C10. Ferrofluid bearings can be divided into two different concepts, pocket bearings and pressure bearings.

7.1.2 Load and stiffness

The main conclusions that can be taken from the research on the load and stiffness behaviour of the bearing can be summarized by the following bullets.

- C11. A ferrofluid pocket bearing has in general a higher load capacity and a higher stiffness than a ferrofluid pressure bearing.
- C12. A ferrofluid pocket bearing has in general a lower damping than a ferrofluid pressure bearing.
- C13. The method proposed to describe the load and stiffness behaviour of the bearing showed to be correct.
- C14. The findings give a better understanding on how to design a bearing according to some desired specifications concerning load and stiffness.
- C15. The magnetic field in-between two nearby magnets can be modelled with the summation of two parabolic functions forming a saddle point.
- C16. The ferrofluid bearing also works in the absence of gravity.
- C17. Trail formation reduces the flight height of the bearing due to a smaller difference in magnetic field across the ferrofluid seal.
- C18. The method proved to be able to explain that trail formation can cause a permanent change in flight height due to air escaping that causes a reduced maximum load capacity.

7.1.3 Friction behaviour

The main conclusion that can be taken from the research on the friction behaviour of the bearing can be summarized by the following bullets.

- C19. The friction model presented in literature was wrong due to the assumption of having net fluid transport over the length of the bearing.
- C20. The flow in-between the two bearing pads can be modelled with a summation of a Poiseuille flow and a Couette flow
- C21. The Couette flow and the Poiseuille flow are such in magnitude that there is no fluid transport over the length of the bearing
- C22. The findings give a better understanding on how to design a bearing according to some desired specifications concerning the friction behaviour.
- C23. The friction model is also applicable for other systems like the damping of a loudspeaker using ferrofluid.
- C24. A translational motion reduces the seal pressure capacity.
- C25. The trail formation is path and time dependent
- C26. The flow field of the trail formation can be modelled with a half Poiseuille flow having a no stress condition at the free surface
- C27. The ferrofluid bearing is an interesting concept to be used as a cheap and simple system to avoid stick-slip.

7.2 Recommendations for future research

The recommendations are split into five different parts. The first part discusses some general recommendations of the project. The second part discusses a possible master project that demonstrates a new system based on the new knowledge gained in this research. The third part discusses a potential master project on more research on the friction models and more validation on the models that already exist. The fourth section discusses another potential master project in which systems using ferrofluid is modelled. The fifth section discusses some recommendations for the PhD project on ferrofluid in the maritime sector that starts in January.

7.2.1 General recommendations

- R1. Extend to electrorheological fluids (same theories should be applicable for these fluids).
- R2. Use a ferrofluid bearing for a bearing with three rotational degrees of freedom.
- R3. Investigate what parameters influence the air popping out of the seal.

7.2.2 Ferrofluid bearing demonstrator stage (master thesis)

- R4. Use the derived models to design a new version of the microscopy stage[58], [59], [62].
- R5. Integrate the sandwich like pocket bearing concept with an actuator.
- R6. Investigate the application of electrically conductive ferrofluid[69].

7.2.3 Ferrofluid bearing fundamentals (master thesis)

- R7. Investigate the potential of hydrophobic or oleophobic coatings since they might reduce the trail formation due to a reduced adhesion force.
- R8. Improve the friction model by investigating the validity at high frequencies.
- R9. Improve models of trail formation.
- R10. Experimental validation of rotational friction model.
- R11. Experimental sanity check to check validity of translational friction model.
- R12. Experimental validation of damping model.

- R13. Investigate the influence of the actuator on the behaviour of the bearing.
- R14. Make an accurate model of the bearing (load capacity, but also damping and friction) that can be used for optimization.
- R15. Water compatible ferrofluid to fill gap with fluid to increase the stiffness.

7.2.4 Ferrofluid FEM modelling (master thesis)

- R16. Model ferrofluid in a FEM analyses, challenge is to properly model the air/fluid/solid/magnetic interface. Not much is written about this subject in literature.
- R17. Implement the ferrofluid viscosity model in a FEM analyses.
- R18. Model the diffusion of magnetic particles.
- R19. Model bearings that use the viscosity of a ferrofluid to create levitation.

7.2.5 Ferrofluid in the maritime sector (PhD thesis)

- R20. Study of the properties of oil-based and water-based ferrofluid in combination with (sea) water and/or lubrication oil.
- R21. Investigate the potential to use a ferrofluid seal in a maritime environment.
- R22. Develop and/or find water compatible ferrofluid.
- R23. Investigate the potential and the difficulty of making ferrofluid in-house.
- R24. Study the variable viscosity of ferrofluid in hydrostatic and hydrodynamic bearings.
- R25. Investigate the gain of using a ferrofluid for the hydrostatic regime at low velocity in a hydrodynamic bearing.
- R26. Model a hydrodynamic bearing using a ferrofluid.
- R27. Study the boundaries of ferrofluid stability.

A Useful relations for ferrofluid bearing design

Below a summation of relations is presented that are derived during this project for the use in the design of a ferrofluid bearing. The meaning of the symbols can be found in the beginning of this thesis on page vii or in Fig. 7-1 and Fig. 7-2.

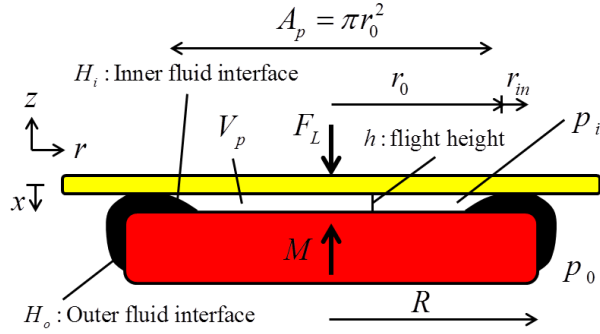


Fig. 7-1: Different symbols used in the relations for the ferrofluid pocket bearing.

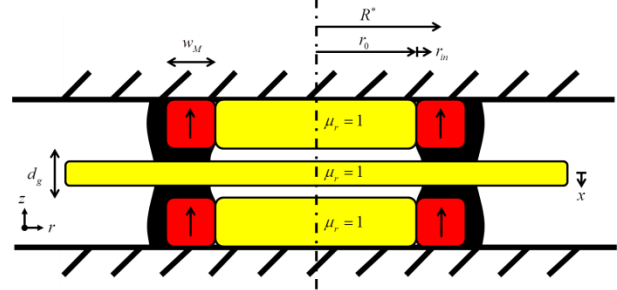


Fig. 7-2: Different symbols used in the relations for the ferrofluid bearing with a sandwich structure using ring magnets.

Viscosity increase due to rotational viscosity:

$$\eta_{\max} = \eta_c (1 + 4\tilde{\phi}) \quad (\text{A.1})$$

Navier-Stokes equation for an incompressible magnetic fluid:

$$\rho \left(\frac{\partial \underline{u}}{\partial t} + \underline{u} \cdot \nabla \underline{u} \right) = -\nabla p + \mu \nabla^2 \underline{u} + \underline{f} + \mu_0 M \nabla H \quad (\text{A.2})$$

$$\nabla \cdot \underline{u} = 0$$

Load of a pocket bearing:

$$F_L = (p_i - p_0) A_p = \mu_0 M (H_i - H_o) A_p \quad (\text{A.3})$$

Load capacity of pressure bearing:

$$F_L = \mu_0 M \int_S H(r) dA \quad (\text{A.4})$$

Stiffness of a pocket bearing:

$$k_{ff} = \mu_0 M A_p \frac{d(H_i - H_o)}{dr_{in}} \frac{dr_{in}}{dx} \quad (\text{A.5})$$

Pneumatic leverage for cylindrical shaped pocket bearing:

$$\frac{dr_{in}}{dx} = \sqrt{\frac{V_p}{4\pi(h-x)^3}} \quad (\text{A.6})$$

Stiffness of a pressure bearing:

$$k_{ff} = \mu_0 M \frac{d}{dx} \int_S H(r) dA \quad (\text{A.7})$$

Stiffness of the volume of the pocket:

$$k_{air} = \left(\frac{V_i}{V_x} \right)^\gamma p_i \gamma \frac{A_p}{h-x} = \left(\frac{h}{h-x} \right)^\gamma p_i \gamma \frac{A_p}{h-x} \quad (\text{A.8})$$

Rotational stiffness of the bearing:

$$k_{rot} = \mu_0 M \frac{d(H_i - H_o)}{dr_{in}} \frac{dr_{in}}{dx} I \quad (\text{A.9})$$

Load of a sandwich structure pocket bearing using ring shaped magnets:

$$F_L = 2\mu_0 M H_{\max} \frac{\pi (R^* - r_0) r_0^3}{(f_{fit,x} w_m)^2 h} x \quad (\text{A.10})$$

Stiffness of a sandwich structure pocket bearing using ring shaped magnets:

$$k_{sand} = 2\mu_0 M H_{\max} \frac{\pi (R^* - r_0) r_0^3}{(f_{fit,x} w_m)^2 h} \quad (\text{A.11})$$

Translational friction of a ferrofluid bearing:

$$F_{fric} = 4\eta \frac{A}{h} U \quad (\text{A.12})$$

Translational damping constant of a ferrofluid bearing

$$c_{trans} = 4\eta \frac{A}{h} \quad (\text{A.13})$$

Load capacity of ferrofluid pocket bearing with including translation:

$$\Delta p = \mu_0 M \Delta H - 6 \frac{\eta U}{h^2} l_{seal} \quad (\text{A.14})$$

Rotational friction of a ferrofluid bearing:

$$T = \eta \frac{J}{h} \omega \quad (\text{A.15})$$

Rotational damping of a ferrofluid bearing:

$$c_{rot} = \frac{T}{\omega} = \eta \frac{J}{h} \quad (\text{A.16})$$

Time constant of trail formation:

$$\bar{t} \sim \frac{\eta \bar{r}^{-2}}{\mu_0 M H h^2} \quad (\text{A.17})$$

B Ferrofluid pressure bearing

A ferrofluid pressure bearing is a type of bearing that does not use a pocket of air to carry a load; the load capacity is purely generated by the pressure induced in the ferrofluid due to an external magnetic field. This appendix derives from the work presented in chapter 4, the relations for the load capacity F_L and stiffness k_{ff} of this type of bearing. The load capacity of the bearing can be calculated with the use of relation (4.3) by integrating the pressure distribution over the whole contact area of the ferrofluid.

$$F_L = \int_S p(r) dA = \mu_0 M \int_S H(r) dA \quad (\text{B.1})$$

The stiffness of the bearing can be modelled by deriving the force over its displacement. In the case of a bearing that uses no pocket for carrying the load it can be described by the following relation:

$$k_{ff} = \frac{dF_L}{dx} = \mu_0 M \frac{d}{dx} \int_S H(r) dA \quad (\text{B.2})$$

Comparing the results of these relations with those of the pocket bearing discussed in chapter 4 leads to the conclusion that the pocket bearing has in general a higher load capacity, a higher stiffness and a lower friction. Fig. 7-3 and Fig. 7-4 give the pressure distribution of respectively a pressure bearing and a pocket bearing. From the comparison can be seen that the pocket bearing has a higher load since it is predominantly defined by the peaks in pressure instead of the whole distribution. A higher load capacity for the same displacement also means that the pocket bearing has a higher stiffness. The lower friction of the bearing is caused by the lower surface area of the fluid since there is only fluid at the outside of the magnet.

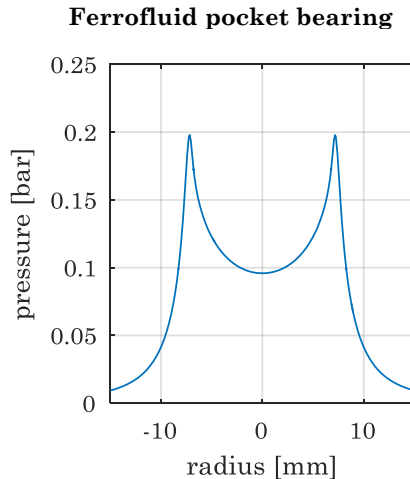


Fig. 7-3. This figure describes the modelled pressure distribution of a ferrofluid pressure bearing using the magnet presented in Fig. 4-2 at a 0.2mm distance from the surface. The figure shows that the pressure distribution follows the shape of the magnetic field.

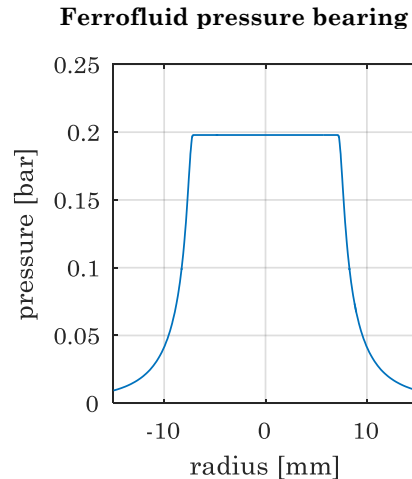


Fig. 7-4. This figure describes the modelled pressure distribution of a ferrofluid pocket bearing with the same configuration as Fig. 7-3. The figure shows that the pressure distribution is predominately defined by the height of the pressure peaks.

C Damping

This appendix presents the work done on the damping model of a ferrofluid pocket bearing. The damping is defined as the force needed to change the distance between the two bearing faces with a certain velocity. This is an important parameter in the systems since it influences the dynamics like oscillation time, response time and vibrational stability. This damping is developed by the squeeze flow in-between the two bearing surfaces when they move towards or away from each other. A model of this is generated by the use of the Reynolds equation and is inspired by the work of [70].

This appendix does not present an accurate damping model, but it does provide a model from which some good understanding could be generated. The first paragraph presents a model from the damping of a squeeze flow of a disk shaped volume between two parallel plates, no influence of a ferrofluid is considered here yet. The second paragraph adds an additional ring to that model with another viscosity. The third paragraph presents a model from which the behaviour of the damping of a pocket bearing could be understood with the use of the models of the previous two paragraphs.

C.1 Model for squeeze flow damping

This section presents the derivation of the damping model for a squeeze flow. This is done with the Reynolds equation for squeeze films in cylindrical coordinates [71], [72]. The derivation assumes that the volume between the bearing pads is completely filled with one normal fluid. This means that the effect of the ferrofluid and the seal is not yet considered in this section. The derivation assumes that the fluid behaves Newtonian, there is a low Reynolds number flow, the pressure across the fluid is negligible and the fluid film thickness is much less than the radius.

$$\frac{\partial}{\partial r} \left(\frac{\rho h^3}{12\eta} r \frac{\partial p}{\partial r} \right) + \frac{1}{r} \frac{\partial}{\partial \theta} \left(\frac{\rho h^3}{12\eta} \frac{\partial p}{\partial \theta} \right) = r \frac{\partial(\rho h)}{\partial t} \quad (\text{C.1})$$

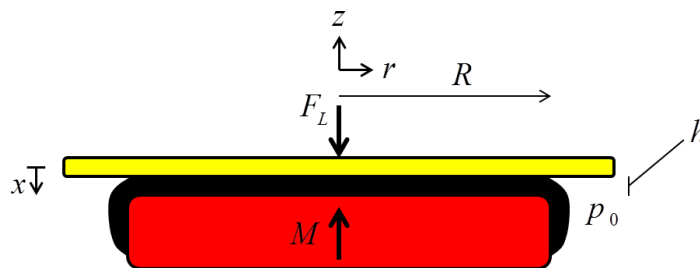


Fig. 7-5: Symbols used in the derivation.

The equation can be reduced to the following form by assuming a constant density and viscosity.

$$\begin{aligned} \frac{\rho h^3}{12\eta} \frac{\partial}{\partial r} \left(r \frac{\partial p}{\partial r} \right) + \frac{\rho h^3}{12\eta} \frac{1}{r} \frac{\partial}{\partial \theta} \left(\frac{\partial p}{\partial \theta} \right) &= r \rho \frac{\partial h}{\partial t} \\ \frac{\partial}{\partial r} \left(r \frac{\partial p}{\partial r} \right) + \frac{1}{r} \frac{\partial}{\partial \theta} \left(\frac{\partial p}{\partial \theta} \right) &= \frac{12\eta}{h^3} r \frac{\partial h}{\partial t} \end{aligned} \quad (\text{C.2})$$

The bearing in consideration here is axisymmetric which means that there is no pressure gradient in θ -direction. This gives the following form:

$$\frac{\partial}{\partial r} \left(r \frac{\partial p}{\partial r} \right) = \frac{12\eta}{h^3} r \frac{\partial h}{\partial t} \quad (\text{C.3})$$

Integrating the formula gives:

$$r \frac{\partial p}{\partial r} = \frac{12\eta}{h^3} r^2 \frac{\partial h}{\partial t} + C_1 \quad (\text{C.4})$$

The pressure gradient in the centre of the bearing is zero. Applying this boundary condition of $\frac{\partial p}{\partial r} = 0$ for $r = 0$ shows that $C_1 = 0$.

$$\begin{aligned} 0 &= \frac{12\eta}{h^3} 0 \frac{\partial h}{\partial t} + C_1 \\ C_1 &= 0 \end{aligned} \quad (\text{C.5})$$

Rearranging equation (C.4), applying the boundary condition and integrating again writes to the following form:

$$p = \frac{3\eta}{h^3} r^2 \frac{\partial h}{\partial t} + C_2 \quad (\text{C.6})$$

The pressure at the outside of the bearing pads should be zero. Applying this boundary condition of $p = 0$ for $R = r$ yields the following result:

$$\begin{aligned} \frac{3\eta}{h^3} R^2 \frac{\partial h}{\partial t} + C_2 &= 0 \\ C_2 &= -\frac{3\eta}{h^3} R^2 \frac{\partial h}{\partial t} \end{aligned} \quad (\text{C.7})$$

The pressure distribution between the bearing pads can now be expressed by the following equation:

$$\begin{aligned} p &= \frac{3\eta}{h^3} r^2 \frac{\partial h}{\partial t} - \frac{3\eta}{h^3} R^2 \frac{\partial h}{\partial t} \\ &= \frac{3\eta}{h^3} (r^2 - R^2) \frac{\partial h}{\partial t} \end{aligned} \quad (\text{C.8})$$

The force can now be calculated by integrating the pressure distribution of the whole surface of the bearing pads. This is done in the following equation:

$$\begin{aligned} F &= \int_S p dA = \frac{3\eta}{h^3} \frac{\partial h}{\partial t} \int_0^R \int_0^{2\pi} (r^2 - R^2) r dr d\theta \\ &= \frac{3\eta}{h^3} \frac{\partial h}{\partial t} \int_0^R \int_0^{2\pi} (r^3 - rR^2) r dr d\theta \\ &= \frac{3\eta}{h^3} \frac{\partial h}{\partial t} \int_0^{2\pi} \left(\frac{R^4}{4} - \frac{R^4}{2} \right) d\theta \\ &= \frac{3\eta}{h^3} \frac{\partial h}{\partial t} 2\pi \left(-\frac{R^4}{4} \right) \\ &= -\frac{3\pi\eta R^4}{2h^3} \frac{\partial h}{\partial t} \end{aligned} \quad (\text{C.9})$$

From this the damping constant can be derived to be:

$$c = \frac{F}{u} = -\frac{3\pi\eta R^4}{2h^3} \quad (\text{C.10})$$

C.2 Model for squeeze flow of damping with two different viscosities

This section will derive a model for a squeeze flow damping with two different viscosity regions. One region is located at the inside as a disk and the other region is located at the outside as a ring. The model presented here is only valid if the radiuses of the regions are much larger than distance between the two bearing faces.

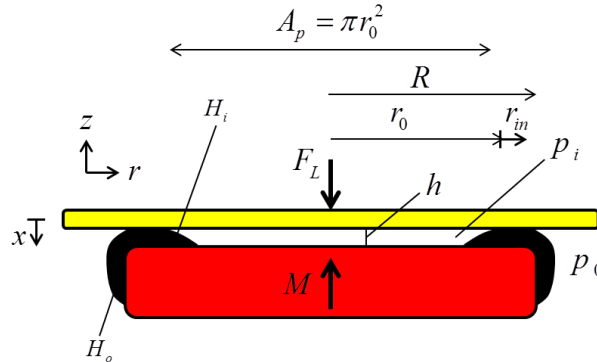


Fig. 7-6. The figure presents the different symbols used in the derivations.

The behaviour of the inner region can still be modelled with the method presented in the previous section. So the damping of the pocket can be described by the following equation:

$$c_p = \frac{F}{u} = -\frac{3\pi\eta_{in}R_{in}^4}{2h^3} \quad (C.11)$$

The contribution of the outer region can be approximated by first assuming a fully filled disk with the size of both regions combined. Now assume a fully filled disk with the size of only the inner region. The difference of these two damping values approximates the damping of the outer region. This model is presented by the following equation:

$$c_s = \frac{F}{u} = -\frac{3\pi\eta_s(R_{out}^4 - R_{in}^4)}{2h^3} \quad (C.12)$$

This method is not applicable if the width of the outer region $(R_{out}^4 - R_{in}^4)$ is not much smaller than the distance between the bearing surfaces. The effects at the ends of the fluid film become too dominant and introduce a lot of uncertainty.

C.3 Model for ferrofluid pocket bearing damping

This section discusses the approximation for the damping of a ferrofluid pocket bearing. The damping can be divided into two parts, an inner part consisting of the pocket and an outer part consisting of the seal. The damping of the inner part can be calculated with the use of relation (C.10), but the damping of the outer part is a bit trickier. The magnitude of the magnetic field changes the viscosity of the fluid which causes a change of viscosity over the region. The length of the region is in many cases also not much shorter than the distance between the bearing faces. These two effects cause the use of equation (C.12) to be relatively inaccurate. Though the equation is still useful to get an understanding of how in general the different parameters are changing the damping of the system. Increasing the viscosity and increasing the seal length will cause the damping to decrease. Increasing the distance between the two bearing faces will cause the damping to decrease.

D Additional measurements bearings

This section presents the some additional measurements done during the experiments. The full load and stiffness range is measured and presented. The amount of fluid that was added to the system was measured after the measurement by weighing the amount of fluid that came of the bearing. The weight that was measured is 0.875gram which corresponds to a volume of 0.634ml . The value for the magnetic field intensity at the outer fluid interface of the seal has a negligible change due to the fluid reservoir. This static value can be derived by measuring how high the fluid builds up on top of the magnet. The height is measured to be 1.4mm which corresponds to a magnetic field intensity of 1.3×10^5 A/m. According to Fig. 7-9, the radial position of the outer fluid interface is 13.3mm . Assume for maximum compression, the outer interface will expand to a radial position of 14mm which corresponds to 1×10^5 A/m.

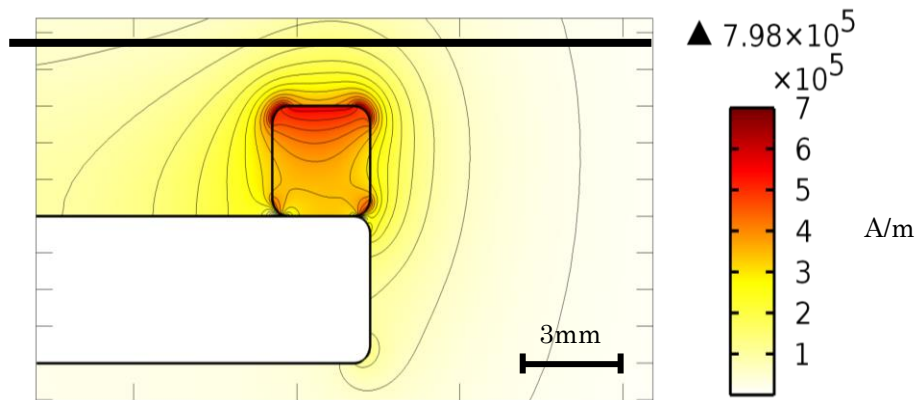


Fig. 7-7. This picture presents the magnetic field or the magnet configuration used in the experiments. The black line presents the initial position of the plate.

D.1 Lower part force vs displacement

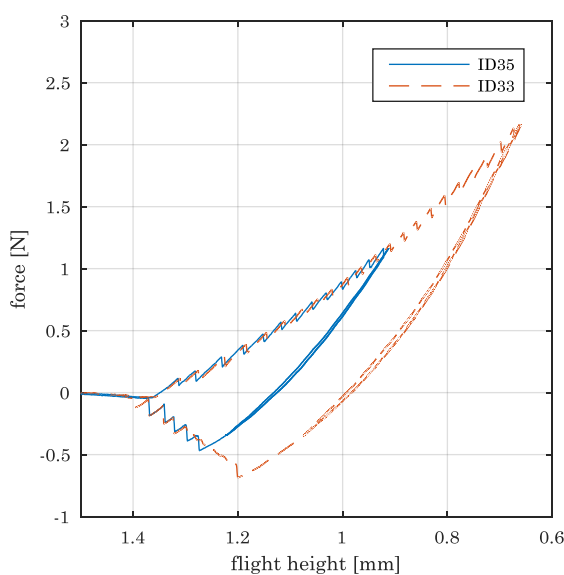


Fig. 7-8. This figure presents the load curve of the lower part of the range.

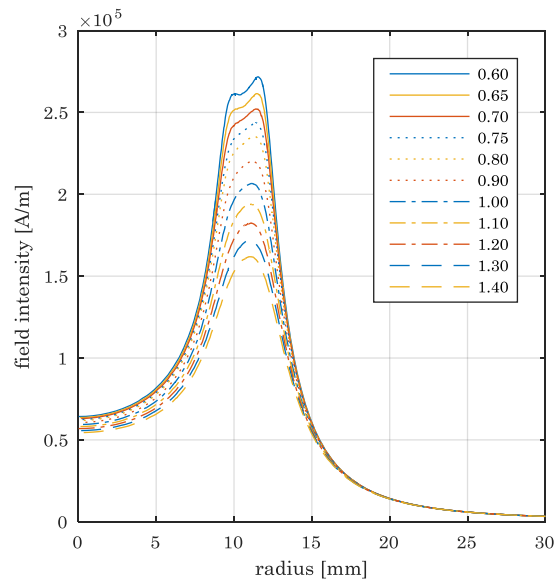


Fig. 7-9. The figure presents the magnetic field intensity for different flight height as function of the radius of the bearing. The value of 1.4mm corresponds to a system without the nonmagnetic bearing face.

D.2 Middle part force vs displacement

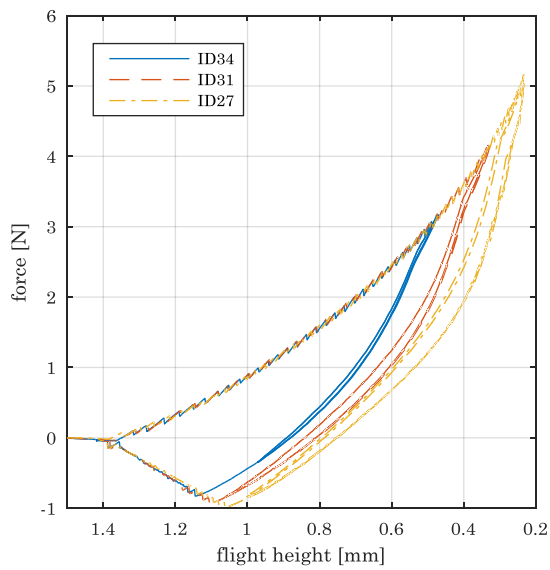


Fig. 7-10. This figure presents the load curve of the middle part of the range. Interesting to note is that some hysteresis is visible caused by air escaping across the inner seal of the bearing.

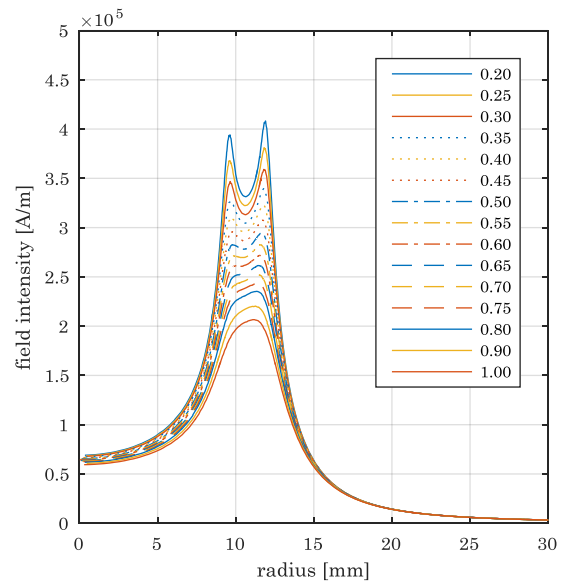


Fig. 7-11. The figure presents the magnetic field intensity for different flight height as function of the radius of the bearing.

D.3 Upper parts force vs displacement

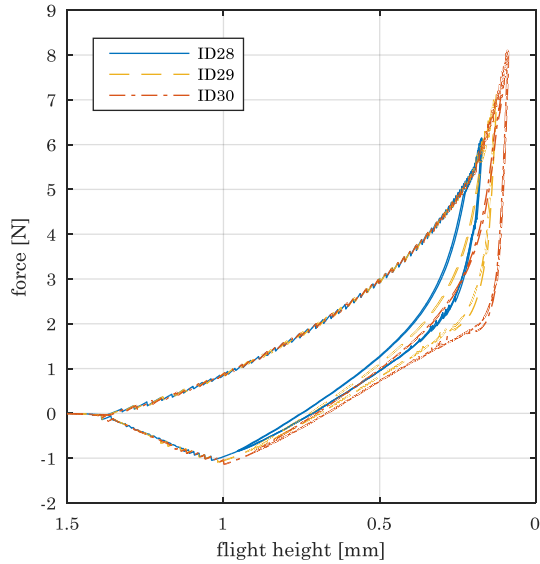


Fig. 7-12. This figure presents the load curve of the middle part of the range. Note that a lot of hysteresis occurs at high loads. This is caused by both the air escaping across the inner seal and the squeeze film damping in-between the two bearing faces.

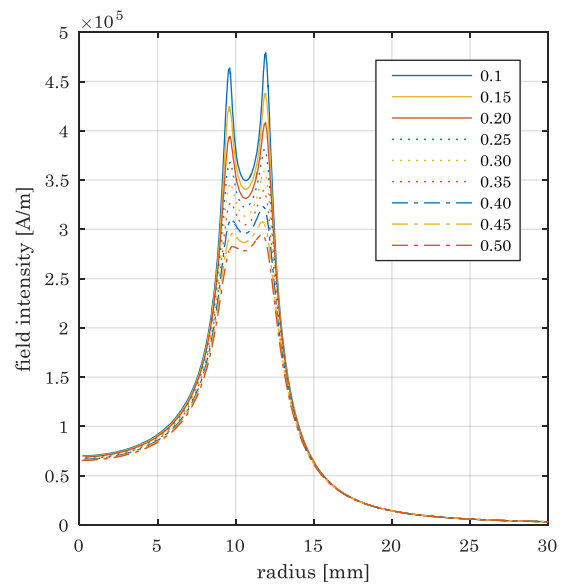


Fig. 7-13. The figure presents the magnetic field intensity for different flight height as function of the radius of the bearing.

D.4 Long run

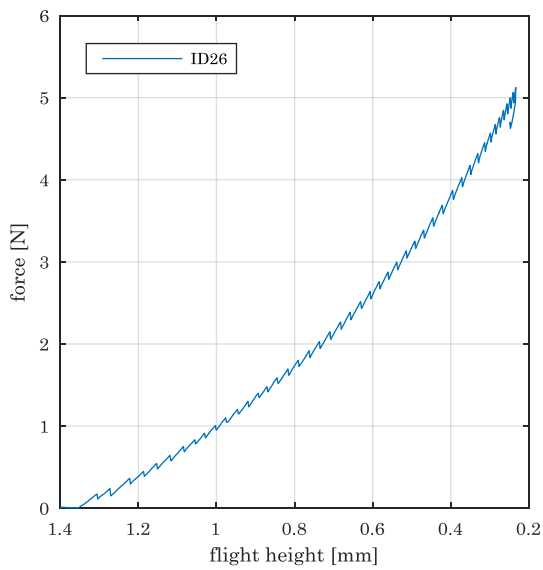


Fig. 7-14. This figure presents the force curve measurement that had as goal to measure the stability of the bearing.

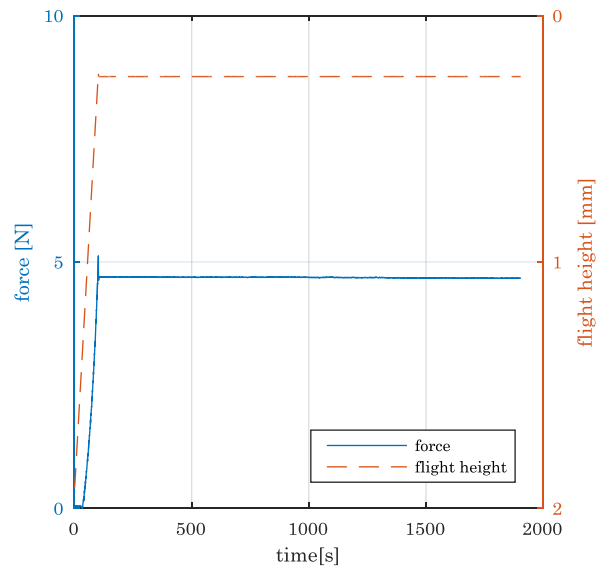


Fig. 7-15. This figure presents the force over time of the measurements that investigated the stability of the bearing over time. It can be seen that over a long time no air escapes from the seal.

D.5 Sandwich experiment overload

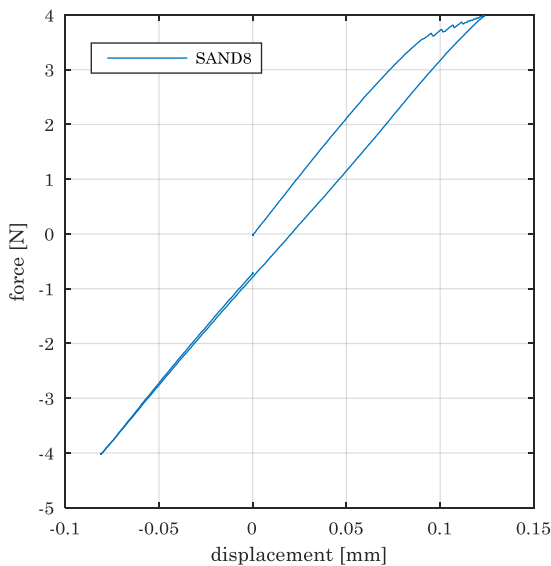


Fig. 7-16. This figure presents the air escaping from the configuration in a bearing with a sandwich like configuration. It shows that overloading the bearing causes a permanent change in position where it has zero force.

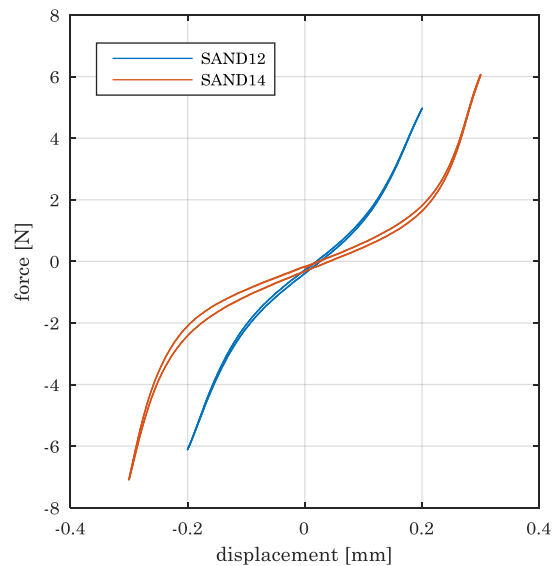


Fig. 7-17. This figure presents the load curve of a sandwich like structure at which a lot of air is escaped. It shows that the bearing comes into a lower stiffness region caused by the inner fluid interfaces that have moved to a position with a small magnetic field gradient.

E Change of concentration due to field gradient

During the experiments it is observed that there is a change in magnetization of the ferrofluid over time. The fluid that was used is the APG513A from Ferrotec of which the different specifications can be found in appendix J. This section discusses whether diffusion might be causing this.

E.1 Experimental results

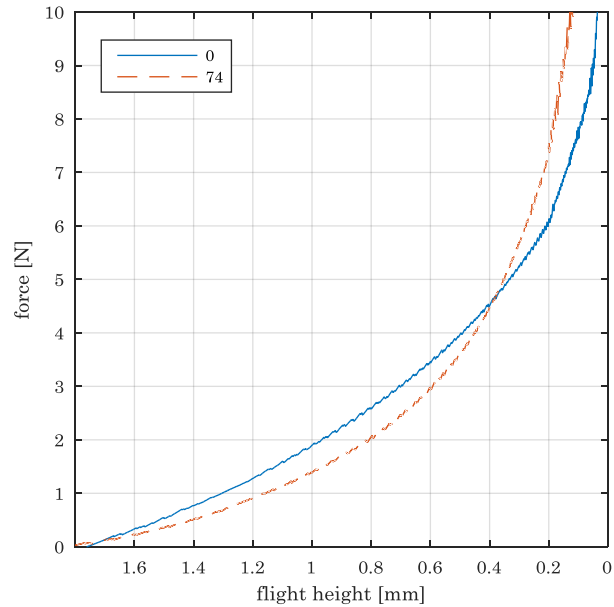


Fig. 7-18. The blue solid line presents the load curve at the initial moment. The red dashed line presents the load curve after 74 hours. It can be observed that the load capacity of the system becomes larger near the magnet and lower far away from the magnet. This can most probably be explained by an increase in magnetization near the magnet and a decrease in magnetization far away from the magnet due to diffusion of particles.

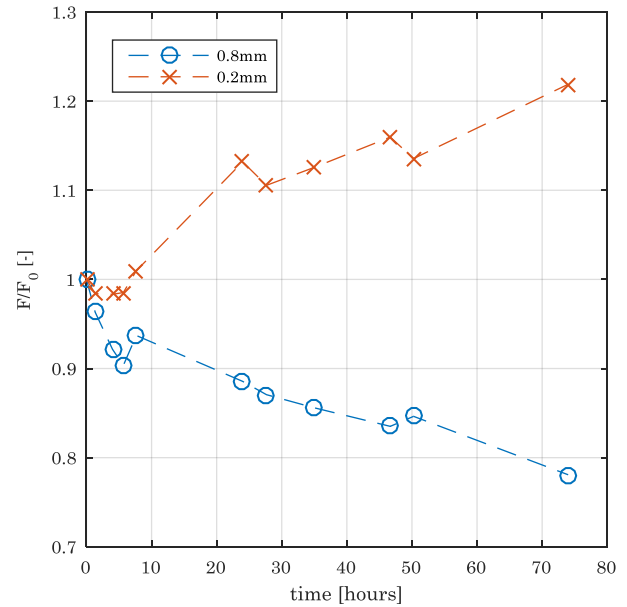


Fig. 7-19. The line with crosses presents the load capacity at a flight height of 0.2mm at different measurements over time. The line with circles presents the load capacity at a flight height of 0.8mm at different measurements over time.

E.2 Modelling

The change of concentration in a substance can be modelled by the following expression:

$$\frac{\partial c}{\partial t} + \nabla \cdot \underline{J} = 0 \quad (\text{E.1})$$

The flux of the particles can be expressed with [73]:

$$\underline{J} = J_d + J_f = -\frac{kT}{3\pi\eta d} \nabla c + c \frac{\mu_0 M_d V_d}{3\pi\eta d} \nabla H \quad (\text{E.2})$$

This leads to the following relation:

$$\frac{\partial c}{\partial t} = \frac{1}{6\pi\eta r} (kT(\nabla^2 c) - \nabla(c\mu_0 V_d M_d \nabla H)) \quad (\text{E.3})$$

In the assumption of a constant gradient in the magnetic field, this can be written to:

$$\frac{\partial c}{\partial t} = \frac{1}{6\pi\eta r} (kT(\nabla^2 c) - \mu_0 V_d M_d \nabla H \nabla c) \quad (\text{E.4})$$

$$6\pi\eta r \frac{\partial c}{\partial t} = kT \nabla^2 c - \mu_0 V_{mag} M_0 \nabla H \nabla c \quad (\text{E.5})$$

This equation is solved by using COMSOL with the relation written to the following form.

$$\frac{\partial c}{\partial t} = \frac{kT}{6\pi\eta r} \nabla^2 c - \frac{\mu_0 V_{mag} M_0 \nabla H}{6\pi\eta r} \nabla c \quad (\text{E.6})$$

$$\frac{kT}{6\pi\eta r} = \frac{1.4 \times 10^{-23} \times 293}{6\pi \cdot 0.15 \times 5 \times 10^{-9}} = 2.9 \times 10^{-13} \quad (\text{E.7})$$

$$\frac{\mu_0 V_{mag} M_0 \nabla H}{6\pi\eta r} = \frac{4\pi \times 10^{-7} \frac{\pi}{6} (10 \times 10^{-9})^3 \times 3.3 \times 10^5 \frac{5 \times 10^5}{0.003}}{6\pi \cdot 0.15 \times 5 \times 10^{-9}} = 2.6 \times 10^{-9} \quad (\text{E.8})$$

This lead to the following result:

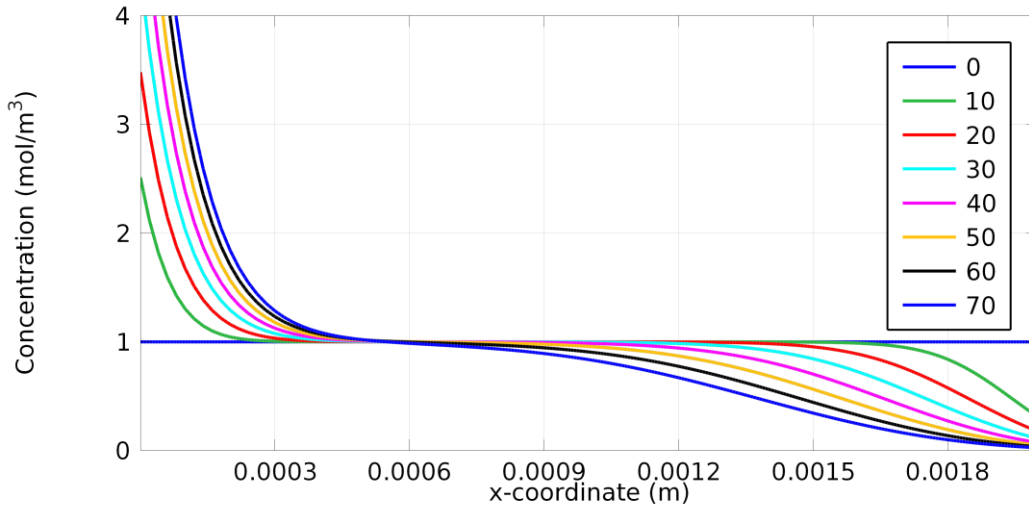


Fig. 7-20. This figure presents the diffusion over time modelled with COMSOL. The graph shows a higher diffusion than expected.

From the graph can be seen that the modelled situation does not correspond with the measured change in magnetization. The change in concentration close to the magnet and close to the air interface is much larger than the change in concentration observed in the experiments. It does correspond that at one third of the distance a negligible change in concentration occurs. The results from the calculation mean most probably that the system cannot simply be modelled with one dimensional diffusion due to a gradient in the magnetic field of one sized particles.

The ferrofluid is in real a fluid with different sizes of particles from which the larger one may form chains. The size of a particle has a lot of influence on the diffusion kinematics. Even by only considering the small particles, a too large diffusion is modelled.

It seems likely though from these results that the change of concentration over time is caused by a diffusion process. For a pocket bearing this means that standing still too long may cause the seal to leak air due to a local decrease in magnetization caused by diffusion. It is not clear whether the particles also show sedimentation but this is very well possible due to the large increase in concentration near the magnet.

F Magnetorheological fluids

A magnetorheological fluid can be defined as a fluid that has paramagnetic properties without having a colloidal stability. The magnetic properties are obtained by suspending the particles in a carrier fluid. No colloidal stability is obtained due to the large size of the particles needed for the higher magnetization strength. Relation (2.5) showed that the magnetization of a magnetic fluid increases with particle diameter. The particles of a magnetorheological fluid are that big that the magnetic energy E_{mag} and/or the gravitational energy E_{grav} are much larger than the thermal energy E_{therm} . The absence of colloidal stability reveals itself by particle aggregation due to the magnetic interaction of the particles and sedimentation of the particles due to the gravitational field or the magnetic field gradient. This particles aggregation and sedimentation changes the rheological properties and since the magnitude of this effect is a function of the magnetic field, the rheological properties can be controlled by the magnetic field.

G Assumptions

There are a lot of assumptions done in the derivation of the models presented in chapter 4 and 5. This section presents the different assumptions that are taken into consideration for the derivation of the model for the sandwich structure. Some examples of assumptions are given as follows. The contribution of the magnetic field gradient in y-direction is neglected which makes the described stiffness conservative. The outer interfaces are assumed to not influence the behaviour, but in fact they do a bit, making the system stiffer. The fluid interfaces are assumed to be vertical which is in reality not true, the pneumatic leverage may in reality be lower describing a lower stiffness than reality. A list containing assumptions that are considered for the models presented for the sandwich experiment presented in section 4.4 are given as follows:

- Stiffness of ferrofluid itself
- Uncertainty on the magnetization strength of ferrofluid
- Ferrofluid has colloidal stability
- Fitted shape of the magnetic field
- COMSOL model of field
- Stiffness of the air (volume)
- Stiffness of the setup is adiabatic
- Outer fluid interface does not contribute
- Uniformity of the fluid
- Capillary force
- Inner fluid interface is vertical
- Inner fluid interface stays vertical
- Measurement of gap height
- Strength of magnet
- Plate is in the middle
- Linear pneumatic leverage
- Test bench well calibrated
- Test bench properly aligned
- COMSOL model fits the magnetic field of the experiment well
- Velocity effects can be neglected (Neglects viscous and inertial terms)

H Air pocket stiffness derivation

This section discusses the derivation of the stiffness of an air pocket in a sandwich like bearing configuration. The derivation starts with assuming a polytropic process:

$$p_1 V_1^\gamma = p_2 V_2^\gamma = C \quad (\text{H.1})$$

At which polytropic index γ is defined as:

$$\gamma = \frac{c_p}{c_v} \quad (\text{H.2})$$

This leads to the following relation for the pressure in the top and in the bottom pocket:

$$\begin{aligned} p_T &= \frac{p_i V_i^\gamma}{V_T^\gamma} = p_i \left(\frac{V_i}{V_T} \right)^\gamma \\ p_B &= \frac{p_i V_i^\gamma}{V_B^\gamma} = p_i \left(\frac{V_i}{V_B} \right)^\gamma \end{aligned} \quad (\text{H.3})$$

The following relation derives from relation (H.1):

$$\begin{aligned} \frac{d}{dx}(p_1 V_1^\gamma) &= \frac{d}{dx}(p_2 V_2^\gamma) = 0 \\ &= p_1 \gamma V_1^{\gamma-1} \frac{dV_1}{dx} + V_1^\gamma \frac{dp_1}{dx} = 0 \end{aligned} \quad (\text{H.4})$$

This means that the gradient in pressure can be described as follows:

$$\frac{dp_1}{dx} = -p_1 \gamma \frac{V_1^{\gamma-1}}{V_1^\gamma} \frac{dV_1}{dx} = -p_1 \gamma \frac{1}{V_1} \frac{dV_1}{dx} \quad (\text{H.5})$$

An expression for the volume can be generated by the following relation:

$$\begin{aligned} V_{PT} &= A_p (h + x) \\ V_{PB} &= A_p (h - x) \end{aligned} \quad (\text{H.6})$$

The gradient of the volume can be described as follows:

$$\frac{dV_{PT}}{dx} = \frac{d}{dx} A_p (h + x) = A_p \quad (\text{H.7})$$

$$\frac{dV_{PB}}{dx} = \frac{d}{dx} A_p (h - x) = -A_p \quad (\text{H.8})$$

These relations result in the following expressions:

$$\begin{aligned} \frac{dp_T}{dx} &= -p_T \gamma \frac{1}{V_{PT}} \frac{dV_{PT}}{dx} = -p_T \gamma \frac{1}{V_{PT}} A_p \\ \frac{dp_B}{dx} &= -p_B \gamma \frac{1}{V_{PB}} \frac{dV_{PB}}{dx} = p_B \gamma \frac{1}{V_{PB}} A_p \end{aligned} \quad (\text{H.9})$$

Now the stiffness of the springs can be written as follows:

$$\begin{aligned}
k_T &= \frac{dF_T}{dx} = \frac{d}{dx}(-p_T A_P) = p_T \frac{dA_P}{dx} + A_P \frac{dp_T}{dx} \\
&= p_T \frac{dA_P}{dx} + p_T \gamma \frac{1}{V_{PT}} A_P^2 \\
k_T &= \frac{dF_B}{dx} = \frac{d}{dx}(p_B A_P) \\
&= p_B \frac{dA_P}{dx} + p_B \gamma \frac{1}{V_{PB}} A_P^2
\end{aligned} \tag{H.10}$$

With the assumption of $\frac{dA_P}{dx} \approx 0$, this writes to:

$$\begin{aligned}
k_T &= p_T \gamma \frac{A_P^2}{V_{PT}} = p_T \gamma \frac{A_P^2}{A_P (h+x)} = p_T \gamma \frac{A_P}{h+x} \\
k_B &= -p_B \gamma \frac{A_P^2}{V_{PB}} = p_B \gamma \frac{A_P^2}{A_P (h-x)} = p_B \gamma \frac{A_P}{h-x}
\end{aligned} \tag{H.11}$$

With the use of relation (H.3), this can be written to:

$$\begin{aligned}
k_T &= p_T \gamma \frac{A_P}{h+x} = \left(\frac{V_i}{V_T} \right)^\gamma p_i \gamma \frac{A_P}{h+x} \\
k_B &= -p_B \gamma \frac{A_P}{h-x} = - \left(\frac{V_i}{V_B} \right)^\gamma p_i \gamma \frac{A_P}{h-x}
\end{aligned} \tag{H.12}$$

The ration between the volumes is equal to:

$$\begin{aligned}
\frac{V_i}{V_T} &= \frac{A_P(h)}{A_P(h+x)} = \frac{h}{h+x} \\
\frac{V_i}{V_B} &= \frac{A_P(h)}{A_P(h-x)} = \frac{h}{h-x}
\end{aligned} \tag{H.13}$$

Now combining (H.12) with (H.13) leads to the following relation:

$$\begin{aligned}
k_T &= \left(\frac{V_i}{V_T} \right)^\gamma p_i \gamma \frac{A_P}{h+x} = \left(\frac{h}{h+x} \right)^\gamma p_i \gamma \frac{A_P}{h+x} \\
k_B &= \left(\frac{V_i}{V_B} \right)^\gamma p_i \gamma \frac{A_P}{h-x} = \left(\frac{h}{h-x} \right)^\gamma p_i \gamma \frac{A_P}{h-x}
\end{aligned} \tag{H.14}$$

This leads to the final relation of the combined stiffness of the upper and bottom pocket.

$$k_{total} = k_T + k_B = \left(\frac{h}{h+x} \right)^\gamma p_i \gamma \frac{A_P}{h+x} + \left(\frac{h}{h-x} \right)^\gamma p_i \gamma \frac{A_P}{h-x} \tag{H.15}$$

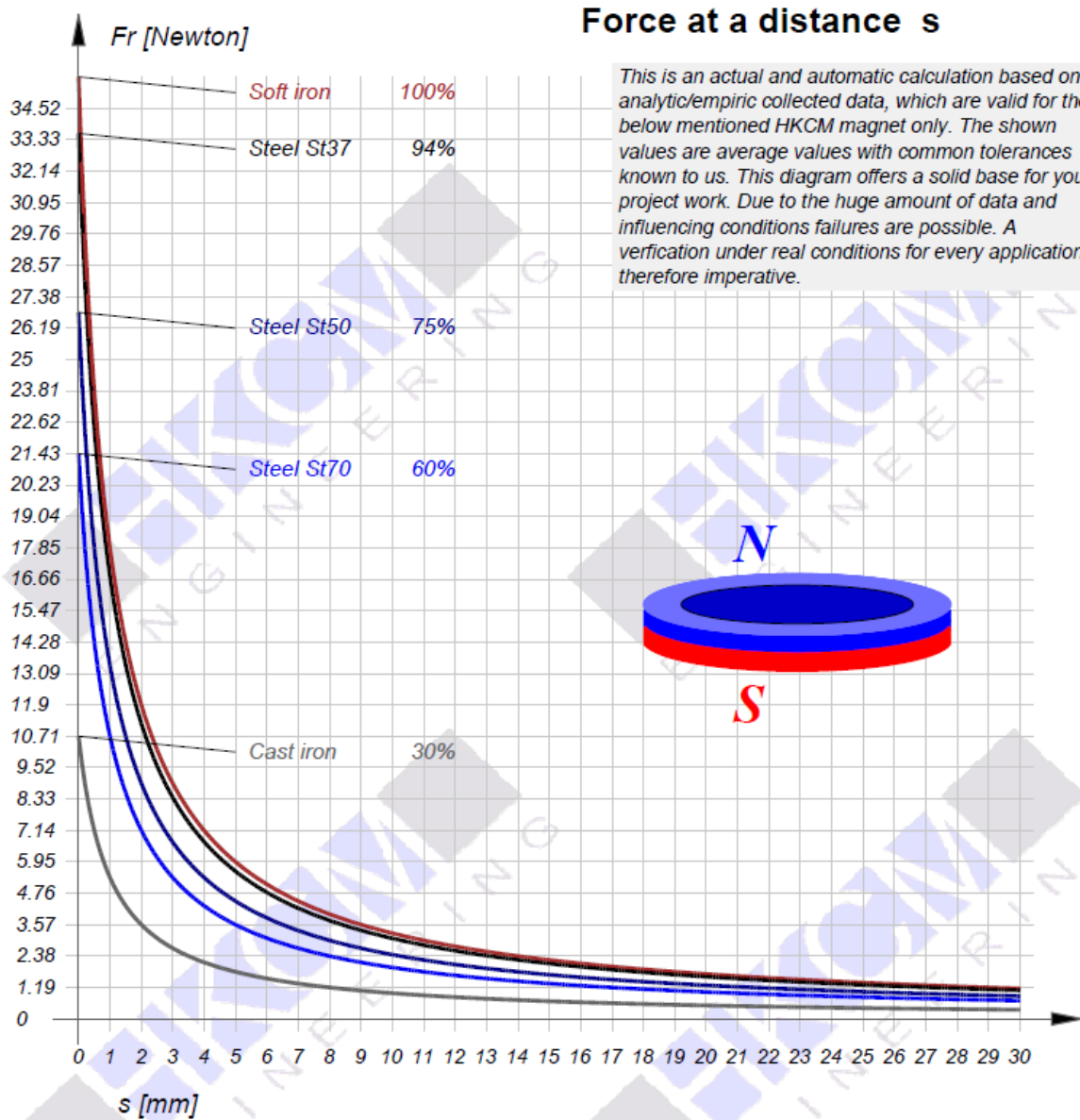
I Specifications magnet

Magnet-Ring R24.5x18.5x03Zn-35SH

Tolerances : DIN ISO 2768-1m
ROHs (2011/65/EU) & REACH (2007/EU)
Outer diameter(D) = 24.5 mm
Inner diameter(d) = 18.5 mm
Height(H) = 3 mm
Material, Grade: Neodymium NdFeB / 35SH / 279kJ/m3
Coating: Zinc
Poles = ax
max.operation temperature = 150 °C
Flux density inside the magnet 1.17 Tesla
Temperature coefficient flux = 0.11% per 1°K
Dead weight: 4.536 g
Holding force on a steel plate 35.71 Newton
Weight, which the magnet can lift: 3.64 kg



HKCM Engineering e.K.
 Langebrueckstr. 24
 D-24340 Eckernfoerde
 p: +49 (0) 4351 878 015
 f: +49 (0) 4351 878 130
 e: magnet@hkcm.de
 w: <https://www.hkcm.de>
 VAT-Id No.: DE 814 756 521



J Specifications ferrofluid APG513A from Ferrotec

Special-Ferrofluid for cooling in full range speakers and woofers with moderate temperature environment. Suitable for low temperatures. Tolerance to high humidity and water is moderate. This ferrofluid was chosen because it is discussed extensively in literature. The ferrofluid might not have the best performance compared to other ferrofluids, but there is a lot of knowledge about this performance. This helps to link the things we expect from theory with the things we see in practice.

Parameter	Value	Unit	Source
Saturation magnetization	0.044	T	[32]
	32×10^3	A/m	
Viscosity	$0.15 \pm 10\%$	kg/ms	[32]
Pour point	-60	°C	[32]
Density	1380	kg/m ³	[32]
Carrier liquid	Synthetic ester	-	[32]
Thermal conductivity	150	mW/mK	[32]
Thermal expansion coefficient	7.5×10^{-4}	1/K	[32]
Anisotropy constant	$K_a = 4.3 \times 10^4$	J/m ³	[74] or Fig. 2-14
Attempt period	$\tau_0 = 10^{-9}$	s	[75]
Magnetization core	63	emu/g	[76]
	3.3×10^5	A/m	[76]
	4.5×10^5	A/m	[27]
Surfactant thickness	~ 2 (estimate)	nm	[27]
Density magnetite	5.18	g/cm ³	[27]
Mean size particle	10	nm	[27]

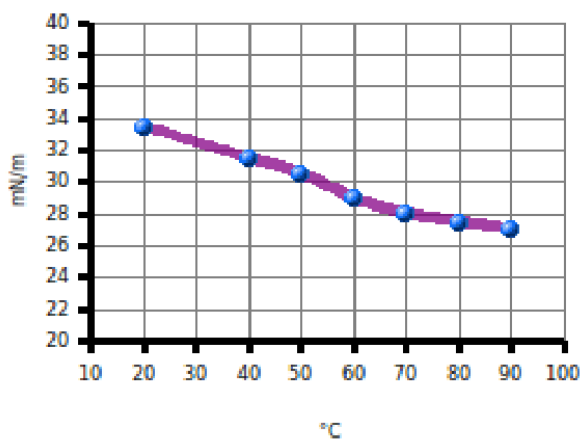


Fig. 7-21. The figure presents the surface tension over the temperature. Figure from [32]

K Zwick

Kalibrierschein / Calibration Certificate

Kunde <i>Customer</i>	Technische Universiteit Delft	Ergebnisdatei <i>Result file</i>	182823.kal
Prüfer <i>Tester</i>	Mohn	Temperatur <i>Temperature</i>	24.0 °C
Kalibrierdatum <i>Date of calibration</i>	22.07.2008	AB-Nr. der Maschine <i>Machines AB no.</i>	2152437
Typ des Kraftaufnehmers <i>Type of load cell</i>	KAF-TC	Werk-Nr. der Maschine <i>Serial no. of the machine</i>	182822
Werk-Nr. Kraftaufnehmer <i>Load cells serial number</i>	182823	Anzeige <i>Display</i>	PC
Nennkraft <i>Nominal force</i>	1000.000 N	Auflösung a der Maschine <i>Machines resolution a</i>	0.42% bei 0.2% FN

Verwendete Gebrauchsnormale und Prüfgeräte:
Working standards and test devices used:

Belastungskörpersatz Nr.02
Digitalkompensator DK 38, Nr. 53374
Kraftaufnehmer 2kN, Nr. 102130042

Wir bestätigen hiermit, daß der oben beschriebene Kraftaufnehmer kalibriert wurde.
Die gemessenen Werte der Kraftmesseinrichtung liegen innerhalb der zulässigen Abweichungen nach DIN EN ISO 7500-1. Die jeweilige Messunsicherheit ist mit zweifacher Standardabweichung bei jeder Stufe angegeben. Die Kraftmesseinrichtung kann in den geprüften Meßbereichen wie folgt eingesetzt werden:

*We hereby confirm that the above named load cell has been calibrated.
The force measurement devices measured values are within the permissible tolerances according to DIN EN ISO 7500-1
The measuring uncertainty is given at each step considered with a double standard deviation. The force measurement device can be put to use as follows in the tested measurement ranges.*

DIN EN ISO 7500-1 Klasse 1 (2.00 N ... 1.00 kN)
DIN EN ISO 7500-1 Klasse 0.5 (10.00 N ... 1.00 kN)

Für die Einhaltung der angemessenen Frist zur Wiederholung der Kalibrierung ist der Benutzer verantwortlich. Wir verweisen auf die Norm DIN 51220 und auf die speziellen Prüf- und Kalibriernormen.

*The user is responsible for keeping to an appropriate deadline for the repetition of calibration.
We draw standard DIN 51220, and the special test and calibration standards to you attention*

Dies ist ein elektronisch erstelltes Dokument, welches ohne Unterschrift gültig ist
This is an electronically created documnet and is therefore valid without signature.

Ergebnisse Zug / results tensile :

wahrer Wert <i>real Value</i>	Maschinenanzeige <i>Machine display</i>	relative Anzeigeabweichung <i>rel. accuracy</i>	relative Wiederholpräzision <i>rel. repeatability</i>	relative Umkehrspanne <i>rel. reversibility</i>	relative Messunsicherheit <i>rel. uncertainty</i>
2.000 N	1.999 N	-0.05 %	0.24 %	-0.04 %	0.35 %
5.000 N	4.999 N	-0.02 %	0.05 %	-0.07 %	0.23 %
10.000 N	9.990 N	-0.10 %	0.03 %	-0.07 %	0.21 %
20.000 N	20.006 N	0.03 %	0.03 %	-0.02 %	0.20 %
50.000 N	50.015 N	0.03 %	0.01 %	-0.01 %	0.20 %
100.000 N	100.040 N	0.04 %	0.01 %	0.00 %	0.20 %
99.907 N	100.000 N	0.09 %	0.28 %	-0.39 %	0.20 %
199.980 N	200.000 N	0.01 %	0.39 %	-0.02 %	0.26 %
400.200 N	400.000 N	-0.05 %	0.09 %	0.06 %	0.12 %
599.920 N	600.000 N	0.01 %	0.02 %	0.03 %	0.12 %
799.830 N	800.000 N	0.02 %	0.09 %	-0.07 %	0.12 %
1.000 kN	1.000 kN	-0.01 %	0.07 %	-0.01 %	0.12 %

Ergebnisse Druck / results compression :

wahrer Wert <i>real Value</i>	Maschinenanzeige <i>Machine display</i>	relative Anzeigeabweichung <i>rel. accuracy</i>	relative Wiederholpräzision <i>rel. repeatability</i>	relative Umkehrspanne <i>rel. reversibility</i>	relative Messunsicherheit <i>rel. uncertainty</i>
2.000 N	2.004 N	0.21 %	0.33 %	-0.53 %	0.37 %
5.000 N	5.005 N	0.11 %	0.18 %	-0.18 %	0.25 %
10.000 N	10.009 N	0.09 %	0.06 %	-0.09 %	0.21 %
20.000 N	20.029 N	0.14 %	0.06 %	-0.03 %	0.21 %
50.000 N	50.023 N	0.05 %	0.04 %	0.01 %	0.20 %
100.000 N	100.020 N	0.02 %	0.02 %	0.01 %	0.20 %
100.400 N	100.000 N	-0.40 %	0.40 %	-0.06 %	0.27 %
200.180 N	200.000 N	-0.09 %	0.25 %	0.04 %	0.17 %
400.250 N	400.000 N	-0.06 %	0.11 %	0.10 %	0.12 %
600.040 N	600.000 N	-0.01 %	0.07 %	0.10 %	0.12 %
800.540 N	800.000 N	-0.07 %	0.01 %	-0.03 %	0.12 %
999.900 N	1.000 kN	0.01 %	0.04 %	0.05 %	0.12 %

L Previous projects containing ferrofluids

L.1 Master thesis

Year	Student name	Project name	ref
2013	Veen, Simon van	Planar Ferrofluid Bearings for Precision Stages	[5]
2014	Café, Max	Nanometer precision Six Degrees of Freedom Planar Motion Stage with Ferrofluid Bearings	[58]
2015	Mok, Gihin	The design of a planar precision stage using cost effective optical mouse sensors	[61]
2015	Habib, Haris	Design of a three DOF planar precision stage using a single Position Sensitive Detector	[62]

L.2 Bachelor projects

Year	Student names	Project name	
2011	Assenberg, Max Mulders, Nigel Schrier, Bram Sjoukes, Joost	Ontwerp een kruistafel met ferrofluid oplegging	[77]
2011	Morsink, Diederik Lieverink, Daniel Lanphen, Linda Fekkes, Marte	Ontwerp van een USB Microscooptafel	[78]
2012	Bommel, Lotte van Hoeven, Tom van der Los, Marc Mostovoy, Nikita	Ferrofluid lagering met grote draagkracht	[79]
2013	Joziasse, Bart Jong, Bart de Meerkerk, Mike van Kuipers, Steven	Horizontale trillingsisolatie met behulp van een ferrofluid vlaklager	[80]
2013	Leeuwen, Menno van Potma, Olivier le Roy, Florrie Speelman, Tim	Vertikale trillingsdemping voor precisie onderzoek	[81]

M References

- [1] R. P. Feynman, "Plenty of Room at the Bottom," no. December, 1959.
- [2] S. S. Ge, T. H. Lee, and S. X. Ren, "Adaptive friction compensation of servo mechanisms," *Int. J. Syst. Sci.*, vol. 32, no. 4, pp. 523–532, 2001.
- [3] P. Ouwehand, "Novel Nanometer precision Planar Positioning stage using Pre-sliding friction," Delft University of Technology, 2015.
- [4] R. Deng, S. Van Veen, M. Café, J. W. Spronck, and R. H. M. Schmidt, "Linear Nano-Positioning Stage using Ferrofluid Bearings," no. June, p. 4, 2014.
- [5] S. van Veen, "Planar Ferrofluid Bearings for Precision Stages," Delft University of Technology, 2013.
- [6] S. S. Papell, "Low viscosity magnetic fluids obtained by the colloidal suspension of magnetic particles," US Patent 3 215 572, 1965.
- [7] R. E. Rosensweig, "Buoyancy and stable levitation of a magnetic body immersed in a magnetizable fluid.," *Nature*, vol. 210, no. 5036, pp. 613–614, 1966.
- [8] E. H. William, "Method of and means for detecting defects in paramagnetic material," US Patent 1 426 384, 1922.
- [9] J. Rabinow, "Magnetic Fluid Clutch," *Tech. News Bull. United States Bur. Stand. (Washington, D. C.)*, vol. 32, p. 7, 1948.
- [10] J. Rabinow, "The Magnetic Fluid Clutch," *Trans. Am. Inst. Electr. Eng.*, vol. 67, no. 2, p. 1308, 1948.
- [11] J. Rabinow, "Magnetic fluid torque and force transmitting device," US Patent 2 575 360, 1951.
- [12] M. R. Jolly, J. W. Bender, and J. D. Carlson, "Properties and Applications of Commercial Magnetorheological Fluids," *J. Intell. Mater. Syst. Struct.*, vol. 10, no. 1, pp. 5–13, 1999.
- [13] S. S. Papell, "No Title," *Space Daily*, no. 211, 1963.
- [14] R. E. Rosensweig, J. N. Nestor, and R. S. Timmens, "No Title," *Br. Inst. Chem. Eng. Inst. Chem. Eng. Jt. Meet.*, p. 15, 1965.
- [15] S. W. Charles and J. Popplewell, "Chapter 8 Ferromagnetic liquids," *Handb. Ferromagn. Mater.*, vol. 2, pp. 509–559, 1980.
- [16] K. Raj, *Ferrofluids: Applications*. Elsevier, 2001.
- [17] M. D. Cowley and R. E. Rosensweig, "The interfacial stability of a ferromagnetic fluid.," *J. Fluid Mech.*, vol. 30, no. 04, pp. 671–688, 1967.
- [18] R. E. Rosensweig, R. Kaiser, and G. Miskolczy, "Viscosity of magnetic fluid in a magnetic field," *J. Colloid Interface Sci.*, vol. 29, no. 4, pp. 680–686, 1969.
- [19] J. P. McTague, "Magnetoviscosity of Magnetic Colloids," *J. Chem. Phys.*, vol. 51, no. 1969, p. 133, 1969.
- [20] M. I. Shliomis, "Magnetic fluids," *Uspekhi Fiz. Nauk*, vol. 112, no. 3, p. 427, 1974.
- [21] R. E. Rosensweig, "Magnetic fluid seals," 1971.
- [22] R. E. Rosensweig, "Bearing arrangement with magnetic fluid defining bearing pads," US Patent 3 612 630, 1971.
- [23] R. E. Rosensweig, "Magnetic fluid pneumatic bearings," 1973.
- [24] C. Scherer and J. A. Marinda, "Introduction to the magnetic fluids bibliography," *J. Magn. Magn. Mater.*, vol. 289, pp. 484–485, Mar. 2005.
- [25] S. Odenbach, "Magnetic fluids," *Adv. Colloid Interface Sci.*, vol. 46, pp. 263–282, Dec. 1993.
- [26] K. Raj and A. F. Chorney, "Ferrofluid technology - An overview," *Indian J. Eng. Mater. Sci.*, vol. 5, no. December, pp. 372–389, 1998.
- [27] S. Odenbach, "Recent progress in magnetic fluid research," *J. Phys. Condens. Matter*, vol. 16, no. 32, pp. R1135–R1150, 2004.
- [28] P. Didukh, A. Slawska-Waniewska, J. M. Greneche, and P. C. Fannin, "Magnetic properties of ferrofluid with cobalt ferrite particles," in *Physics of Magnetism '99*, 2000, vol. 97, no. 3, pp. 587–590.
- [29] S. Odenbach, *Colloidal magnetic fluids: basics, development and application of ferrofluids*, no. 763. Berlin: Springer Verlag, 2009.
- [30] S. Odenbach and S. Thurm, "Magnetoviscous Effects in Ferrofluids," in *Ferrofluids SE - 10*, vol. 594, S. Odenbach, Ed. Springer Berlin Heidelberg, 2002, pp. 185–201.
- [31] M. I. Shliomis, "Effective viscosity of magnetic fluids," *Sov. Phys. JETP*, vol. 24, no. 6, pp. 1291–1294, 1972.

- [32] Ferrotec, “Ferrofluid Data Sheet APG 500 series,” 2013.
- [33] M. Martsenyuk, Y. L. Raikher, and M. I. Shliomis, “On the kinetics of magnetization of suspensions of ferromagnetic particles,” *Sov. J. Exp. Theor. Phys.*, vol. 38, no. 2, p. 413, 1974.
- [34] S. Odenbach and H. Störk, “Shear dependence of field-induced contributions to the viscosity of magnetic fluids at low shear rates,” *J. Magn. Magn. Mater.*, vol. 183, no. 1–2, pp. 188–194, 1998.
- [35] S. Thurm and S. Odenbach, “Particle size distribution as key parameter for the flow behavior of ferrofluids,” *Phys. Fluids*, vol. 15, no. 6, p. 1658, 2003.
- [36] P. C. Jordan, “Association phenomena in a ferromagnetic colloid,” *Mol. Phys.*, vol. 25, no. January 2015, pp. 961–973, 1973.
- [37] A. Y. Zubarev, S. Odenbach, and J. Fleischer, “Rheological properties of dense ferrofluids. Effect of chain-like aggregates,” *J. Magn. Magn. Mater.*, vol. 252, no. 0, pp. 241–243, 2002.
- [38] S. Odenbach and H. Müller, “Stationary Off-Equilibrium Magnetization in Ferrofluids under Rotational and Elongational Flow,” *Phys. Rev. Lett.*, vol. 89, no. 3, p. 037202, 2002.
- [39] A. Lange, R. Richter, and L. Tobiska, “Linear and nonlinear approach to the Rosensweig instability,” *GAMM-Mitteilungen*, vol. 30, no. 1, pp. 171–184, 2007.
- [40] N. H. Black and H. N. Davis, *Practical Physics*. The MacMillan Co., USA, 1913.
- [41] G. F. Maxwell, “Ferrofluid.” 2006.
- [42] J. L. Neuringer and R. E. Rosensweig, “No Title,” *Phys. Fluids*, vol. 7, p. 1964, 1964.
- [43] N. Bayat, A. Nethe, J. M. Guldbakke, J. Hesselbach, V. A. Naletova, H.-D. Stahlmann, E. Uhlmann, and K. Zimmermann, “Technical Applications,” in *Colloidal Magnetic Fluids SE - 6*, vol. 763, S. Odenbach, Ed. Springer Berlin Heidelberg, 2009, pp. 1–72.
- [44] M. Kciuk and R. Turczyn, “Properties and application of magnetorheological fluids,” *J. Achiev. Mater. ...*, vol. 18, no. 1, pp. 127–130, 2006.
- [45] P. P. Phulé, “Magnetorheological (MR) fluids: Principles and applications,” *Smart Mater. Bull.*, vol. 2001, no. 2, pp. 7–10, 2001.
- [46] J. Popplewell, “Technological applications of ferrofluids,” *Phys. Technol.*, vol. 15, no. 3, pp. 150–156, 1984.
- [47] K. Raj, B. Moskowitz, and R. Casciari, “Advances in ferrofluid technology,” *J. Magn. Magn. Mater.*, vol. 149, no. 1–2, pp. 174–180, 1995.
- [48] K. Raj and R. Moskowitz, “Commercial applications of ferrofluids,” *J. Magn. Magn. Mater.*, vol. 85, no. 1–3, pp. 233–245, 1990.
- [49] R. E. Rosensweig, “Magnetic Fluids,” *Annu. Rev. Fluid Mech.*, vol. 19, no. 1, pp. 437–461, Jan. 1987.
- [50] C. Scherer and A. M. Figueiredo Neto, “Ferrofluids: properties and applications,” *Brazilian Journal of Physics*, vol. 35. scielo, pp. 718–727, 2005.
- [51] J. Wang and G. Meng, “Magnetorheological fluid devices: principles, characteristics and applications in mechanical engineering,” *Proc. Inst. Mech. Eng. Part L J. Mater. Des. Appl.*, vol. 215, no. 3, pp. 165–174, 2005.
- [52] R. L. Bailey, “Lesser Known Applications of Ferrofluids,” *J. Magn. Magn. Mater.*, vol. 39, pp. 178–182, 1983.
- [53] K. D. Ridler, A. B. Gosling, and G. M. Edge, “Linear bearing for parallel tracking arm,” 4,065,188, 1977.
- [54] S. Sudo, Y. Takaki, Y. Hashiguchi, and H. Nishiyama, “Magnetic Fluid Devices for Driving Micro Machines,” *JSME Int. J. Ser. B*, vol. 48, no. 3, pp. 464–470, 2005.
- [55] J. M. Guldbakke and J. Hesselbach, “Development of bearings and a damper based on magnetically controllable fluids,” *J. Phys. Condens. Matter*, vol. 18, no. 38, pp. S2959–S2972, 2006.
- [56] E. Uhlmann and N. Bayat, “High precision positioning with ferrofluids as an active medium,” *CIRP Ann. - Manuf. Technol.*, vol. 55, no. 1, pp. 415–418, 2006.
- [57] G. Millet and A. Hubert, “Design of a 3 DOF displacement stage based on ferrofluids,” *ACTUATORS’06*, pp. 656–659, 2006.
- [58] M. Café, “Nanometer precision Six Degrees of Freedom Planar Motion Stage with Ferrofluid Bearings,” Delft University of Technology, 2014.
- [59] M. Café and J. Spronck, “Nanometer precision Six Degree s of Freedom Planar Motion Stage with Ferrofluid Bearings,” *DSPE Conf. Precis. Mechatronics*, pp. 43–46, 2014.
- [60] B. Assadsangabi, M. H. Tee, and K. Takahata, “Electromagnetic Microactuator Realized by Ferrofluid-Assisted Levitation Mechanism,” *J. Microelectromechanical Syst.*, vol. 23, no. 5, pp. 1112–1120, 2014.

-
- [61] G. Mok, "The design of a planar precision stage using cost effective optical mouse sensors," Delft University of Technology, 2015.
- [62] H. Habib, "Department of Precision and Microsystems Engineering Design of a three Degrees of Freedom planar precision stage using a single Position Sensitive Detector," 2015.
- [63] B. Assadsangabi, M. H. Tee, and K. Takahata, "Ferrofluid-Assisted Levitation Mechanism for Micromotor Applications," *2013 Transducers Eurosensors XXVII 17th Int. Conf. Solid-State Sensors, Actuators Microsystems*, no. June, pp. 2720–2723, 2013.
- [64] A. Einstein, "On the Motion of Small Particles Suspended in a Stationary Liquid, as Required by the Molecular Kinetic Theory of Heat," *Ann. Phys.*, vol. 322, no. 8, pp. 549–560, 1905.
- [65] P. E. Dupont, "Avoiding stick-slip through PD control," *IEEE Trans. Automat. Contr.*, vol. 39, no. 5, pp. 1094–1097, 1994.
- [66] R. Ravaut, G. Lemarquand, and V. Lemarquand, "Mechanical properties of ferrofluid applications: Centering effect and capacity of a seal," *Tribol. Int.*, vol. 43, no. 1–2, pp. 76–82, 2010.
- [67] T. a. Osman, G. S. Nada, and Z. S. Safar, "Static and dynamic characteristics of magnetized journal bearings lubricated with ferrofluid," *Tribol. Int.*, vol. 34, no. 6, pp. 369–380, 2001.
- [68] T. a. Osman, G. S. Nada, and Z. S. Safar, "Different magnetic models in the design of hydrodynamic journal bearings lubricated with non-Newtonian ferrofluid," *Tribol. Lett.*, vol. 14, no. 3, pp. 211–223, 2003.
- [69] M. George and W. Ferrin, "Electrically conductive ferrofluid bearing and seal apparatus and low-viscosity electrically conductive ferrofluid used therein," 4,673,997, 1984.
- [70] J. Stefan, "Versuche uber die scheinbare adhesion," *Sitz. Kais. Akad. Wiss. Math. Nat. Wien*, vol. 69, no. 2, pp. 713–735, 1874.
- [71] B. J. Hamrock and S. R. Schmid, *Fundamentals of Fluid Film Lubrication Second Edition*. 2004.
- [72] G. W. Stachowiak and A. W. Batchelor, *Engineering Tribology*, 4th ed. Elsevier Inc., 2014.
- [73] S. Odenbach, *Ferrofluids*, no. 594. Berlin; New York: Springer, 2002.
- [74] A. Tari, J. Popplewell, and S. W. Charles, "Observation of Spin Glass Behaviour in Ferrofluids," *J. Magn. Magn. Mater.*, vol. V, no. 15–18, pp. 1125–1126, 1980.
- [75] P. C. Fannin and S. W. Charles, "The study of a ferrofluid exhibiting both Brownian and Neel relaxation," *J. Phys. D. Appl. Phys.*, vol. 22, pp. 187–191, 2000.
- [76] G. D. Moeser, K. a. Roach, W. H. Green, T. A. Hatton, and P. E. Laibinis, "High-gradient magnetic separation of coated magnetic nanoparticles," *AIChE J.*, vol. 50, no. 11, pp. 2835–2848, 2004.
- [77] M. Assenberg, N. Mulders, B. Schrier, and J. Sjoukes, "Ontwerp een kruistafel met ferrofluid oplegging," 2011.
- [78] D. Morsink, D. Liefferink, L. Lanphen, and M. Fekkes, "Ontwerp van een USB Microscooptafel," Delft University of Technology, 2011.
- [79] L. Van Bommel, T. Van Der Hoeven, M. Los, and N. Mostovoy, "Ferrofluid lagering met grote draagkracht," Delft University of Technology, 2012.
- [80] B. Joziassse, B. de Jong, M. van Meerkerk, and S. Kuipers, "Horizontale trillingsisolatie met behulp van een ferrofluid vlaklager," Delft University of Technology, 2013.
- [81] M. van Leeuwen, O. Potma, F. le Roy, and T. Speelman, "Vertikale trillingsdemping voor precisie onderzoek," Delft University of Technology, 2013.